

Texas Southern University

Digital Scholarship @ Texas Southern University

Dissertations (2016-Present)

Dissertations

5-2022

Discovery of OJT010 as a Novel Inhibitor of Severe Acute Respiratory Syndrome Coronavirus 2

Manvir Kaur

Follow this and additional works at: <https://digitalscholarship.tsu.edu/dissertations>



Part of the [Other Pharmacy and Pharmaceutical Sciences Commons](#)

Recommended Citation

Kaur, Manvir, "Discovery of OJT010 as a Novel Inhibitor of Severe Acute Respiratory Syndrome Coronavirus 2" (2022). *Dissertations (2016-Present)*. 16.
<https://digitalscholarship.tsu.edu/dissertations/16>

This Dissertation is brought to you for free and open access by the Dissertations at Digital Scholarship @ Texas Southern University. It has been accepted for inclusion in Dissertations (2016-Present) by an authorized administrator of Digital Scholarship @ Texas Southern University. For more information, please contact haiying.li@tsu.edu.

DISCOVERY OF OJT010 AS A NOVEL INHIBITOR OF SEVERE ACUTE
RESPIRATORY SYNDROME CORONAVIRUS 2

DISSERTATION

Presented in Partial Fulfillment of the Requirements for
the Degree Doctor of Philosophy in the Graduate School
of Texas Southern University

By

Manvir Kaur, B.D.S., M.H.A.

Texas Southern University

2022

Approved By

Omonike Olaleye, Ph. D, MPH.

Chairperson Dissertation Committee

Gregory H. Maddox, Ph.D.

Dean, Graduate School

Approved By

Omonike Olaleye Ph.D., MPH.
Chairperson, Dissertation Committee

03/29/2022
Date

Dong Liang, Ph.D.
Committee Member

03/29/2022
Date

Ya Fatou Njie Mbye, Ph.D.
Committee Member

03/29/2022
Date

Hector Miranda, Ph.D.
Committee Member

03/29/2022
Date

© Copyright by Manvir Kaur 2022

All Rights Reserved

**DISCOVERY OF OJT010 AS A NOVEL INHIBITOR OF SEVERE
ACUTE RESPIRATORY SYNDROME CORONAVIRUS 2**

By

Manvir Kaur, Ph.D.

Texas Southern University, 2022

Professor Omonike Olaleye Ph.D., MPH. Advisor

The current pandemic of coronavirus disease (COVID-19) caused by the highly infectious pathogen, severe acute respiratory syndrome coronavirus 2 (SARS-CoV-2), represents a global public health challenge. The emergence of deadly SARS-CoV-2 variants with mutations on the viral genes has made it more imperative to discover therapeutics that target the host receptors for COVID-19 treatment. Therefore, our research has targeted the critical host entry receptor: Angiotensin-converting enzyme-2 (ACE2) for SARS-CoV-2 entry into the human cells.

SARS-CoV-2 is an enveloped RNA beta coronavirus that infects human cells via interaction with the ACE2 receptor, followed by viral replication and virus dissemination. Spike protein of SARS-CoV-2 has a receptor-binding domain (RBD), which binds to the host ACE2 receptor. ACE2 is an essential component of the Renin-Angiotensin System (RAS) that converts Angiotensin II (Ang II) to Angiotensin 1-7, a potent vasopressor. Even though ACE2 facilitates viral entry, it provides defense against acute lung injury,

indicating that the ACE2/Ang 1-7 pathway must be carefully manipulated to reduce SARS-CoV-2 induced lung injuries.

Herein, we discovered that OJT010 targets the interaction between RBD and rhACE2 without inhibiting the exopeptidase activity of rhACE2. Our findings reveal that OJT010 binding to rhACE2 may potentially preserve its physiological function and prevention exacerbation of the disease. Furthermore, it will potentially prevent non-target cardiac toxicities observed in other ACE2 modulating drugs. Moreover, we discovered that OJT010 inhibits the cellular entry and further replication of the SARS-CoV-2 and B.1.617.2 Delta Variant in three independent assays; Infection Induced Cytopathic Effect (CPE), Nanoluciferase reporter assay (NLRV), and Pseudotyped Lentiviral assay. In addition, we have also assessed the molecular interactions of the compounds with the host and viral receptor using molecular dynamic simulation of the best-fit docking complex to elucidate the binding sites of OJT010. Next, we have determined the pharmacokinetics (PK) parameters of OJT010 in healthy rats. We have further advanced into a hamster of model SARS-CoV-2 infection to evaluate the efficacy of OJT010 against SARS-COV-2 infection *in vivo*.

Based on our findings, OJT010 represents a promising drug that could be further evaluated as a lead series in developing chemotherapeutics for COVID-19 treatment.

TABLE OF CONTENTS

	Page
LIST OF FIGURES.....	viii
LIST OF TABLES.....	x
LIST OF ABBREVIATIONS.....	xii
VITA.....	xiv
DEDICATION.....	xv
ACKNOWLEDGEMENT.....	xvi
CHAPTER	
1. INTRODUCTION.....	1
2. LITERATURE REVIEW.....	6
2.1 Severe Acute Respiratory Syndrome Coronavirus 2 (SARS-Cov-2) ...	6
2.1.1 Pathophysiological, and Epidemiological features	6
2.1.2 Origin of SARS-CoV-2.....	8
2.1.3 Genome of SARS-CoV-2.....	10
2.1.4 Cellular Entry/Life Cycle of SARS-CoV-2.....	12
2.2 FDA Approved Therapeutics for COVID-19 Treatment.....	15
2.2.1 Remdesivir	15
2.2.2 Monoclonal Antibodies.....	18
2.2.3 Immune Modulators	19
2.2.4 Paxlovid (Ritonavir-Boosted Nirmatrelvir)	20
2.2.5 Molnupiravir.....	21
2.2.6 Vaccines.....	22

2.3	Drug Discovery and Development for the Treatment of COVID- 19...	24
2.3.1	Pharmacological Targets for Drug Discovery in COVID-19 Pathogenesis Pathway	25
2.3.1.1	Viral Targets.....	25
2.2.1.2	Spike Protein.....	25
2.3.1.3	Nonstructural Proteins.....	29
2.3.1.4	SARS-CoV-2 Proteases	29
2.3.1.5	RNA-dependent RNA Polymerase	29
2.3.2	Host Targets	31
2.3.2.1	Structure of ACE2.....	31
2.3.2.2	Substrate Specificity of ACE2.....	32
2.3.2.3	Expression of ACE2	33
2.3.2.4	Physiological Role of ACE2	34
2.3.3	Host Proteases	37
2.3.4	Auxiliary SARS-CoV-2 Receptors	38
2.3.5	SARS-CoV-2 Co-Receptor.....	38
2.4	Discovery of OJT010 as a Novel Inhibitor of SARS-CoV-2.....	39
2.4.1	Primary Pharmacology of OJT010	40
2.4.2	Toxicology of OJT010 in Animals.....	45
2.4.3	Pharmacokinetics and Metabolism of OJT010.....	46
2.4.4	Clinical efficacy of OJT010.....	47
3.	DESIGN OF STUDY.....	49
3.1	Central Hypothesis and Specific Aims.....	49

3.2	Specific Aim 1	50
3.2.1	Specific Aim 1 Sub Aim (1a)	50
3.2.2	Specific Aim 1 Sub Aim (1b)	50
3.2.3	Specific Aim 1 Sub Aim (1c)	51
3.3	Specific Aim 2	52
3.3.1	Specific Aim Sub Aim (2a)	52
3.3.2	Specific Aim Sub Aim (2b)	52
3.3.3	Specific Aim Sub Aim (2c)	52
3.4	Specific Aim 3	53
3.5	Materials and Methods for Pharmacological Studies	54
3.5.1	COVID-19 Spike-ACE2 Binding Assay Kit	54
3.5.2	ACE2 Inhibitor Screening Assay.....	55
3.5.3	ACE 1 Exopeptidase Activity	56
3.5.4	Materials and Methods for Pseud typed Lentivirus Assay	57
3.5.6	Antiviral assays using SARS-CoV-2 <i>In vitro</i>	59
3.5.7	Infection Induced Cytopathic Effect (CPE)	59
3.5.8	Cytotoxicity of OJT010 in CPE Assay	60
3.5.9	Nanoluciferase Reporter Virus Assay	61
3.5.10	Cytotoxic effect of OJT010 in NLRV assay	62
3.5.11	Effect Synergism of OJT010 with Remdesivir on SARS-CoV-2 Infection	63
3.5.12	Data analysis	65
3.6	Molecular Docking and Simulation Study.....	66

3.6.1	Protein (hACE2-RBD) Acquisition and Preparation	66
3.6.2	Molecular Docking between Proteins and Drug	66
3.6.3	Molecular Docking between ACE2-Spike protein	67
3.6.4	Molecular Dynamic (MD) Simulations	67
3.6.5	Post-Dynamic Analysis	69
3.6.5.1	Binding Free Energy Calculations.....	69
3.7	Materials for Pharmacokinetic Study	70
3.7.1	Chemicals and Drugs	70
3.7.2	Supplies.....	71
3.7.3	Equipment, Apparatus and Software	73
3.7.4	Animals	75
3.8	Methods for Pharmacokinetic Study.....	76
3.8.1	LC-MS/MS Assay Development	76
3.8.2	Chromatography.....	76
3.8.3	MS/MS Detection	77
3.8.4	Standard and Quality Control Samples.....	78
3.8.5	Plasma and Urine Sample Preparation	79
3.9	Pharmacokinetic Studies	79
3.9.1	General animal procedures	79
3.9.2	Evaluation of Oral Bioavailability	80
3.9.3	Pharmacokinetic Analysis	81
4.	RESULTS AND DISCUSSION.....	84
4.1	Effects of OJT010 and OJT009 on rhACE2 and RBD Assay	84

4.2	Effects of OJT010 and OJT009 on rhACE2 Exopeptidase Activity....	87
4.2.1	Effects of OJT010 on Exopeptidase Activity of ACE.....	91
4.3	Efficacy of OJT010 against SARS-CoV-2 and Spike (B.1.617.2 Delta Variant) in a Pseudo virus assay.....	92
4.4	Efficacy of OJT010 against SARS-CoV-2 infection induced Cytopathic Effect (CPE) in Vero E6 cells.....	94
4.5	Cytotoxicity Effects of OJT010 in Vero E6 cells.....	99
4.6	Effect of OJT010 on the Replication of SARS-CoV-2 Nanoluciferase Reporter Virus Assay 549 cells.....	101
4.7	Cytotoxicity of OJT010 in A549 lung Cells using NLRV Assay.....	107
4.8	Efficacy of OJT010 against B.1.617.2 Delta Variant Infection-Induced Cytopathic Effect (CPE)	109
4.9	Effect of Combination of Remdesivir and OJT010 on the Replication of SRAS-CoV-2 in NLRV assay.....	116
4.10	Inhibitory Mechanism of OJT010 as Potent Blockers of Molecular Interaction between SARS-CoV-2 Spike protein and Human Angiotensin-converting Enzyme-2.....	118
4.11	Single Dose Pharmacokinetic Studies Evaluating Oral Bioavailability	122
4.12	Multiple-dose Pharmacokinetic Study to Obtain Steady-State Concentrations	126
5.	SUMMARY AND CONCLUSION	132
	REFERENCES	138

LIST OF FIGURES

FIGURE		PAGE
1	Genome organization of SARS-CoV 2.....	11
2	The Life Cycle of SARS-CoV-2.....	14
3	Mechanism of SARS-CoV-2 Inhibition by Remdesivir	17
4	NIH Treatment Guidelines for COVID-19	23
5	Structure of SARS-CoV-2 Spike protein.....	28
6	SARS-CoV-2 Targeting ACE2 Receptor and Entry in Infected Cell	36
7	Synergism of OJT010 and Remdesivir.....	64
8	Effect of OJT010 and OJT009 on the interaction of rhACE2 and SARS-CoV-2 Spike (RBD) protein.....	86
9	Effect of OJT010 and OJT009 on the Exopeptidase Activity of ACE2.....	90
10	Effect of OJT010 on the Exopeptidase Activity of ACE	91
11	Efficacy of Reference Inhibitors against SARS-CoV-2 Induced Cytopathic Effect (CPE) in Vero E6 cells.....	97
12	Cytotoxicity of OJT010 in VeroE6 cells.....	99
13	Efficacy of OJT010 against SARS-CoV-2 in Nanoluciferase Reporter Assay in A549 cells.....	102
14	Efficacy of Reference Inhibitors against SARS-CoV-2 NLRV in Vero E6 cells.....	105
15	Cytotoxicity of OJT010 in A549 Lung Cells.....	107
16	Efficacy of OJT010 against Delta Variant of SARS-CoV-2 in Infection Induced Cytopathic Effect (CPE) assay	110
17	Efficacy of Reference Inhibitors against Delta SARS-CoV-2 CPE in Vero E6 cells	114
18	Effect of Combination of OJT010 and Remdesivir on SARS-CoV-2 Replication in NLRV assay	117
19	Mean Plasma Concentration-Time Profile of OJT010 following Single IV (50 mg/kg) Dose in Rats.....	124
20	Mean Plasma Concentration-Time Profile of OJT010 following Single oral (250 mg/kg) Dose in Rats.....	125

21	Mean Plasma Concentration-Time Profile of OJT010 following Multiple Oral (2500 and 400 mg/kg) dosing in Rats.....	131
----	---	-----

LIST OF TABLES

TABLES		PAGE
1	Electronic Parameters for MS/MS Acquisition of OJT010 and IS	78
2	Effect of OJT010 and OJT009 against the Binding of rhACE2 and RBD of Spike	87
3	Effect of OJT010 on the SARS-CoV-2 and Delta Variant Pseudo typed Lentivirus Infection in Vero E6 cells.....	93
4	Activity of OJT010 and Reference Compounds against SARS-CoV-2 Induced Cytopathic Effect in Vero E6 Cells.....	98
5	Cytotoxicity of OJT010 in Vero E6 Cells, in Comparison to Reference Inhibitors of SARS-CoV-2.....	100
6	Activity of OJT010 and Reference Compounds against SARS-CoV-2 infection using NLRV assay in A549 lung cells	106
7	Cytotoxicity of OJT010 in A549 Cells, in comparison, to Reference Inhibitors of SARS-CoV-2.....	108
8	Activity of OJT010 and Reference Compounds against Delta Variant of SARS-CoV-2 in CPE assay.....	115
9	Thermodynamic Binding Free Energy Profiles for the Spike RBD towards hACE2 before and after ligands binding at RBD-hACE2.....	120
10	Thermodynamic Binding Free Energy Profiles for the ligands at the hACE2-Spike RBD site.....	120
11	Results of Binding Energies and Interactions Between Ace-2 And Sars-Cov-2 Spike `Before and After Drugs Bind to Exopeptidase Site of ACE2.....	121
12	Thermodynamic Binding Free Energy Profiles for the ligands at the hACE2 binding site of hACE2-Spike RBD.....	121
13	Pharmacokinetic Parameters and Oral Bioavailability of OJT010 after Single Oral Dose Study.....	123

14	Pharmacokinetic Parameters and Oral Bioavailability of OJT010 after multiple dosing.....	128
15	Plasma Concentrations of OJT010 following Oral Administration.....	129

LIST OF ABBREVIATIONS

SARS-CoV-2	Severe Acute Respiratory Syndrome Coronavirus-2
MERS-CoV	Middle East Respiratory Syndrome Coronavirus
SARS-CoV-1	Severe Acute Respiratory Syndrome Coronavirus
COVID-19	Coronavirus Disease 2019
FDA	Food And Drug Administration
EUA	Emergency Use Authorization
ACE2	Angiotensin-Converting Enzyme 2
S	Spike Glycoprotein
PD	Peptidase Domain
ORF	Open Reading Frames
Nsps	Nonstructural Proteins
E	Envelope
N	Nucleocapsid
M	Membrane
ACE	Angiotensin-Converting Enzyme
ANG II	Angiotensin II
HCoV	Human Coronaviruses
TMPRSS2	Transmembrane Protease, Serine 2
RBD	Receptor-Binding Domain (RBD)
CPE	Infection Induced Cytopathic Effect (Cpe)
NLRV	Nanoluciferase Reporter Assay (NLRV)
RdRP	RNA-Dependent RNA Polymerase (RdRp)

PLPro	Papain-Like Protease
3CLpro	3C-Like Protease
%	Percentage
μg	Microgram
μL	Microliter
μM	Micromolar
Cl	Clearance
IS	Internal Standard
IV	Intra Venous
PO	Per Os (Oral)
DP	Declustering Potential
CE	Collision Energy
CXP	Collision Cell Exiting Potential
EP	Entrance Potential
ESI	Electrospray Ionization
LC-MS/MS	Liquid Chromatography Tandem Mass Spectrometry
MRT	Mean Residence Time
PK	Pharmacokinetics
HPLC	High Performance Liquid Chromatography
MS	Mass Spectrometry
CYP	Cytochrome P450
DMSO	Dimethyl Sulfoxide
DI	Deionized Water

VITA

November 4. Born, India

2013..... Bachelor of Dental Surgery,
Gian Sagar Dental College and
Hospital, India

2015-2017..... Master of Healthcare Administration
Texas Southern University

2017-2022..... Graduate Research Assistant,
College of Pharmacy and Health
Science, Texas Southern University

Major Field..... Pharmaceutical Science

DEDICATION

To the unconditional love and support of my family & my nephews, Ayaan, and Jaiveer Singh.

ACKNOWLEDGEMENT

I have received a lot of help and support in this journey and in writing this dissertation. I want to take a moment to express my gratitude to my mentors and my friends who assisted me throughout my Ph.D. studies.

It is a great pleasure to offer my heartfelt gratitude to Dr. Omonike Olaleye, my mentor, philosopher, and guide. Thank you for your consistent support and guidance throughout this project. Your insight and knowledge have always steered me through this process. I'm grateful for our scientific conversations and late-night lab experiments. Your passion for drug discovery has kept me going and encouraged me to excel in this field.

I would also like to thank my committee members, Dr. Dong Liang, Dr. Ya Fatou Njie Mbye, and Dr. Hector Miranda, for their guidance and scientific advice and for sharing your valuable expertise. Special thanks to Dr. Liang, whose support allowed my studies to go the extra mile. I'm also thankful for your comment and recommendations on this dissertation.

I am grateful to Dr. Anuoluwapo Egbejimi and Dr. Kehinde Idowu for their scientific discussions and guidance during my studies. I am thankful to Dr. Jing Ma and Dr. Yang Wang for assisting with the conduct of animal experiments.

I would like to give special thanks to Dr. Maria Rincon Nigro, who supported me and put up with stress. I want to thank Tolulope Adebusuyi for being a wonderful colleague in the lab. Working with you guys was a lot of fun.

This research was supported, in part, by research infrastructure support from RCMI grant number 5U54MD007605-28 from NIMHD/NIH.

CHAPTER 1

INTRODUCTION

Severe acute respiratory syndrome coronavirus 2 (SARS-CoV-2), a novel virus, has quickly escalated into an unexpected and devastating pandemic of coronavirus disease 2019 (Morens & Fauci, 2020). As of March 12th, 2022, over 450 million cases have been detected, with more than 6 million deaths recorded worldwide (@JohnsHopkins, 2022). It has become a public health crisis, which has not only overwhelmed the health care system but has also affected the global economy (Shang et al., 2021). Because of the severity of the continuing COVID-19 pandemic, it is imperative to develop antiviral drugs, vaccines, and antibodies as quickly as possible.

While there has been substantial development in developing therapeutics, treatment options for COVID-19 remained extremely limited (@US_FDA, 2022a). Although vaccination is an effective measure, limitation in global access and uncertainties about the duration of protection represents significant challenges to overcome. Moreover, with the emergence of SARS-CoV-2 variants it's now more evident that simply two doses of vaccines are not enough to contain the spread of SARS-CoV-2 (J. L. Bernal et al., 2021; Burki, 2022).

Despite the fact that the Food and Drug Administration (FDA) has approved numerous drugs, including antivirals, corticosteroids, monoclonal antibodies and immune modulators, only one drug; remdesivir is fully authorized to treat COVID-19 (@US_FDA, 2022a).

More recently, two new drugs, Molnupiravir and Paxlovid, were also granted an emergency use authorization (EUA) for the treatment of COVID-19 infection in adults and pediatric patients ("Molnupiravir for treatment of COVID-19," 2022; "Paxlovid for treatment of COVID-19," 2022). However, no therapies have been shown to speed up the viral clearance and prevent transmission. As a result, SARS-CoV-2 continues to spread globally, contributing to high morbidity and mortality (@JohnsHopkins, 2022). Moreover, due to cost and availability, it's unlikely that these treatments will be available to low and middle-income countries (Andrew Hill, 2022). Furthermore, there is a possibility that monotherapy will cause escape mutants over time. Therefore, it is essential to explore innovative strategies in antiviral drug discovery to contain this pandemic.

Understanding the structure of SARS-CoV-2 and its interaction with host protein, may aid in the development of more effective antiviral therapies. SARS-CoV-2 is a positive-sense single-stranded RNA beta coronavirus that infects human cells via interaction with the Angiotensin-converting enzyme 2 receptor, followed by viral replication and virus dissemination (Walls et al., 2020; Q. Wang et al., 2020; Wrapp et al., 2020; Yan et al., 2020). Structural studies have shown that the receptor-binding

domain of spike glycoprotein (S) of the SARS-CoV-2 binds to the host cell receptor that triggers the fusion between the viral membrane and cellular membrane, resulting in entry of SARS-CoV-2 into the cell. This interaction has been confirmed as an initial and critical step in the viral infection (Walls et al., 2020; Q. Wang et al., 2020; Wrapp et al., 2020; Yan et al., 2020). The binding between the RBD of the SARS-CoV-2 subunit to the peptidase domain (PD) of ACE2 is emerging as a promising therapeutic target.

The COVID-19 global emergency has raised an urgent need to develop antiviral drugs, which prompted scientists worldwide to discover novel and potent therapeutics agents against SARS-CoV-2. However, the traditional screening and lead optimization approaches are expensive ventures, and highly resources and time-consuming (Wouters et al., 2020). Therefore, more innovative methods and faster strategies are needed to facilitate drug discovery. Given the severity of the pandemic, repurposing of clinically approved drugs to expedite the traditional process of drug discovery is an emerging strategy, with low cost, shorter development period, and minimum risk of failure (Pushpakom et al., 2019).

Drug repurposing is a highly promising approach to accelerate the development process by identifying novel therapeutic opportunities for FDA-approved drugs that have already been shown to be safe and effective in humans for other indications (Pushpakom et al., 2019). The rationale behind drug repurposing is that the same molecular pathways may be involved in different diseases, or a drug molecule may have pharmacological activity on other targets, suggesting a new possible indication of use (Pushpakom et al.,

2019). For example, remdesivir was initially developed against the Ebola virus and is now being repurposed for COVID-19 (Consortium et al., 2021). In fact, multiple repurposed drugs are being tested in clinical trials for COVID-19 treatment (Saul & Einav, 2020).

To discover new antivirals among repurposed drugs for COVID-19, this study discusses the serendipity of OJT010 as a novel antiviral that showed superior pharmacological efficacy at the molecular and cellular level against SARS-CoV-2 in the micromolar range. OJT010 is a mucolytic agent used to treat respiratory diseases and is well tolerated and safe (Nobata et al., 2006; Olivieri et al., 1987). It has been shown to improve the clinical course of respiratory diseases and reduce the incidence of postoperative pulmonary complications (Fegiz, 1991). In this study, we explored the effects of OJT010 on disrupting the interaction between recombinant human ACE2 (rhACE2) and the RBD of the S protein of SARS-CoV-2. We also determined the impact of OJT010 on viral replication through three individual assays: Nanoluc Reporter Virus and SARS-CoV-2 infection-induced cytopathic effect using wild type and delta variants of SARS-CoV-2 and Pseudotyped lentiviral assay.

Furthermore, we have assessed the effect of combination therapy of OJT010 with remdesivir against SARS-CoV-2. Additionally, we have also determined the cytotoxicity of OJT010 in comparison to other clinically approved drugs. Next, we have also investigated the impact of OJT010 on the exopeptidase activity of rhACE2. We have determined the pharmacokinetic parameters of OJT010 in healthy rats. Herein, we found

that OJT010 effectively modulated the interaction between rhACE2 and RBD of spike protein in the micromolar range. We also discovered that OJT010 inhibited replication of wild and delta variants of SARS-CoV-2 in NLRV, CPE, and Pseudotyped virus assay in the micromolar range. Furthermore, we are reporting for the first time that OJT010 doesn't inhibit the exopeptidase activity of rhACE2. Altogether, the potent efficacy, excellent safety, and pharmacologic profile of OJT010, along with its affordability and availability, makes it a promising candidate for drug repurposing as possible prophylactic and treatment options against SARS-CoV-2 infection.

CHAPTER 2

LITERATURE REVIEW

2.1 Severe Acute Respiratory Syndrome Coronavirus 2

In December 2019, a newly recognized illness spread through the Huanan Seafood Wholesale Market in Wuhan, China, and worldwide. It started with an upper respiratory tract infection and quickly escalated into pneumonia and eventually respiratory failure (Z. N et al., 2020). The etiological agent was a new coronavirus called SARS-CoV-2 that caused a disease named COVID-19 (Lu et al., 2020). The disease quickly expanded globally, and by March 11, 2020, it was declared a pandemic. As of February 21, 2022, COVID 19 has affected 188 countries worldwide, with over 500 million confirmed cases and a death toll of over 5 million (@JohnsHopkins, 2022).

2.1.1 Pathophysiological, and Epidemiological Features

Patients with SARS-CoV-2 infections have diverse clinical outcomes with mild to moderate symptoms such as fever, cough, fatigue, headache, diarrhea, and shortness of

breath: subset progresses to severe acute respiratory distress syndrome (ARDS) with massive alveolar damage and impaired lung function (Guan et al., 2020; Mason, 2020; Yang et al., 2020). Although the respiratory tract is the gateway for SARS-CoV-2 infection, reports of extrapulmonary manifestations involving cardiovascular, renal, gastrointestinal, hematologic, and neurologic systems are increasing, suggestive of a vascular infection rather than a purely respiratory disease (Ellul et al., 2020; Gross et al., 2020; Gupta et al., 2020).

Around 80% of patients infected with SARS-CoV-2 are asymptomatic or have mild to moderate illness primarily affecting the upper respiratory tract. While the remaining 20% will develop severe symptomatic infection necessitating hospitalization, 5% will require ventilation support in the Intensive Care Unit (ICU) (Wu & McGoogan, 2020). Individuals, particularly those over the age of 65 and those who have comorbid conditions such as respiratory disorders, diabetes, cardiovascular and cerebrovascular disease are at an increased risk of death (C. N et al., 2020). More importantly, male patients are more susceptible to this disease and are significantly impacted by it. Men, especially older accounted for nearly 70% of those infected with SARS-CoV-2 (Yang et al., 2020).

Clinical stages of infection are associated with pathogenic events that occur once the virus infects the lungs. Clinical symptoms and pathogenic events associated with any infectious disease, particularly COVID-19, should be viewed through the damage-response lens. Various elements and factors can tip the balance in favor of the host or

pathogen (Pirofski & Casadevall, 2018). Thus, the virus may occasionally act as an initiator rather than a perpetrator. The host's forces are released due to the virus's presence that causes uncontrolled inflammatory immune responses, which drives cytokines storm and causes tissue and organ damage (D. P et al., 2020; Z et al., 2020).

2..1.2 Origin of SARS-CoV-2

In the past two decades before COVID 19, two other significant coronaviruses; Severe Acute Respiratory Syndrome Coronavirus (SARS-CoV) and Middle East Respiratory Syndrome Coronavirus (MERS-CoV) have been identified and to date, seven coronaviruses have been discovered (Lu et al., 2020; Zhang & Holmes, 2020).

Coronaviruses are members of the “Nidovirales” family of viruses. The coronavirus family comprises four subgenera (alpha, beta, gamma, and delta coronaviruses). Human coronavirus (HCoV) falls under the two of these genera (alpha coronaviruses and beta coronaviruses). HCoV-229E and HCoV-NL63 are alpha coronaviruses that infect humans, whereas HCoV-HKU1, HCoV-OC43, MERS-CoV, SARS-CoV, and SARS-CoV-2 are beta coronaviruses that infect humans (Chan et al., 2015; Lefkowitz et al., 2018).

SARS-CoV-2 is a positive-sense single-stranded RNA beta coronavirus that infects human cells via interaction with the ACE2 receptor, followed by viral replication and virus dissemination (Wrapp et al., 2020; Yan et al., 2020; Yan et al., 2022). The

sudden emergence and rampant spread of SARS-CoV-2 have raised several questions on its genomic evolution and genetic recombination.

SARS-CoV-2 shares 79% of structural identity with SARS-COV and 50% with MERS-CoV (Kim et al., 2020). The genome of SARS-CoV-2 is closely related to the bat coronavirus RaTG13/2013 (RaTG13), sharing 96 % sequence identity, implying that both viruses share a common ancestor (Kim et al., 2021). Nevertheless, the SARS-CoV-2 genome also shows evidence of genetic recombination with at least two different viruses from different clusters, inferring that this virus might not be directly transferred from bats to humans or could be a result of convergent evolution. Moreover, the uncanny resemblance in a sequence of S1 protein of SARS-CoV-2 among human isolates, which is uncommon for RNA viruses, indicates a recent recombination event that happened in the intermediate host before jumping to the human (Zhang & Holmes, 2020). Concurrent evidence has found high sequence similarities between RBD of pangolin CoV and SARS-CoV-2 and proposed them as a potential reservoir species, suggesting the possibility of pangolins serving as an intermediate host before jumping into the human (Sun et al., 2020).

2.1.3 Genome of SARS-CoV-2

SARS-CoV-2 is an enveloped positive-sense single-stranded RNA virus with a genome of around 30 kb (Lu et al., 2020). SARS-CoV-2 genome encodes five major open reading frames (ORFs) (Michel et al., 2020). The two large ORF1a and ORF1b occupy the two-thirds length of the viral RNA. Upon-cell entry, the genomic RNA is translated to make proteins from two ORFs; ORF1a and ORF1b. The ORF1a is translated to produce polypeptide1a, which is then cleaved into 11 nonstructural proteins (nsps). The ORF1b yields a large polypeptide translated into 15nsps (Kim et al., 2020). The viral proteases nsp3 and nsp5, which have a papain-like protease (PLpro) domain and a 3C-like protease (3CLpro) domain, are responsible for the proteolytic cleavage (Kim et al., 2020). The viral genome serves as a template for replication and transcription, mediated by the RNA-dependent RNA polymerase (RdRP) activity of the nsp12 protein. Negative-sense RNA intermediates are produced to serve as templates for creating positive-sense genomic and subgenomic RNAs (sgRNAs). The structural proteins bundle the gRNA to assemble progeny virions. The remaining part of the genome is translated into structural proteins Spike (S), Envelope (E), Nucleocapsid (N), and Membrane (M) proteins, and several accessory proteins whose functions are yet to be discovered. According to the present annotation, SARS-CoV-2 has at least six accessory proteins (3a, 6, 7a, 7b, 8, and 10) (Kim et al., 2021).

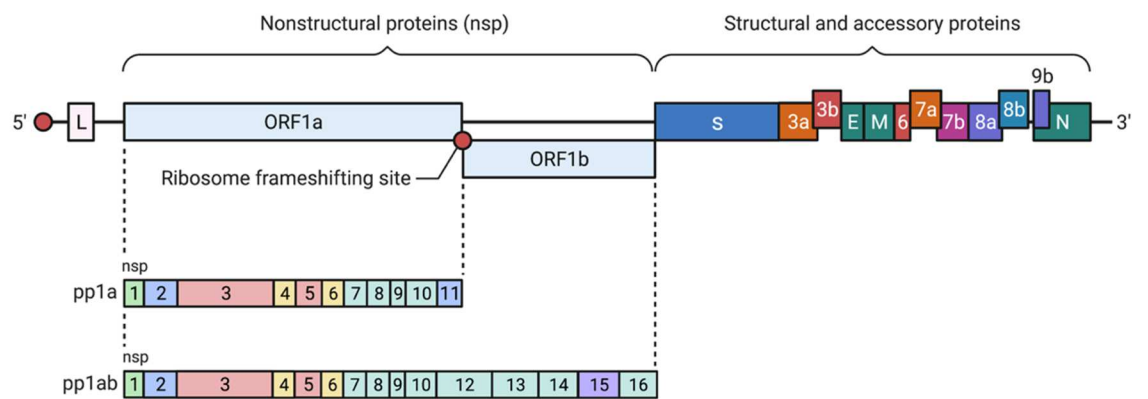


Figure 1: Genome Organization of SARS-CoV-2

Reprinted from "Genome Organization of SARS-CoV", by BioRender, August 2020, retrieved from <https://app.biorender.com/biorendertemplates/t5f99ec8322469900a3546483-genome-organization-of-sars-cov> Copyright 2022 by BioRender.

2.1.4 Cellular Entry/Life Cycle of SARS-CoV-2

SARS-CoV-2 enters the cell by two main pathways:

1. Endocytic pathway
2. Cell fusion pathway

Structural studies have shown that the spike glycoprotein of the SARS-CoV-2 binds to the host cell receptor and fuses the viral membrane with a cellular membrane (Wrapp et al., 2020). The first pathway involves receptor-mediated endocytosis, whereas the second pathway involves plasma membrane fusion following S protein attachment with ACE2 receptor (Jackson et al., 2022). The trimeric S protein of SARS-CoV-2 is cleaved into S1 and S2 during their biosynthesis in virus-producing cells by furin, a host protease (Xia et al., 2020). The S protein contains non-covalently associated S1 and S2 subunits in mature virions. S1 includes the receptor-binding domain, which binds to the peptidase domain (PD) of its cognate receptor angiotensin-converting enzyme 2, whereas S2 is responsible for membrane fusion.

The binding of S1 to the host receptor ACE2 exposes another cleavage site on S2 (Walls et al., 2020; Q. Wang et al., 2020; Wrapp et al., 2020; Yan et al., 2020). The S2 subunit is cleaved by the host transmembrane protease, serine 2 (TMPRSS2), at the cell surface or by cathepsin L in the endosomes, following the endocytic pathway. A two-step sequential protease cleavage by host cell proteases at S1/S2 and the S2 sites is

crucial for viral entry into the host cells (Hoffmann et al., 2020; Ou et al., 2020). This interaction has been confirmed as an initial and critical step in the viral infection (Walls et al., 2020; Q. Wang et al., 2020; Wrapp et al., 2020; Yan et al., 2020). The binding between the RBD of the SARS-CoV-2 subunit to the peptidase domain of ACE2 is emerging as a promising therapeutic target.

Following-cell entry, the viral RNA is released into the host cytosol. The SARS-CoV-2 gRNA serves as mRNA to translate the two large polyproteins, which are further cleaved by viral proteases, into nonstructural proteins (Lu et al., 2020; Meyer et al., 2021). The SARS-CoV-2 genome serves as a template for replication and transcription, mediated by the RNA-dependent RNA polymerase (RdRP) activity of the nsp12 protein (Gao et al., 2020). The four structural proteins (S, M, E, and N) required for the virion assembly are translated by host ribosomes. Then mature virions are released from the cell by lysosomal trafficking from the infected cell (Malone et al., 2022).

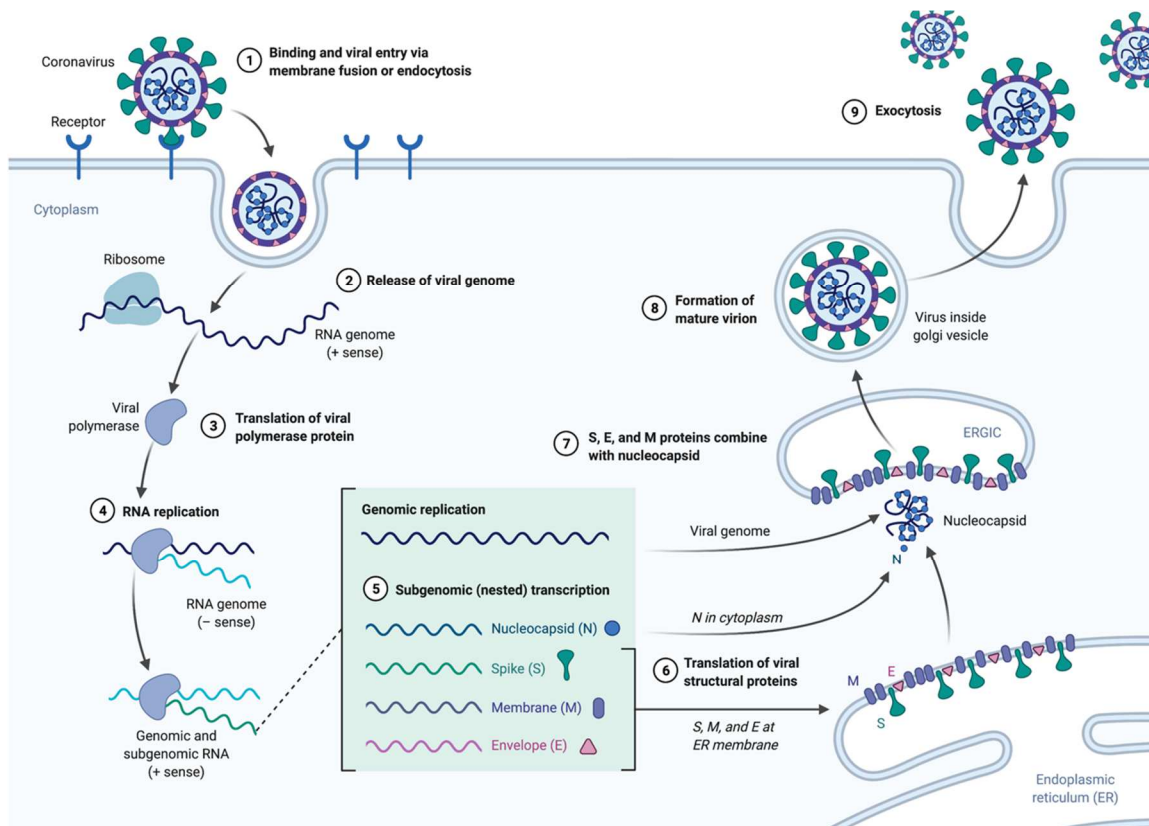


Figure 2: The Life Cycle of SARS-CoV-2

Reprinted from "Coronavirus Replication Cycle", by BioRender, July 2020, retrieved from <https://app.biorender.com/biorender-templates/t-5e56d97d1b689000850f8f93-coronavirus-replication-cycle>.

2.2 FDA Approved Therapeutics for COVID-19 Treatment

The COVID-19 pandemic has sparked a tremendous search and investment worldwide to identify effective treatments at all stages of the disease. On a global scale, numerous attempts have been made to determine the appropriate therapeutic drugs to treat COVID-19 (Bugin & Woodcock, 2021). In the past two years, FDA has approved three vaccines and a single fully authorized drug for the treatment of COVID-19 (@US_FDA, 2022a). However, a few more drugs are approved under EUA against SARS-CoV-2 (@US_FDA, 2022a). This section will briefly discuss the approved vaccines and treatments measures for COVID 19.

2.2.1 Remdesivir

Remdesivir (GS-5734), a viral RNA-dependent RNA polymerase inhibitor, is the only FDA-approved drug for the treatment of COVID-19. A nucleotide analog prodrug is metabolized in cells to yield pharmacologically active remdesivir triphosphate (RDV-TP) that inhibits the viral RdRP (Agostini et al., 2018; Grein et al., 2020; Teoh et al., 2020). It has a broad-spectrum antiviral activity against several viruses, including SARS-CoV, MERS-CoV, and Ebola (Gordon, Tchesnokov, Feng, et al., 2020; J. Wang et al., 2021). Biochemical studies showed that the RdRp could use RDV-TP as a substrate and incorporate RDV-TP into the growing RNA product. Unlike with many other classic chain terminators, inhibition is not seen immediately after incorporation of RDV-TP, but instead, it's delayed by three more nucleotides before it induces an irreversible chain

termination (Gordon, Tchesnokov, Woolner, et al., 2020; Jordan et al., 2018; Siegel et al., 2017; J. Wang et al., 2021). Although the clinical efficacy and safety of remdesivir for COVID-19 treatment have been evaluated in various clinical trials, early studies provided conflicting evidence on its effectiveness among hospitalized COVID-19 patients (M et al., 2021; McCreary et al., 2022). Because the available evidence is insufficient to recommend either for or against routine remdesivir treatment for all hospitalized patients with moderate COVID-19, it is left on clinicians to determine the appropriate use of remdesivir in COVID-19 patients (Consortium et al., 2021; G et al., 2021; Grein et al., 2020; Paladugu & Donato, 2020).

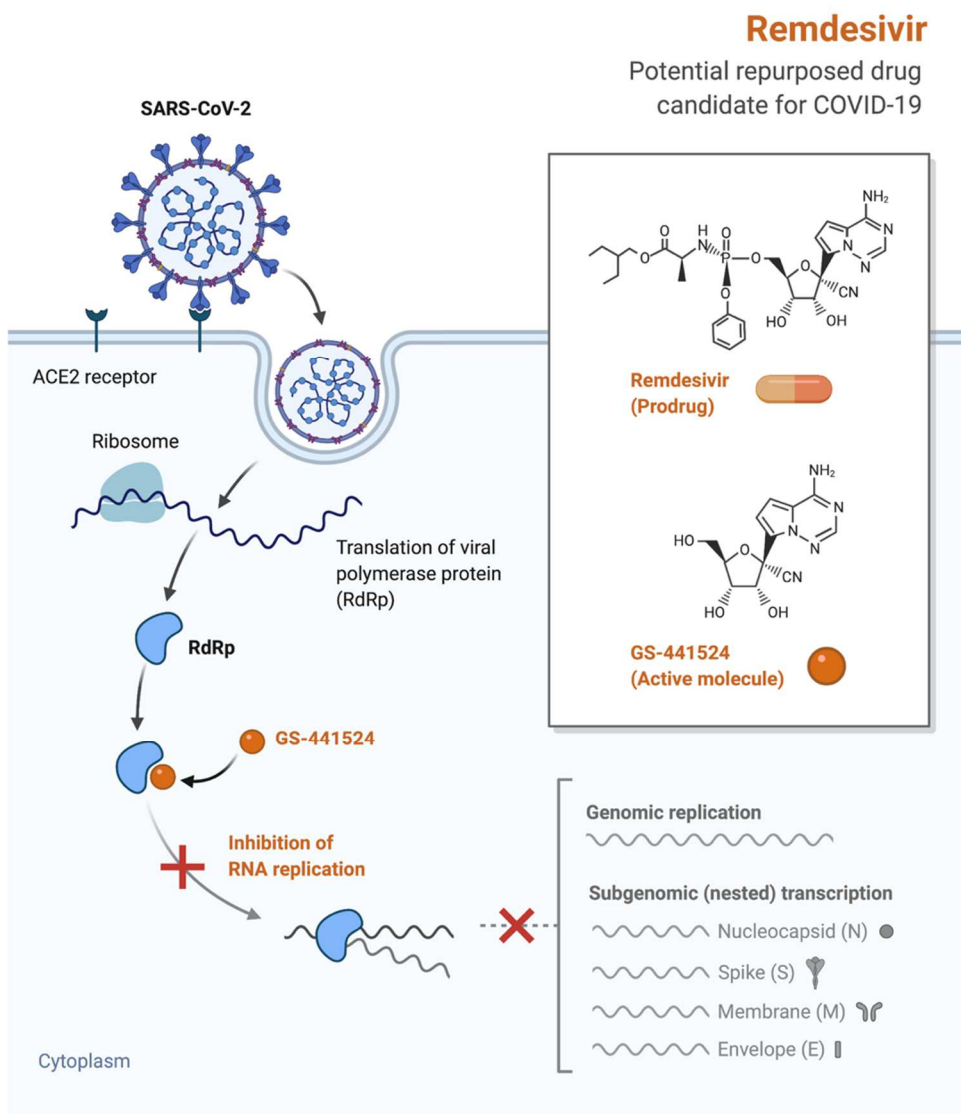


Figure 3: Mechanism of SARS-CoV-2 Inhibition by Remdesivir

Reprinted from "Remdesivir: Potential Repurposed Drug Candidate for COVID-19 (Portrait)", by BioRender, April 2020, retrieved from <https://app.biorender.com/biorender-templates/figures/all/t-5ea056e2183b5d00b114231f-remdesivir-potential-repurposed-drug-candidate-for-COVID-19>- Copyright 2022 by BioRender.

2.2.2 Monoclonal Antibodies

Monoclonal antibodies are lab-made molecules engineered to mimic the immune system to counteract harmful pathogens such as viruses like SARS-CoV-2 (J et al., 2022). FDA has approved four monoclonal antibodies under EUA for the treatment of COVID-19 (@US_FDA, 2020).

- a) Bamlanivimab plus etesevimab,
- b) Casirivimab plus imdevimab (REGEN-COV)
- c) Sotrovimab
- d) Tixagevimab plus cilgavimab
- e) Bebtelovimab

The anti-SARS-CoV-2 antibodies target different epitopes of spike protein: S1-RBD, S1-NTD, or the S2 region. They prevent/block the interaction of RBD with the ACE2 and interfere with the S2-mediated membrane fusion process, preventing viral particles from entering the host cell and thus reducing viral infections (Group et al., 2022; Group et al., 2021).

SARS-CoV-2, like other infectious organisms, can mutate over time, making specific treatments ineffective against variants such as the omicron (VanBlargan et al., 2021; P. Wang et al., 2021). Therefore, recently FDA revised its recommendation and advised to limit the use of bamlanivimab plus etesevimab and Casirivimab plus

imdevimab (REGEN-COV) because of the preclinical evidence demonstrating lack of efficacy and reduced neutralizing activity of these antibodies against the recently emerged omicron variants of the SARS-CoV-2 (@US_FDA, 2022b; Group, 2022; Weinreich et al., 2021).

2.2.3 Immune Modulators

According to our current understanding of COVID-19, the immune system plays a significant role in defining the disease's severity. SARS-CoV-2 interacts closely with an individual's immune system, resulting in many clinical manifestations. Most SARS-CoV-2 infected people are asymptomatic, which shows that this virus can elicit a robust, resistant response (Group et al., 2021).

The immune system can become hyperactive in COVID-19 infection, leading to disease progression (D. P et al., 2020). To prevent the disease progressing to its most severe manifestations, the immune system must be addressed and controlled in addition to the virus-targeting treatment approaches. Immune modulators can aid in the reduction of hyper inflammation (Feuillet et al., 2021; Paces et al., 2020).

FDA has issued an EUA for Corticosteroids; dexamethasone, Interleukin-6 inhibitors: tocilizumab (or sarilumab), and Janus kinase (JAK) inhibitors: baricitinib (or tofacitinib) (@US_FDA, 2022a). Tocilizumab is a monoclonal antibody that decreases inflammation by blocking the interleukin-6 receptor in the COVID patient's (Group,

2021; Gupta et al., 2021). However, due to conflicting evidence on their approved dose and pharmacokinetics of these drugs, they are only recommended in patients with severe or critical COVID-19.

2.2.4 Paxlovid (Ritonavir-Boosted Nirmatrelvir)

Nirmatrelvir is an orally bioavailable, reversible inhibitor of the main protease (3CLPro) of SARS CoV-2. The 3CLPro viral protease plays a critical role in viral replication by cleaving the two viral polyproteins (Owen et al., 2021). Nirmatrelvir is a potent inhibitor of all alpha and beta coronavirus known to infect humans (Pillaiyar et al., 2016). Nirmatrelvir is co-administered with ritonavir (marketed under the brand name Paxlovid), a potent cytochrome P450 3A4 inhibitor, and enhances the pharmacokinetic of nirmatrelvir. It is necessary to take ritonavir to raise nirmatrelvir concentrations to desired therapeutic ranges (Hammond et al., 2022). However, nirmatrelvir boosted with ritonavir can cause significant drug-induced toxicity (Owen et al., 2021; Pillaiyar et al., 2016). In the EPIC-HR trial, ritonavir-boosted nirmatrelvir significantly reduced the risk of hospitalization or death in non-hospitalized adults with laboratory-confirmed SARS-CoV-2 infection by 89 percent when compared to the placebo (Hammond et al., 2022). Based on the recent preprint Paxlovid potentially inhibited viral variants of SARS-CoV-2 in two separate *in vitro* assays (Vangeel et al., 2022).

2.2.5 Molnupiravir

Molnupiravir is the oral prodrug of the nucleoside analog beta-D-N4-hydroxycytidine (Jayk Bernal et al., 2022; "Molnupiravir for treatment of COVID-19," 2022). In phase II clinical trials, administration of molnupiravir caused a 30 % reduction in hospitalization or death compared to the placebo group (A. J. Bernal et al., 2021). It has a broad range of antiviral activity against a wide range of RNA viruses (Costantini et al., 2012; Painter et al., 2019; Reynard et al., 2015; Sheahan et al., 2020; Yoon et al., 2018). Molnupiravir was originally discovered as an inhibitor of the influenza virus, later repurposed for SARS-CoV-2 (Reynard et al., 2015). Molnupiravir has a comparable potency to remdesivir against SARS-CoV-2 *in vitro* (Sheahan et al., 2020; Tao et al., 2021).

The mechanism of action includes lethal mutagenesis; RdRp uses molnupiravir as a substrate during replication instead of cytidine triphosphate or uridine triphosphate (Sheahan et al., 2020). Uptake of molnupiravir by viral RNA-dependent RNA-polymerases introduces mutations that cause an error catastrophe during the viral replication (Kabinger et al., 2021; Zhou et al., 2021). However, due to lack of safety data, the long-term harms of molnupiravir remains a matter of concern.

As a mutagenic ribonucleoside antiviral agent, the possibility exists that molnupiravir will be metabolized by the human cells and might be incorporated into the host DNA, leading to mutations (Kabinger et al., 2021; Zhou et al., 2021). Moreover, it's

been proposed that random mutagenesis occurring in the viral genome due to the molnupiravir mechanism of action over time might generate new variants of SARS-CoV-2 due to increased diversity in viral sequence (CJ et al., 2021). In the absence of research evidence regarding safety and efficacy, molnupiravir might only be favoured to treat high-risk groups.

2.2.6 Vaccines

To date, FDA has approved three vaccines as preventive measures against covid 19

- a) Pfizer-BioNTech COVID-19 Vaccine
- b) Moderna COVID-19 vaccine
- c) The Janssen COVID-19

The mRNA vaccines are nucleoside-modified RNA that encodes the full-length spike protein of SARS-CoV-2, modified by two proline mutations (Walsh et al., 2020). The spike protein is locked in the prefusion conformation that mimics the intact virus and elicits an immune response to provide antigenicity (Walsh et al., 2020). Both Pfizer and Moderna vaccines are 95% and 94.1% efficacious at preventing COVID-19 illness and severe disease. At the same time, the Janssen COVID-19 vaccine is 77-85% efficacious at preventing strong to critical COVID-19 infection (Baden et al., 2021; Polack et al., 2020; Sadoff et al., 2021).

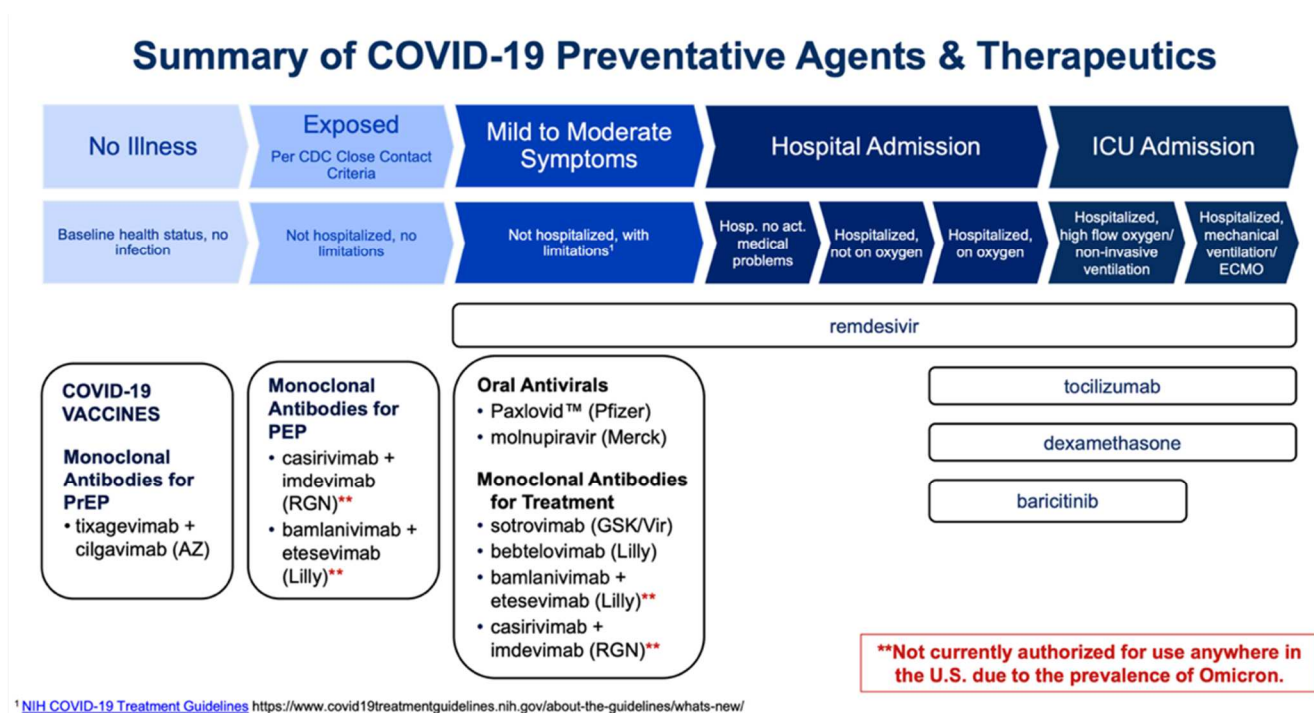


Figure 4: NIH Treatment Guidelines for COVID-19

US State and Health Services. NIH guidelines for the treatment of COVID-19. Retrieved from (<https://aspr.hhs.gov/COVID-19/Therapeutics/Documents/USG-COVID19-Tx-Playbook.pdf>)

2.3 Drug Discovery and Development for the Treatment of COVID-19

Why need still need new therapeutics for COVID-19?

Several vaccines and drugs have been developed to prevent and treat COVID-19. Some have been proven to be efficacious and safe to a certain level. Despite this, relying solely on the available treatments would be unwise for several reasons. The range of challenges that need to be addressed are limited availability, high cost, need for parenteral administration and monitoring in a health care setting. Moreover, the SARS-CoV-2 continues to mutate. The emerging viral variants such as highly infectious Delta and Omicron have become more immune to the currently approved vaccine, monoclonal antibodies, and drugs. Therefore, there is a need for safe and effective oral treatments for COVID-19 that can be taken in the earliest stages of infection to prevent its progression to more severe disease, hospitalization, and death. Such treatment would help mitigate the spread of the infection, hospitalization, and mortality. Thus, reducing the burden on the healthcare system and global economy.

A better understanding of viral and host pathways that are crucial for infection and viral survival will help in the development of potent and targeted antiviral. In the following section, I will discuss the critical viral and host proteins and enzymes involved viral life cycle.

2.3.1 Pharmacological Targets for Drug Discovery in COVID-19

Pathogenesis Pathway

Severe acute respiratory syndrome coronavirus 2, a novel and highly pathogenic virus, continues to pose a public health threat worldwide. To date, new SARS-CoV-2 variants with mutations in the viral genes are quickly spreading (VP, AB, et al., 2022). To contain the pandemic, efficient therapeutic measures are needed now more than ever. In order to develop effective therapeutic interventions against SARS-CoV-2 infection, it is required to inhibit critical viral entry and post-entry processes by targeting viral enzymes or host receptors.(VP, C, et al., 2022). I will briefly discuss important proteins of the virus that could be targeted to develop countermeasures against SARS-CoV-2.

2.3.1.1 Viral Targets

The structural proteins, (S, E, M, N) proteases and replication enzymes play an essential function in the viral life cycle and are an attractive pharmacological target for drug discovery.

2.3.1.2 Spike Protein

The S protein is a type 1 membrane protein responsible for receptor recognition, attachment, and membrane fusion. In its functional form the monomeric S protein assembles as a homotrimer. The S1 subunit is organized into four subdomains:

- a) N terminal domain
- b) C terminal domain is also known as RBD domain
- c) SD1 and SD2 subdomains

The S2 subunit contains an N-terminal fusion peptide, two heptad repeats, a transmembrane domain, and a cytoplasmic tail. The S protein exists in various configurations and undergoes substantial structural rearrangement between the prefusion and post-fusion stages. In the prefusion location, the binding of ACE2 destabilizes the S1 subunit, resulting in the shedding of S1 and the S2 subunit transitioning to a stable post-fusion configuration. The receptor-binding domain of S1 undergoes hinge-like conformational motions to engage a host cell receptor, temporarily hiding or exposing the determinants of receptor binding. The S protein is a target for antibody-mediated neutralization because of its essential function, and analysis of the prefusion S structure would provide atomic-level information to assist the vaccine design and development (Jackson et al., 2022; Wrapp et al., 2020).

The binding between the RBD of the SARS-CoV-2 subunit to the peptidase domain of ACE2 is emerging as a promising therapeutic target. *In vitro* studies have demonstrated that recombinant soluble ACE2 (Monteil et al., 2020) and ACE2-Fc (Lei et al., 2020) have potential applications in the prevention and treatment of SARS-CoV-2 infection. Moreover, small molecules that can interact with the majority of RBD residues or ACE2 residues could potentially disintegrate the binding and prevent SARS-CoV-2 entry into the cells (Gil et al., 2020).

Although the other three structure proteins: E, M, N, have gained attention and are indispensable for viral functioning, structural information on these proteins is limited. Nucleocapsid protein plays a multifaceted role in viral infection and is responsible for packing viral RNA into ribonucleoprotein complexes. The M protein is embedded in the viral membrane and is responsible for assembling the new viral particles with the host cell. Finally, the envelope protein is involved in the recruitment of the endoplasmic reticulum through its interaction with the M protein (Mariano et al., 2020).

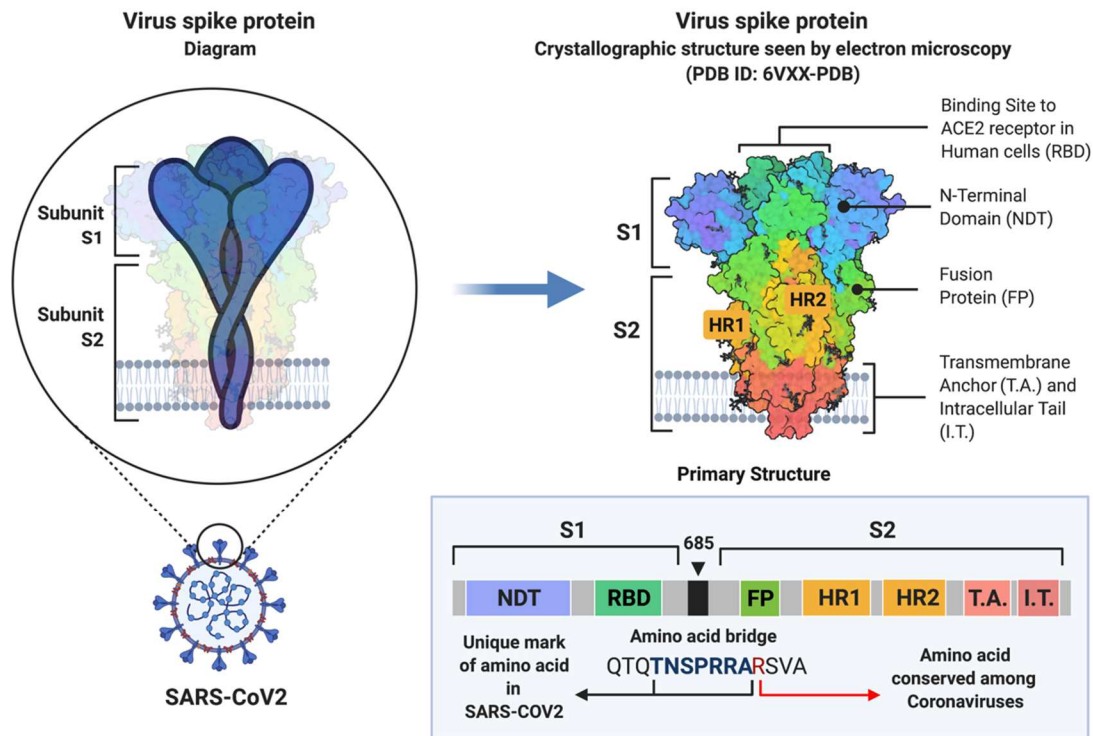


Figure 5: Structure of SARS-CoV-2 Spike Protein

Reprinted from "An In-depth Look into the Structure of the SARS-CoV2 Spike Glycoprotein", by BioRender, August 2020, retrieved from <https://app.biorender.com/biorender-templates/figures/5e99f5395fd61e0028682c01/t-5f1754e62baea000ace86904-an-in-depth-look-into-the-structure-of-the-sars-cov2-spike-g> Copyright 2022 by BioRender.

2.3.1.3 Nonstructural Proteins

The role of most nsps has been reported; however, the function of nsps is still to be discovered (Lu et al., 2020). Although any nsp could be used as a druggable target, its essentiality in the viral life cycle and the availability of structural studies increase the chances of success. Based on this criteria, two major proteases (3C-like and papain-like protease), and RNA-dependent RNA polymerase (RdRP), are studied extensively to discover therapeutic for COVID19.

2.3.1.4 SARS-CoV-2 Proteases

3C-like protease (3CLPro) and papain-like protease (PLpro) cleave two large polyproteins, pp1a and pp1ab, and generate mature nsps. Because of their essentiality in processing the polyproteins, both proteases are crucial for viral replication and are attractive drug targets among coronaviruses. Currently, two inhibitors of 3CLpro: lopinavir and ritonavir, are approved for the COVID-19 treatment (Hilgenfeld, 2014; L. Zhang et al., 2020).

2.3.1.5 RNA-dependent RNA Polymerase

RdRp is a critical enzyme in the life cycle of coronaviruses and other RNA viruses. This enzyme is structurally and functionally conserved across viruses with RNA

genomes from various families. RdRp is a central component involved in the replication and transcription of the RNA genome (Gao et al., 2020). The lack of a human analog for this enzyme and its importance in the virus's life cycle makes this enzyme a critical therapeutic target for antiviral development. The only approved drug for COVID-19, remdesivir, is an RdRp inhibitor (@US_FDA, 2022a).

2.3.2 Host Targets

Although targeting viral proteins is a good strategy, emerging viral variants pose a risk for the emergence of escape mutants against antivirals targeting viral proteins and enzymes. Therefore, our research has focused on blocking the first step of viral fusion of SARS-CoV-2 spike protein receptor-binding domain (RBD) with host receptor; Angiotensin-converting enzyme 2 (ACE2) and thereby prevent the cellular entry of SARS-CoV-2 into the human cells.

2.3.2.1 Structure of ACE2

ACE2 is an integral type 1 membrane-bound zinc metalloprotease, which functions exclusively as a carboxypeptidase. This metalloprotease is consisted of 805 amino acids, with a 17 amino acid signal sequence at the N terminal and a putative C-terminal membrane anchor (Towler et al., 2004). Although ACE2 exists as a membrane protein anchored to the plasma membrane, it can also be found in the plasma or other body fluids as a soluble, truncated enzyme lacking transmembrane and cytosolic domain that can cleave the C-terminal residue from angiotensin I and II (Tipnis et al., 2000).

The extracellular region of the ACE2 is composed of two domains: the N-terminal zinc metallopeptidase domain and a C-terminal domain. The metallopeptidase domain of ACE2 is subdivided into two subdomains (I & II). These two subdomains together form a deeply recessed proteolytic active site of the enzyme. The zinc-binding site is situated

near the bottom of the active site. ACE2 contains a single HEXXH + E zinc-binding consensus sequence. The zinc ion is coordinated by His374, His 378, Glu 402, and one water molecule. A chloride ion is bound in the subdomain II coordinated by Arg169, Trp477, and Lys481 (Towler et al., 2004).

Two forms of mammalian ACE have been identified: somatic ACE containing two catalytic domains and germinal ACE with a single domain. The catalytic domain of ACE2 shares 42 % of structural resemblance to each of the catalytic domains of ACE. ACE2 also shares a 33% similarity to the somatic angiotensin-converting enzyme, a peptidyl dipeptidase, in the regions surrounding the catalytic domain (Donoghue et al., 2000; Tipnis et al., 2000; Towler et al., 2004).

2.3.2.2 Substrate Specificity of ACE2

ACE2 is a member of the M2 zinc metalloproteinase family along with somatic and testicular forms of ACE. ACE2 has a different substrate and inhibitor specificity from ACE, and hence its physiological function differs from ACE. Moreover, ACE inhibitors (lisinopril, captopril, and enalaprilat) cannot inhibit the activity of ACE2 (Tipnis et al., 2000). The rationale behind this could be that specific ACE inhibitors are designed to compete with peptides that are cleaved to release C-terminal dipeptides. In ACE2, the binding pocket (S2') is smaller. It can only accommodate one amino acid instead of a second terminal peptide bond compared with that of testicular ACE (Tipnis et al., 2000). Therefore, the positioning of inhibitors in the active site of ACE2 may not be

in the correct conformation to affect the cleavage of single amino acid from the C terminus of the substrate (Towler et al., 2004). However, EDTA, a metal chelating agent, completely inhibited the catalytic activity of ACE2 at 10mM (Tipnis et al., 2000).

Unlike ACE, ACE2 has only a single catalytic domain compared to two N & C-terminal domains of somatic ACE. Furthermore, ACE2 specifically acts as carboxypeptidase rather than dipeptidyl peptidase (Tipnis et al., 2000). ACE2 can cleave a single hydrophobic or basic residue from the C-terminal of peptides. It cleaves basic arginine residues from angiotensin I and II (Ang). Bradykinin, which has c-terminal arginyl residue, is not hydrolyzed by ACE2. The amino acid residue present generally determines the peptidase cleavage site within four to five positions of the scissile bond. Proline and leucine are preferred at the P1' position for substrate hydrolysis (Tipnis et al., 2000).

2.3.2.3 Expression of ACE2

The expression of ACE2 is highly tissue specific. It is mainly expressed in the heart, gastrointestinal system, kidney, and testis of the human tissue (Donoghue et al., 2000). Immunohistochemical analysis shows that ACE2 is localized in the endothelium of most intramyocardial vessels, including capillaries, veins, coronary arteries. In kidney cells, the expression of ACE2 was also present throughout the endothelium and in smooth muscle cells. In the gastrointestinal system, ACE2 is primarily expressed in ileum, duodenum, jejunum, caecum, and colon (Harmer et al., 2002).

2.3.2.4 Physiological Role of ACE2

ACE2 has distinct physiologic functions apart from acting as a receptor for SARS-CoV-2. It plays a vital role in regulating the renin-angiotensin system (RAS) to maintain blood pressure homeostasis, as well as fluid and electrolyte balance (Boehm & Nabel, 2002; Corvol et al., 1995; Crackower et al., 2002; Donoghue et al., 2000; Skeggs et al., 1980; Tipnis et al., 2000). Angiotensin-converting enzyme (ACE) and ACE2 are homologs but play different RAS roles; ACE generates Angiotensin II (Ang II), whereas ACE2 inactivates AngII by cleaving the C-terminal residues from it, generating Ang 1-7, a negative regulator of the RAS system (Boehm & Nabel, 2002; Corvol et al., 1995; Crackower et al., 2002; Donoghue et al., 2000).

Consequently, ACE2 has a beneficial role in many diseases such as lung injury, hypertension, cardiovascular diseases, and diabetes (Tikellis & Thomas, 2012). ACE2 cleaves the C-terminal Leu to Ang I to generate Ang 1-9. Similarly, it hydrolyzes the C-terminal residues from three other vasoactive peptides: neurotensin, kinetensin, des-Arg bradykinin, Ang I, Ang II, and dynorphin A(1-3) and the apelin peptides (Tipnis et al., 2000).

In SARS-CoV-2 infection, binding of spike protein to its receptor ACE2 causes downregulation of its expression resulting in increased levels of Ang II, strongly associated with viral load and lung injury (Liu et al., 2020). Similarly, in the influenza A (H7N9) virus, elevated levels of Ang II are linked to disease progression and severity and

may predict patient mortality (Huang et al., 2014). The renin-angiotensin pathway has been shown to play a critical role in acute pulmonary injury, and ACE2 has a protective role in the acute pulmonary failure (Kuba et al., 2005). Previous studies have shown the protective function of ACE2 against lung injury in a mouse model. Interestingly, only catalytically active recombinant human ACE2 could rescue the lung function, suggesting a possible therapy to treat acute lung injury (Y et al., 2005). In 2 phase II clinical trials, the administration of ACE2 decreased Ang II and increased Ang 1–7 levels. However, the administration of ACE2 did not show any improvement in physiological or clinical measures of ARDS (Khan et al., 2017). Therefore, potential inhibitors that could increase ACE2 exopeptidase activity and block RBD and ACE2 interaction represent an exciting therapeutic option against SARS-CoV-2 infection.

Although ACE2 facilitates viral entry, it provides defense against acute lung damage, indicating that the ACE2/Ang 1-7 pathway can be carefully manipulated to reduce SARS-CoV-2 induce lung injuries (Imai et al., 2005; Kuba et al., 2005). It is already known that the enzymatic site of ACE2 is different from the binding site of RBD, and potent ACE2 inhibitor MLN-4760 has no effect on the interaction of RBD with ACE2 (B et al., 2021). Thus, a drug that can target the critical interaction between SARS-CoV-2 S glycoprotein and human ACE2, without inactivation of this enzyme and blocking its crucial beneficial function, represents an exciting therapeutic possibility to combat SARS-CoV-2 infection.

SARS-CoV-2 Entry through Host ACE2

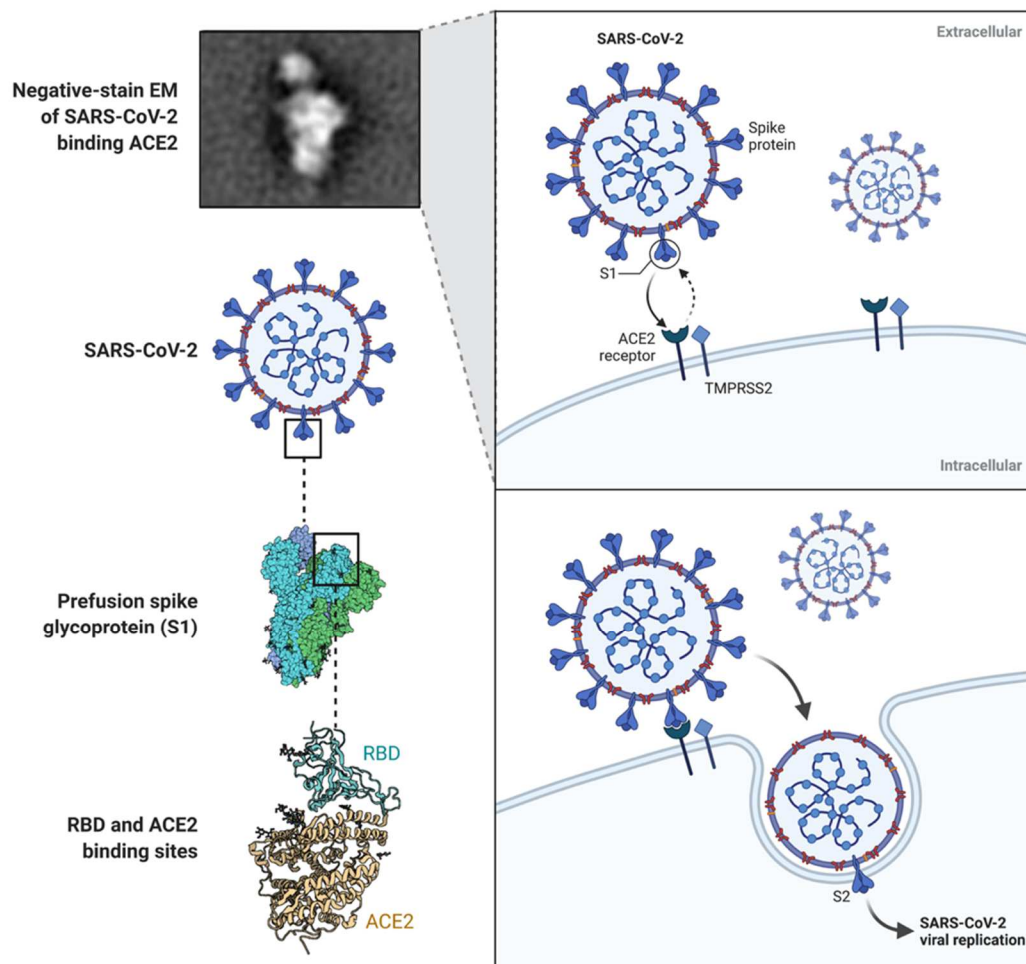


Figure 6: SARS-CoV-2 Targeting ACE2 Receptor and Entry in Infected Cell

Reprinted from "SARS-CoV-2 Targeting of ACE2 Receptor and Entry in Infected Cell", by BioRender, August 2020, retrieved from <https://app.biorender.com/biorender-templates/figures/5e99f5395fd61e0028682c01/t-5f9ae195d8c66d00a335fc7f-sars-cov-2-targeting-of-ace2-receptor-and-entry-in-infected-> Copyright 2022 by BioRender.

2.3.3 Host Proteases

Three host proteases play a crucial role in the viral life cycle. Proteolytic cleavage of S at S1/S2 and the S2' site protein by host proteases activates the SARS-CoV-2 and increases its infectivity. Cleavage of the S protein can occur at the plasma membrane (Furin and TMPRSS2) or in the endosomes before membrane fusion (Cathepsin B/L) (Hoffmann et al., 2020; Xia et al., 2020). TMPRSS2 is a type II membrane serine protease essential for many physiological and pathological processes. It is widely expressed in several organs and tissues, including the prostate, respiratory tract, gastrointestinal tract, kidney, and pancreas (Wettstein et al., 2022). It activates SARS-CoV-2 by proteolytic cleavage at the S2 site, which triggers plasma membrane fusion and release of viral RNA into the cytoplasm (Hoffmann et al., 2020). Furin-mediated cleavage at S1/S2 is required for subsequent activation by TMPRSS2. In TMPRSS2 negative cells, the S1/S2 site cleavage is mediated by endosomal protease cathepsin B/L. Inhibition of cathepsin activity by chloroquine and hydroxychloroquine was unsuccessful for the treatment of COVID-19, possibly because of the presence of other proteases such as furin and TMPRSS2 (Hoffmann et al., 2020).

Even though TMPRSS2 mediate S protein cleavage leads to increased uptake and processing of SARS-CoV-2, cellular entry is partially blocked by a clinically proven TMPRSS2 inhibitor camostat (Hoffmann et al., 2020). Therefore, inhibitors of furin and TMPRSS2 might be an option for potential therapeutics for COVID-19. However, unlike

TMPRSS2, furin is essential for normal development; thus, prolonged inhibition of this enzyme might be associated with unwanted adverse effects (Xia et al., 2020).

2.3.4 Auxiliary SARS-CoV-2 Receptors

Several host receptors function as co-receptors or cofactors and aid in viral entry into the cell, such as heparin sulfate, NRP1, and Scavenger receptor class B member 1 (SRB1) (Cantuti-Castelvetri et al., 2020; Wei et al., 2020). Heparin sulfate binds to the S protein and promotes viral infectivity (Q. Zhang et al., 2020). Similarly, the overexpression of the SCARB1 gene, which encodes SRB1 protein stimulates infection, whereas its knockdown decreased the infection (Wei et al., 2020). Another receptor, NRP1, binds to the CendR motif (RRARR) at the S1-S2 junction and increases SARS-CoV-2 infectivity (Cantuti-Castelvetri et al., 2020).

2.3.5 SARS-CoV-2 Co-Receptor

AXL is a plasma membrane-associated member of the Tyro3/Axl/Mer (TAM) family of tyrosine kinase receptors that regulate innate immunity and promote apoptotic cell clearance (Morales et al., 2021). AXL was previously discovered to be a Zika virus receptor, allowing the virus to enter human glial cells and facilitate infection by downregulating interferon signaling. It also acts as a dengue virus entry factor and enhances the entry of filoviruses. AXL has recently been identified as another important entry receptor that stimulates the entry of SARS-CoV-2 into respiratory system cells. The

association of the SARS-CoV-2 Spike protein's N-terminal domain (NTD) with AXL enhances viral entry into human cells (S. Wang et al., 2021).

2.4 Discovery of OJT010 as a Novel Inhibitor of Severe Acute Respiratory Syndrome Coronavirus 2

To limit the spread of COVID-19, new protective measures are needed to save the lives of millions of people. This could be achieved quickly by repurposing old drugs to accelerate drug discovery without lengthy preclinical and clinical studies. Previously several research efforts have been made to repurpose old drugs against SARS-CoV-2. Several clinical trials have been conducted to find effective measures to treat COVID-19. Until March 2022, 7633 clinical trials have been registered to develop drugs and vaccines for COVID 19 (Bugin & Woodcock, 2021). OJT010 is a demethylated metabolite of OJT009. Both drugs are clinically approved mucolytic agents used to treat respiratory diseases with excellent safety and tolerability (M & B, 2008). OJT010 has a wide range of clinical properties, including secretolytic activity, anti-inflammatory, anti-antioxidant, local anesthetic, antiviral, antibacterial, and antifungal (M & B, 2008; PR, 2010). It was also recently reported that it is approved to treat COVID-19 in China (H et al., 2021). Based on the plethora of preclinical and clinical evidence on its antiviral and anti-inflammatory properties, we proposed that OJT010 might prevent or inhibit the entry and replication of SARS-CoV-2.

2.4.1 Primary Pharmacology of OJT010

The mechanism of action of OJT010 has been extensively investigated in multiple studies. It has a broad range of effects, including mucokinetic properties, mucociliary activity, and stimulation of surfactant production (H et al., 1987; K et al., 2006). It also acts anti-inflammatory and antioxidant agent by balancing inflammatory reactions to relieve symptoms of cough and cold. Its local anesthetic effect helps alleviate symptoms of sore throat (D et al., 1994; KM et al., 2008; PR, 2010).

Apart from these, recent studies have drawn more attention to its role in the autophagy-lysosomal pathway, a critical process for inhibiting viral proteins and further dissemination (Magalhaes et al., 2018). Furthermore, OJT010 suppresses the influenza virus's proliferation in the airway and improves mice's survival rate (B et al., 2002). Additionally, OJT010 potentiates antibiotic activity in the lungs by increasing their concentrations (M & B, 2008; R et al., 1987). It has gained attention due to its activity as a GCase chaperone to treat neurodegenerative diseases (A et al., 2020).

More recently, it has been evaluated as an antiviral agent against SARS-CoV-2 for the potential treatment of COVID-19 (BF et al., 2021; SB et al., 2020). I will briefly discuss the role of OJT010 in various diseases.

Mucokinetic and Mucociliary Properties: SARS-CoV-2 infects mainly alveolar Type 2 (AT2) epithelial cells in the lungs. AT2 plays an essential role in surfactant production. OJT0010 increases surfactant production, ciliary activity, and bronchial secretions, which aid in clearing viral particles (B et al., 2002; Z. P et al., 2020). It accumulates in lamellar bodies (LB) found in AT2 cells and elicits calcium release from lamellar bodies, which triggers the fusion of LB with the plasma membrane leading to surfactant release (P & M, 2021). OJT010 has shown a dose-dependent increase in surfactant production, thereby maintaining the alveolar function, and preventing an alveolar collapse *in vivo* in rats, rabbits, guinea pigs, and ferrets (H et al., 1987; M & B, 2008).

Antioxidative and Anti-Inflammatory Activities: OJT0010 suppresses viral proliferation by upregulating anti-inflammatory factors. In a mouse study of acute lung injury, OJT0010 significantly reduced proinflammatory cytokines, such as tumor necrosis factor- α (TNF- α), interleukin-6 (IL-6), and transformation growth factor- β 1 (TGF- β 1), reduced lung inflammation and accelerated recovery from acute lung injury induced by lipopolysaccharide (KM et al., 2008; X et al., 2004).

Moreover, OJT0010 inhibits histamine release, LTC₄, IL-4, IL-13, and LTB₄ from mast cells, basophils, and monocytes (BF et al., 1999). It decreases the concentration of TNF- α , interleukin (IL)-2, IL-1, IL-4, IL-6, IL-13, interferon (IFN)- γ , and TGF- β 1 in the broncho-alveolar lavage (BF et al., 1999).

Interestingly, it has high affinity for lung tissue, resulting in 20 times higher concentration than blood after oral or IV administration with no toxicity (Choi et al., 2018). It also acts as a free radical scavenger and decreases the release of reactive oxygen species from polymorphonuclear and mononuclear cells, thus prevent against oxidative damage (D et al., 1994). Moreover, co-treatment of OJT0010 with another antibiotic, including beta-lactams, glycopeptides, macrolides, nitrofurans, and rifamycin's, increases their concentration in lung tissue and airway surface fluid levels (V & GS, 2019).

Local Anesthetic: OJT0010 is a potent inhibitor of neuronal voltage-gated Na⁺ and Ca⁺ channels (M & B, 2008). It acts as a chaperone and binds to the active site of the GCCase protein and reduces activity. The binding of OJT0010 to GCCase enables its transportation to the lysosome and release of free active enzymes under acidic conditions. In other tissues, such as the brain, OJT0010 increases intracellular GCCase activity, as reported in studies of rodent and primate models (GH et al., 2009).

Effect on Autophagy: The autophagy and lysosome systems play a crucial role in clearing viral infections. OJT0010 induces autophagy in a dose-dependent manner and mycobacterial death in macrophages. Also, potentiate rifampin activity through an unclear mechanism (Magalhaes et al., 2018; SW et al., 2018)

Ion Homeostasis: OJT010 modulates chloride ion conductance in cystic fibrosis. At 100 μ M, it increases chloride transport across the apical cell membrane of

immortalized cells. A maximum increase in chloride conductance (~8 fold) was seen after 8 h of treatment with OJT010 compared to control (G et al., 2013).

Effect Viral Infection: OJT0010 reduced RV14 infection-induced production of mediators, including IL-1 β , IL-6, and IL-8. It significantly reduced the levels of the p50 and p65 subunits of nuclear factor kappa B (NF- κ B). Furthermore, it reduced the number and fluorescence intensity of acidic endosomes from which RV RNA enters the cytoplasm (C et al., 2020; M et al., 2014).

OJT0010 significantly suppressed the influenza-virus multiplication in the airway of mice and improved the survival rate. Furthermore, it stimulated pulmonary surfactant release, mucus protease inhibitor, immunoglobulin (Ig)-A, and IgG (B et al., 2002; C et al., 2020).

OJT010 is an active demethylated metabolite of OJT009. Both drugs act as mucolytic agents and are widely available over the counter in many countries to treat upper respiratory tract diseases with proven efficacy and safety (D et al., 1987; H et al., 1987; KM et al., 2008; S et al., 1997). OJT009 has been hypothesized to inhibit one of the critical host proteases, TMPRSS2, involved in the SARS-CoV-2 infection pathway (JM et al., 2014). TMPRSS2, an androgen-regulated cell surface serine protease, cleaves the spike protein to aid viral and cell membrane fusion (Hoffmann et al., 2020).

Olaleye et al. discovered for the first time that OJT010 and its progenitor OJT009 inhibit the SARS-CoV-2 infection-induced cytopathic effect at micromolar concentration. In addition, OJT010 and OJT009 effectively modulated the binding between RBD and ACE2 (Olaleye et al., 2020). Lucas et al. discovered OJT009 in a chemical screen to identify a potent, bioavailable TMPRSS2 inhibitor suppressing prostate cancer metastasis *in vivo* (JM et al., 2014). Because of its activity on TMPRSS2, OJT009 is tested in clinical trials against COVID-19. Because of the parent drug, OJT010 was hypothesized to have activity against TMPRSS2 and therefore proposed for further studies to identify its role against SARS-CoV-2 (Li, 2020). There are only a few reports published regarding the role of these two compounds against SARS-CoV-2 infection. In this study, we focused on OJT010, and I will briefly discuss what has already been known about its anti-SARS-CoV-2 activity in the literature.

A study published by Bradfute et al. evaluated the effects of OJT009 and OJT0010 against SARS-CoV-2 in Vero E6 cells. The method used to determine the activity of compounds were cell survival assay, quantitative PCR, and plaque-forming assay. In the cell survival assay, OJT009 had no inhibition of viral infection at 1, 10, and 100 μ M (SB et al., 2020). OJT010 showed a dose-dependent increase in cell survival with maximum activity at 100 μ M. High concentrations of OJT010 has been demonstrated safe in long-term use in Parkinson's disease, pregnant women, and Gaucher disease, and doses of this magnitude are known to lead to lung levels approaching 100 μ M (GH et al., 2009; I et al., 2013). Furthermore, high dose OJT0010 has been shown both safe and effective in reducing inflammatory cytokines (TNF-a and IL-1, IL-6, Nf-

kB) and improve the course of respiratory disorders such as acute respiratory distress syndrome (ARDS) (K et al., 2006).

Another study evaluated the effect of OJT009 and OJT0010 on the cell-cell fusion induced by SARS-CoV-2 infection *in vitro*. OJT009 induced SARS-CoV-2 expression when ACE2 and TMPRSS2 were present together in a dose-dependent manner. At the same time, OJT0010 did not lead to enhancement but a slight decrease in activity at 50 μ M (BF et al., 2021).

A study done by Carpinteria et al. discovered the role of OJT010 as an inhibitor of acid sphingomyelin. Their study identified the role of acid sphingomyelin as an activator of the spike protein. Acid sphingomyelins stimulate the release of ceramides, which promotes viral infections. Inhalation of 20 mM of OJT010 solution decreases sphingomyelin/ceramide activity in nasal epithelial cells, preventing the entry of spike pseudovirus into the cell (A et al., 2021).

2.4.2 Toxicology of OJT010 in Animals

In single-dose toxicity trials (mouse, rat, rabbit, guinea pig, and dog), OJT010 was well tolerated after oral and parenteral administration (Y et al., 2022). Subacute and chronic oral repeated toxicology studies in rat, rabbit, guinea pig, and dog for a period ranging from 26 weeks to 78 weeks showed little to no adverse effects and negligible signs of target organ toxicity with doses up to 2500 mg/kg (rat) and 250 mg/kg (rabbit and dog)

(M & B, 2008). Clinical symptoms of toxicity following overdoses across species were body weight loss, dyspnoea, reduced motoric activity, ataxia, and convulsions. All adverse effects were reversible, and there was no evidence of progression (Y et al., 2022).

The minimum tolerated dose without any adverse effects were 50 mg/kg (rat), 40 mg/kg (rabbit) and 10 mg/kg (dog). Oral doses of OJT010 in rats and rabbits of up to 3000mg/kg and 200mg/kg respectively did not impair early embryonic development. There was no evidence for any embryotoxicity or teratogenicity. Similarly, there was no evidence for a treatment-related tumorigenic potential of OJT010 in mice and rats (H et al., 2022). Overall, OJT010 is an extensively investigated drug with a well-established favorable safety profile in animals, verified by its widespread therapeutic use in humans over the past decade.

2.4.3 Pharmacokinetics and Metabolism of OJT010

The pharmacokinetics of OJT010 has been extensively studied in the mouse, rat, rabbit, and dog. In both animals and humans, gastrointestinal absorption of OJT010 is quick and nearly complete. In humans, absolute oral bioavailability is high, whereas, in animals, it is lower. The rapid and extensive distribution of OJT010 is consistent with its high volume of distribution. It is rapidly and extensively distributed from the blood into tissues.

OJT010 is substantially metabolized into DBAA in animals and humans (3,5 dibromoanthranilic acid). DBAA has a low tissue distribution compared to the parent molecule. Across species, plasma protein binding for OJT010 is low but very strong for its metabolite DBAA. OJT010 has a short half-life in mice and dogs but a moderate half-life in rats and humans.

2.4.4 Clinical efficacy of OJT010

OJT010 is used antenatal and post-natal in newborns to prevent infant respiratory distress syndrome (IRDS) and fetal lung maturity. Healthy pregnant women (24-34 weeks) were given one-two dose of (1g-1.3g) of OJT010 daily, oral or I.V infusion for 1-5 days. Administration of OJT010 to pregnant did not cause any toxicity (M et al., 1987; Paleari et al., 2011). The only reported side effects were nausea and headache. The number of pregnant women enrolled in the study ranged between 20-300 in number. Antenatal uses of OJT010 resulted in a significant decrease in the incidence of IRDS and prenatal morbidity and mortality (C et al., 1997; Y et al., 1995).

OJT010 was highly safe when used in infants with IRDS during the first five days at a dose of 20-30mg daily and reduced the incidence of IRDS associated complications (A et al., 1987; RR et al., 1992). OJT010 administration in the adult population with chronic obstructive lung disorders and lung carcinomas requiring surgeries due to thoracic pathologies or patients with spinal cord injuries has significantly prevented

postoperative complications and improved airway patency in patients with chronic obstructive pulmonary disease (COPD) (E et al., 1994; G, 1991; P & P, 1989). OJT010 was dosed at 1g per day through I.V infusion for the duration of 3-5days. Similar to pregnant women, no significant toxicity was reported by this group. Patients enrolled in the study were between 20-250 in number (E et al., 1994; G, 1991; P & P, 1989).

OJT010 has been extensively studied to prevent and exacerbate upper respiratory diseases, mainly in adults. Long-term use of high-dose OJT010 has reduced the severity and frequency of upper respiratory disorders. Most studies included a population with chronic bronchitis and were treated with a dose of 45- 150mg/day orally from 10-days to 1 year (CH et al., 1987; E et al., 1994). No significant adverse effects were reported during treatment with the drug. Use of OJT010 has shown no toxicity when used at doses of 10-270 mg daily orally for a duration of 10 days to 17 months for the treatment of diseases such as Gaucher's disease, radiation lung injury, sore throat, cystic fibrosis, primary Sjogren's syndrome, secretory otitis media (CH et al., 1987; E et al., 1994).

CHAPTER 3

DESIGN OF THE STUDY

3.1 Central Hypothesis and Specific Aims

OJT010 is an orally bioavailable drug with broad-spectrum antiviral activity against rhinovirus and influenza virus (B et al., 2002). It inhibits viral replication by suppressing the release of inflammatory cytokines and reducing the activation of transcription factor nuclear factor kappa B (NF- κ B) (B et al., 2002). Moreover, it has been shown to decrease the expression and protein levels of intercellular adhesion molecule-1 (ICAM-1), a receptor for rhinovirus (M et al., 2014). Also, it reduces the number of acidic endosomes from which the virus enters the host cytoplasm (C et al., 2020; M et al., 2014). Furthermore, OJT010 plays an essential role in the homeostasis of the chloride ions (G et al., 2013). ACE2 has a chloride binding site, and it is essential for substrate hydrolysis. It also plays an essential role in determining the structural conformation of ACE2, which makes it receptive to binding with RBD of Spike protein (Towler et al., 2004; Vickers et al., 2002). Therefore, modulation of chloride ions by OJT010 may prevent the binding of ACE2 to the SARS-CoV-2 spike protein. In our efforts to identify clinically approved drugs for the potential treatment of COVID-19, our laboratory conducted a screen for inhibitors of SARS-CoV-2 infection. We discovered three compounds that inhibited the SARS-CoV-2 infection-induced cytopathic effect and

had potent activity against ACE2-RBD interaction. These compounds were structurally similar to OJT010. *We hypothesize that OJT010 interaction with ACE2 will block viral entry and inhibit the replication of SARS-CoV-2 in vitro.*

3.2 Specific Aim 1: To Evaluate the Efficacy and Cytotoxicity of OJT010 against SARS-CoV-2 Infection.

3.2.1 (1a) To Determine the Antiviral Activity of OJT010 against SARS-CoV-2 and its Delta Variant B.1.617.2

Rationale: COVID-19, caused by the deadliest SARS-CoV-2, represents a big challenge for the health care system. The scientific community has made numerous efforts to discover drugs that can inhibit the replication of SARS-CoV-2. Repurposing clinically approved drugs is an accelerated pathway to solving the unprecedented situation created by this pandemic. Through a focused search of clinically approved drugs that have activity against SARS-CoV-2, our lab discovered OJT010 as a novel inhibitor of SARS-CoV-2 infection. In this study, we evaluated the efficacy of OJT010 against viral replication using three independent *in vitro* assays.

3.2.2 (1b) To Assess the Cytotoxicity of OJT010 in VeroE6 Kidney and A549 Lung Cells.

Rationale: To determine the effective concentrations against SARS-CoV-2, first, we evaluated the cytotoxicity of OJT010 in the mammalian cell lines. Concentration below the CC_{50} was used in the antiviral assay to determine IC_{50} of OJT010 against SARS-CoV-2. This ensures that the response obtained in the antiviral assay is due to the direct activity of OJT010 against the virus, not due to the cytotoxic effects on the cells.

3.2.3 (1c) To Determine the Efficacy of the Combination of OJT010 with Remdesivir against SARS-CoV-2 in vitro

Rationale: Till now, remdesivir is the only FDA-approved drug for the treatment of COVID -19. However, the clinical efficacy of remdesivir is controversial (Grein et al., 2020). Moreover, a combination of drugs has been used to treat COVID-19 (@US_FDA, 2020; Consortium et al., 2021). In the absence of potent single-agent therapy against SARS-CoV-2, new drugs that could potentiate the activity of already approved antiviral can significantly speed up the clearance of the virus and decrease hospitalization and death. Therefore, we evaluated the effects of OJT010 on remdesivir and vice-versa against SARS-CoV-2.

3.3 Specific Aim 2: To Investigate and Characterize the Impact of OJT010 on the Interaction of rhACE2 and RBD of SARS-CoV-2 and the Exopeptidase Activity of ACE2.

3.3.1 (2a) To Evaluate the effects of OJT010 on the Interaction of rhACE2 and RBD of SARS-CoV-2

3.3.2 (2b) To Determine whether OJT010 Impacts the Exopeptidase Activity of ACE2

Rationale: Interaction of ACE2 with RBD of Spike protein is the most crucial step in the viral life cycle. In addition to direct viral effects, downregulation of ACE2 by SARS-CoV-2 creates an imbalance between the RAS and ACE2/angiotensin (1-7) axis, which further contributes to inflammation and multiple organ injury in COVID-19 (SN et al., 2021). Drugs that can block the interaction between these two proteins will inhibit the entry of SARS-CoV-2 into the cells. This will prevent the infection and damage caused to the host cell by over-activating the immune system in response to the virus challenge.

3.2.3 (2c) To Investigate Binding Sites for OJT010 on the SARS-CoV-2 and Host ACE2 Receptor Through Computational Studies.

Rationale: To understand the molecular mechanism of action of OJT010, we determined the binding amino acid residues for the active sites on the viral and host receptor by molecular docking. Understanding the mechanism of action will provide

insight into the new possible means of OJT010 other than the already known in the literature. Furthermore, this will guide developing an effective treatment plan for OJT010 as a prophylactic or therapeutic agent for the treatment of COVID 19.

3.4 Specific Aim 3: To Determine the In Vivo Pharmacokinetic Parameters of OJT010 in Healthy rats.

Rationale: To advance into *in vivo* efficacy models and clinical studies, it is essential to understand the time course of drug concentration in the body.

Pharmacokinetic and pharmacodynamic (PK/PD) studies in drug discovery and development are vital to translate the preclinical IC_{50} into clinical efficacies. We determined the PK parameters of OJT010 in healthy rats to understand target drug exposure and drug disposition.

3.5 Materials and Methods for Pharmacological Studies

Drugs: OJT010 and Dimethyl sulfoxide (DMSO) (D8418-1Lot#SHBM4129) were purchased from Sigma Aldrich (St. Louis, MO). OJT010 was dissolved in 100 % DMSO at a concentration of 50mM and was further serially diluted in 100% DMSO.

3.5.1 COVID-19 Spike-ACE2 Binding Assay Kit

A Spike (RBD) - ACE2 binding assay kit (Cat # CoV-SACE2-1, Lot# 062320 7066) was purchased from RayBiotech (RayBiotech, 2022). The enzyme-linked immunoabsorbent assay (ELISA) was performed in a transparent flat-bottom 96-well plate, following manufacturer instructions. We prepared 10 mM stock solutions of the compounds in DMSO and serially diluted the compounds in DMSO as follows: 100, 50, 10, 5, 1, 0.5, and 0.1 μ M for OJT009 and OJT010. All experiments were done in triplicates and repeated thrice. Each plate contained a positive control (1% DMSO) and a blank control with no ACE2.

Briefly, 96 well plate pre-coated with recombinant SARS-CoV-2 Spike receptor-binding domain (RBD) protein was incubated 1 μ L of serially diluted compounds in 49 μ L of 1X assay diluent buffer for a duration of 30 mins, at room temperature (22°C) with shaking at 180rpm. After this, 50 μ L of ACE2 protein in 1X assay diluent buffer was added into the 96 well plates, and the reaction was allowed to go on for 2.5 hr at room temperature (22°C) with shaking at 180rpm. After that, the reaction mixture was

discarded, and the plate was washed consecutively four times with 300 μ L 1X wash buffer, followed by the addition of the detection antibody (anti-ACE2 goat antibody) further incubated for one hr at room temperature (22°C) with shaking at 180rpm. Then, the solution was discarded, and the plate was washed as described above.

In the next step, the HRP-conjugated anti-goat IgG was added to each well, and the reaction plates were further incubated for 1 hr at room temperature (22°C) with shaking at 180rpm. Again, the solution was discarded, and the final wash step was repeated as described above. In the final step, 100 μ L of 3,3',5,5'-tetramethylbenzidine (TMB) one-step substrate was added to the reaction mixtures and incubated in the dark at room temperature (22°C) with shaking at 180rpm for an additional 30 mins and then stopped by the addition of 50 μ L stop solution. The absorbance was read immediately at 405 nm using a Beckman Coulter DTX880 multimode plate reader. The data were fitted after the background hydrolysis was adjusted using a special bell-shaped dose-response curve equation in GraphPad prism software 8.4.3.

3.5.2 ACE2 Inhibitor Screening Assay

An ACE2 exopeptidase Inhibitor screening assay kit with the fluorogenic substrate (Catalogue #79923) was purchased from BPS Bioscience (San Diego, CA) and modified to measure the exopeptidase activity of ACE2 in the presence and absence of inhibitors (BPSBioscience, 2022). Following the manufacturer's directions, the fluorescence assay was carried out in a 96-well black flat-bottom plate with a final

reaction volume of 50 μ L. We prepared 50 mM stock solutions of OJT009 and OJT010 in 100% DMSO. We further serially diluted the compounds in DMSO as follows: 500, 250, 100, 50, 10, 1, 0.1 μ M. All experiments were done in triplicates and repeated twice. A positive control of enzyme treated with vehicle alone (2 percent DMSO) and a blank control with no enzyme were included on each plate.

Briefly, each reaction had 24 μ L of purified recombinant human ACE2 protein (0.42ng/ μ L) in ACE2 buffer, one μ L of the compound at different concentrations, and 25 μ L ACE2 fluorogenic substrate. The final volume of the reaction was 50 μ L. The reaction mixtures were incubated for 1 hrs at room temperature (22 C) and protected from light. After that, the fluorescence intensities (λ Excitation = 535nm, λ Emission = 595nm) were measured using a Spectramax iD3 multimode plate reader. The background hydrolysis was subtracted, and the data were fitted to a four-parameter logistic (variable slope) equation using GraphPad prism software 9.1.

3.5.3 ACE 1 Exopeptidase Activity

ACE1 Inhibitor Screening Kit (Cat #MAK422) was purchased from Sigma-Aldrich (St. Louis, MO) and adapted to determine the effect of OJT010 on the enzymatic activity of ACE (Aldrich, 2022). The in vitro colorimetric assay was performed in a transparent flat-bottom 96-well plate. We prepared 50mm and 10mm solutions of Captropil, a known ACE1 inhibitor used as a positive inhibitor control. Stock solutions of the compounds were prepared in 100 % Dimethyl sulfoxide (DMSO) and further serially diluted in

DMSO as follows: 500, 100, 50,10,5,1 and 0.5 μm for OJT010 and the positive control Captopril. All experiments were performed in Quadruplicates. Each plate contained a positive control (1% DMSO) and a blank controls with no ACE1 enzyme. Specifically, 2.5 μl of serially diluted compounds were pre-incubated with 2 μl of ACE1 protein diluted in 38 μl of 1X assay diluent buffer for about 15 mins, at room temperature (22°C). Then, we added 157.5 μl of 1x ACE1 assay buffer (197.5 μl for -ve control) into the 96 well plates. The solution was mixed well and incubated at 37 °C for 15-20 minutes, protected from light. After that, 40 μl of the substrate was added to each well and mixed well. The absorbance was measured immediately at 345 nm (A345) in kinetic mode for 60 minutes.

3.5.4 Material and Methods for Pseud typed Lentivirus Assay

Cell growth conditions and Medium, ACE2 Human Kidney 293 recombinant Cells (ACE2 HEK-293-#79951), Thaw media (#60187-1), Growth media (#79801), Spike (SARS-CoV-2) Pseudotyped Lentivirus (Luciferase Reporter # 79942), Spike S1 Neutralizing Antibody (# 101024), and ONE-Step™ Luciferase Assay System (#60690-1) were purchased from BPS Biosciences (San Diego, CA). The pseudotyped lentivirus contained SARS-CoV-2 Spike protein (Genbank Accession #QHD43416.1) and the firefly luciferase gene under the control of the CMV promoter. Expression of luciferase can be detected after the addition of the substrate. When pseudovirions are incubated with a molecular inhibitor before infection, they will block the spike-mediated cell entry. The

number of blocked viruses can be measured via luciferase reporter activity. (Nie et al., 2020)

Briefly, HEK293 cells were resuspended in thaw media (no puromycin) and cultured in a T25 flask at 37°C in a CO2 incubator. After the first passage, cells were further cultured in growth media (contains puromycin). On the experiment day, ACE2-HEK293 were seeded at the density of 7500 cells per well into a white opaque 96-well cell culture microplate in 90 µl of growth medium. Cells were inoculated with 750 infectious particles (MOI =0.1) of SARS-CoV-2. Before infection, pseudotyped lentivirus (5µl) was preincubated with OJT010 (5µl) at concentrations ranging from 100, 50, 25, and 10 µM and with controls for 30 minutes at room temperature (RT); the reactions were then added to the cells. After 48 hours, 100 µl Luciferase reagent (BPS Bioscience, catalog no. 60690) was added to measure luciferase activity. Luminescence was measured with Spectra max ID3 (molecular devices). The measured luminescence signal was directly proportional to the amount of Pseudo typed lentivirus successfully transduced into the cells. Data are presented as percent inhibition of entry of pseudo-type lentivirus into the HEK293-ACE2 cells (Bioscience, 2022). Infected cells and infected treatment cells (Spike neutralizing antibodies) were positive and negative controls. All experiments were done in duplicates and were repeated twice.

3.5.6 Antiviral assays using SARS-CoV-2 *In Vitro*

Screening Strategy: We will employ a cell-based assay measuring the cytopathic effect (CPE) of the virus infecting Vero E6 host cells. The CPE reduction assay is a popular and widely used assay format to screen for antiviral drugs because of its ease of use in the high throughput screening (HTS) (CB et al., 2008; WE et al., 2007). In this assay, host cells infected with the in this assay, virus-infected host cells die as a result of the virus's hijacking of cellular mechanisms for replication processes. By monitoring the viability of host cells three days after virus inoculation, the CPE reduction assay indirectly measures the effect of antiviral drugs acting through various molecular mechanisms. Anti-viral compounds are identified as those that protect the host cells from the cytopathic effect of the virus, thereby increasing viability.

3.5.7 Infection Induced Cytopathic Effect (CPE)

Vero E6 cells selected for expression of the SARS CoV receptor (ACE2; angiotensin-converting enzyme 2) are used for the CPE assay(W et al., 2003). Cells are grown in MEM/10% HI FBS supplemented and harvested in MEM/1% PSG/ supplemented 2% HI FBS. Cells are batch inoculated with either SARS CoV-2 (M.O.I. ~ 0.002), resulting in 5% cell viability 72 hours post-infection. Compound samples are serially diluted 2-fold in DMSO nine times. Assay Ready Plates (ARPs; Corning 3712BC) pre-drugged with test compounds (90 nL sample in 100% DMSO per well dispensed using a Labcyte ECHO 550) are prepared in the BSL-2 lab by adding 5 μ L

assay media to each well. The plates are passed into the BSL-3 facility, where a 25 μ L aliquot of virus inoculated cells (4000 Vero E6 cells/well) is added to each well in columns 3-22. The wells in columns 23-24 contain virus-infected cells only (no compound treatment). Before virus infection, a 25 μ L aliquot of cells is added to columns 1-2 of each plate for the cell only (no virus) controls. Plates were incubated at 37°C/5%CO₂ and 90% humidity for 72 hours, and then 30 μ L of Cell Titer-Glo (Promega) is added to each well.

Luminescence is read using a Perkin Elmer Envision or BMG CLARIOstar plate reader following incubation at RT for 10 minutes to measure cell viability. Raw data from each test well is normalized to the average signal of non-infected cells (Avg Cells; 100% inhibition) and virus-infected cells only (Avg Virus; 0% inhibition) to calculate % inhibition of CPE using the following formula: % inhibition = $100 * (\text{Test Cmpd} - \text{Avg Virus}) / (\text{Avg Cells} - \text{Avg Virus})$. The SARS CPE assay is conducted in BSL-3 containment with plates being sealed with a clear cover and surface decontaminated prior to luminescence reading (CB et al., 2008; W et al., 2003; WE et al., 2007).

3.5.8 Cytotoxicity of OJT010 in CPE Assay

Compound cytotoxicity is assessed in a BSL-2 counter screen as follows: In each well of assay-ready plates prepared with test compounds as described above, host cells in media are added in 25 μ l aliquots (4000 cells/well). Cells alone (100 percent viability) and cells treated with hyamine at a final concentration of 100M (0 percent viability) serve

as the high and low signal controls for cytotoxic effect in the assay, respectively. The DMSO concentration is kept constant in all wells (0.3 percent), as determined by the dilution factor of stock test compound concentrations. After 72 hours of incubation at 37°C/5 percent CO₂ and 90% humidity, 30µl Cell Titer-Glo (Promega) is added to each well. Following a 10-minute incubation at room temperature, Luminescence was measured using a BMG PHERAstar plate reader to measure cell viability.

3.5.9 Nano luciferase Reporter Virus Assay

A549 cells expressing ACE-2 (obtained from Ralph Barric at UNC) are grown in DMEM high glucose supplemented with 20% HI FBS, 1% NEAA, 100 µg/ml Blasticidin and split 1:6 every three days (remove Blasticidin from the media one passage before using the cells in the assay). On the day of assay, the cells are harvested in DMEM supplemented with 2% HI FBS, 1% HEPES, 1% Pen/Strep. Assay-ready plates pre-drugged with test compounds are prepared in the BSL-2 lab by adding 5µL assay media to each well. The plates and cells are then passed into the BSL-3 facility. A working stock of SARS CoV-2 nanoluciferase reporter virus (NLRV) passaged five times in A549 cells expressing ACE2 is diluted 6000-fold in media containing 160,000 cells per mL (MOI ~ 0.002) and stirred at 200 RMP for approximately 10 minutes. A 25µL aliquot of virus inoculated cells (4000 cells) is added to each well in columns 3-24 of the assay plates. The wells in columns 23-24 do not contain test compounds, only virus-infected cells for the 0% inhibition controls. Prior to virus inoculation, a 25µL aliquot of cells is added to columns 1-2 (no test compounds) of each plate for the cell, only 100% inhibition

controls. After incubating plates at 37°C/5%CO₂ and 90% humidity for 72 hours, 30µL of NanoGlo (Promega) is added to each well. Luminescence is read using a BMG CLARIOstar plate reader (bottom read) following incubation at room temperature for 10 minutes to measure luciferase activity as an index of virus titer. Plates are sealed with a clear cover and surface decontaminated prior to luminescence reading (B et al., 2015).

3.5.10 Cytotoxic effect of OJT010 in NLRV assay

Compound cytotoxicity is assessed in a BSL-2 counter screen as follows: In each well of assay-ready plates prepared with test compounds as described above, host cells in media are added in 25 µl aliquots (4000 cells/well). Cells alone (100 percent viability) and cells treated with hyamine at a final concentration of 100M (0 percent viability) serve as the high and low signal controls for cytotoxic effect in the assay, respectively. The DMSO concentration is kept constant in all wells (0.3 percent), as determined by the dilution factor of stock test compound concentrations. After 72 hours of incubation at 37°C/5 percent CO₂ and 90% humidity, 30µl Cell Titer-Glo (Promega) is added to each well. Following a 10-minute incubation at room temperature, Luminescence was measured using a BMG PHERAstar plate reader to measure cell viability.

3.5.11 The Effect Synergism of OJT010 with Remdesivir on SARS-CoV-2 Infection

Compounds were tested in a dual combination design in the CPE and NLRV assays. The only difference in the experiment was the compound layout and data analysis.

Each combination consisted of seven concentrations of one compound (cmpd B) across a section of the plate with seven concentrations of the second compound (cmpd A) arranged down the same plate section as shown below. Compounds were run in anti-viral and cytotoxicity assays when tested. Serial dilutions were performed to produce 6X concentrations such that a 5 μ L transfer into the assay resulted in the final concentrations indicated (30 μ L total assay volume).

	1	2	3	4	5	6	7	8	9	10	11	12	13	14	15	16	17	18	19	20	21	22	23	24								
A	Cell Control		cmpd B high dose						← cmpd B 7pt DR ←		cmpd B high dose						← cmpd B 7pt DR ←		Positive Control													
B			cmpd A high dose				↓				← cmpd B 7pt DR ←				↓										← cmpd B 7pt DR ←							
C							↓								↓																	
D					→	→	→	→	→	→			→	→	→	→	→	→														
E							↓								↓																	
F							↓								↓																	
G							↓								↓																	
H			→ cmpd A 7pt DR →						→ cmpd A 7pt DR →																							
I			Cell Control		cmpd B high dose						← cmpd B 7pt DR ←		cmpd B high dose												← cmpd B 7pt DR ←		Positive Control					
J					cmpd A high dose				↓				← cmpd B 7pt DR ←				↓															
K							↓								↓																	
L	→	→					→	→	→	→	→	→			→	→	→	→														
M							↓								↓																	
N							↓								↓																	
O							↓								↓																	
P	→ cmpd A 7pt DR →						→ cmpd A 7pt DR →																									

Figure 7: Method for Measuring the Effect of Combination Therapy of OJT010 and Remdesivir (A=OJT010, B=Remdesivir)

3.5.12 Data analysis

The raw data from plate readers are imported into the activity base for all assays, where raw values are associated with compound IDs and test concentrations.

For the antiviral NLRV assay, raw signal values are converted to % inhibition by the following formula:

$$\% \text{ inhibition} = 100 \times (\text{test compound value} - \text{mean value infected cell controls}) / (\text{mean value uninfected cell controls} - \text{mean value infected cell controls}).$$

For the cell viability assay measuring compound cytotoxicity, % cell viability is calculated as follows:

$$\% \text{ viability} = 100 * (\text{test compound value} - \text{mean low signal control}) / (\text{mean high signal control} - \text{mean low signal control}).$$

EC50 and CC50 values are calculated from a four-parameter logistic fit of data using the Xlfit module of Activity base with top and bottom constrained to 100 and 0%, respectively.

Concentration-response graphs of compound combinations were produced in the Graphpad Prism software package.

For synergy analysis, reduced data with associated concentrations and compound ids were imported into, which applies models for detection of synergistic interactions.

The zero-interaction potency (ZIP) model was used.

3.6 Methods for Molecular Docking and Simulation Study

3.6.1 Protein (hACE2-RBD) Acquisition and Preparation

The X-ray crystal structures of the complex of SARS-CoV-2 RBD with hACE-2 (Wild-type (WT)) (PDB code: 6LZG) and Delta variant (PDB ID: 7DF4) were obtained from the RSCB Protein Data Bank (C et al., 2021; Q. Wang et al., 2020). The protein structures were then prepared on the UCSF Chimera software package (Z et al., 2012). The structures of the proteins were prepared by removing water molecules, nonstandard naming, protein residue connectivity. The mucolytic drug (OJT010) was accessed from PubChem (S et al., 2016). The 3-D structures of the drugs were prepared on the Avogadro software package (Hanwell et al., 2012).

3.6.2 Molecular Docking between Proteins and Drug

For molecular docking, Chimera's Autodock was utilized with default docking parameters (O & AJ, 2010), The drug molecules were given Gasteiger charges before docking, and the non-polar hydrogen atoms were fused into carbon atoms. The molecules were then docked first into the hACE-2 catalytic binding pocket, and secondly, at the hACE-2-RBD binding site by defining the grid box with a spacing of 1 Å each and size and (22 × 18 × 22) and (32 × 41 × 25) pointing in x, y and z directions, respectively. The best docking poses for the two drugs were then subjected to molecular dynamics simulations.

3.6.3 Molecular Docking between ACE2-Spike protein

For the protein-protein molecular docking, the Haddock (High Ambiguity Driven Protein-Protein Docking) server was employed, which uses biochemical or biophysical interact data such as chemical shift perturbation data from NMR titration experiments or mutagenesis data (Cyril Dominguez et al., 2003). The binding residues on the two proteins were specified, and all other parameters were left at default settings.

3.6.4 Molecular Dynamic (MD) Simulations

The MD simulation was carried out in the manner outlined by Kehinde et al (I et al., 2019). The simulations were run on the GPU version of the AMBER package (AMBER 18), with the FF18SB variant of the AMBER force field utilized to describe the systems (PC & JO, 2014).

The Restrained Electrostatic Potential (RESP) and General Amber Force Field (GAFF) techniques were employed in ANTECHAMBER to create atomic partial charges for the ligand. AMBER 18's Leap module permitted the addition of hydrogen atoms and Na⁺ counter ions to the ACE2-RBD complex in order to neutralize all systems. The systems were then implicitly suspended within an orthorhombic box of TIP3P water molecules, with all atoms within 10 of any box edge (Jorgensen et al., 1998).

For both solutes, an initial minimization of 2000 steps was performed with a restraint potential of 500 kcal/mol imposed. They were completed in 1000 steps using the steepest descent method, followed by 1000 steps of conjugate slopes. An extra full

minimization of 1000 steps was performed using the conjugate gradient approach with no constraints. For 50 ps, a gradual heating MD simulation from 0 to 300 K was run, ensuring that the systems maintained a fixed number of atoms and a fixed volume. The systems' solutes were subjected to a potential harmonic constraint of 10 kcal/mol and a collision frequency of 1.0 ps. Following heating, each system was subjected to a 500-ps equilibration, with the operating temperature held constant at 300 K. Additional characteristics, such as numerous atoms and pressure, were also kept constant, simulating an isobaric-isothermal ensemble. The Berendsen barostat was used to keep the system pressure at 1 bar (Basconi & Shirts, 2013; GonnetPedro, 2007).

The entire time spent on the MD simulations was 100 ns. The SHAKE algorithm was used in each simulation to constrict hydrogen atom bonds (Ryckaert, 2022; *Ryckaert, J.P., Ciccotti, G. and Berendsen, H.J. (1977) Numerical Integration of the Cartesian Equations of Motion of a System with Constraints Molecular Dynamics of n-Alkanes. Journal of Computational Physics, 23, 327-341. - References - Scientific Research Publishing, 2022*).

Each simulation employed a 2fs step size and an SPFP accuracy model. The simulations matched the isobaric-isothermal ensemble (NPT) with randomized seeding, a constant pressure of 1 bar maintained by the Berendsen barostat (Basconi & Shirts, 2013), a pressure-coupling constant of 2 ps, a temperature of 300 K, and a Langevin thermostat (GonnetPedro, 2007) with a collision frequency of 1.0 ps.

3.6.5 Post-Dynamic Analysis

3.6.5.1 *Binding Free Energy Calculations*

The Molecular Mechanics/GB Surface Area approach (MM/GBSA) was used to compute the free binding energy (Ylilauri & Pentikäinen, 2013). Binding free energy was averaged across 100000 snapshots taken from the 100ns trajectory. This approach computes the free binding energy (ΔG) for each molecular species (complex, ligand, and receptor) as:

$$\Delta G_{\text{bind}} = G_{\text{complex}} - G_{\text{receptor}} - G_{\text{ligand}} \quad (1)$$

$$\Delta G_{\text{bind}} = E_{\text{gas}} + G_{\text{sol}} - TS \quad (2)$$

$$E_{\text{gas}} = E_{\text{int}} + E_{\text{vdw}} + E_{\text{ele}} \quad (3)$$

$$G_{\text{sol}} = G_{\text{GB}} + G_{\text{SA}} \quad (4)$$

$$G_{\text{SA}} = \gamma \text{SASA} \quad (5)$$

The gas-phase energy is denoted by E_{gas} , which is made up of the internal energy E_{int} , the Coulomb energy E_{ele} , and the van der Waals energies E_{vdw} . The E_{gas} was calculated directly from the FF14SB force field terms. The energy contribution from the polar states, G_{GB} , and non-polar states, G_{sol} , were used to calculate the solvation free energy, G_{sol} . Using a water probe radius of 1.4, the non-polar solvation energy, G_{SA} , was calculated from the solvent-accessible surface area (SASA). In contrast, the contribution of the polar solvation, G_{GB} , was determined by solving the GB equation. S and T signify the solute's total entropy and temperature, respectively.

3.7 Materials for Pharmacokinetic Study

3.7.1. Chemicals and Drugs

- Acepromazine (10 mg/mL) injection, purchased from Hospira (Lake Forest, IL), was used as part of the anesthetic cocktail for jugular vein cannulation surgery.
- Bupivacaine HCl injection USP (0.5%, 5mg/mL), purchased from Hospira (Lake Forest, IL), was used to provide post-surgery analgesia to the animals.
- Deionized water, produced in the lab with a Barnstead TM Smart2Pure TM water purification system (Thermo Fisher Scientific, Waltham, MA), was used in OJT010 formulation.
- Formic Acid, purchased from Sigma-Aldrich (St. Louis, MO), was used to enhance the ionization of OJT010 in the LC-MS/MS method development.
- Heparin sodium injection (1000 units/mL), purchased from Hospira (Lake Forest, IL), was used as anticoagulant in animal experiments.
- Ketamine injection (100 mg/mL), purchased from Hospira (Lake Forest, IL), was used as part of the anesthetic cocktail for jugular vein cannulation surgery.
- LC-MS grade acetonitrile, purchased from J.T. Baker Chemical Co. (Phillipsburg, NJ), was used to prepare mobile phase for the quantification of OJT010 by LC-MS/MS.
- LC-MS grade water, purchased J.T. Baker Chemical Co. (Phillipsburg, NJ), was used to prepare mobile phase for the quantification of OJT010 by LC-MS/MS.

- LC-MS grade methanol, procured from Mallinckrodt Baker (Phillipsburg, NJ, USA), was used for solubility studies of OJT010.
- OJT010 (purity \geq 98%) was purchased from Thermofisher (Tewksbury, MA)
- Sodium chloride solution, 0.85 %, (normal saline) purchased from Sigma-Aldrich (St. Louis, MO), was used to dilute dosing solutions for animal dosing.
- OJT010-d5, purchased from Cayman Chemical (Ann Arbor, MI), was used as internal standard (IS) for LC-MS/MS method.
- Xylazine injection (100 mg/mL), purchased from Hospira (Lake Forest, IL), was used as part of the anesthetic cocktail for jugular vein cannulation surgery.

3.7.2 Supplies

- 1 cc sterile tuberculin slip tip syringes and PrecisionGlide® 23 G TW needles, purchased from Becton Dickinson & Co. (Franklin Lakes, NJ), were used during animal experiments for intra-venous dosing and blood sampling.
- Auto-sampler propylene injection vials (Clear; 100 μ L), purchased from ChromTech (Apple Valley, MN), were used to hold samples for injection in the LC-MS/MS assays.
- Auto-sampler propylene injection vials (Clear; 100 μ L), purchased from ChromTech (Apple Valley, MN), were used to hold samples for injection in the LC-MS/MS assays.

- Cotton tipped applicators (6”), purchased from Baxter Healthcare Co (McGaw Park, IL), were used during animal surgeries to stop bleeding and apply topical contents during surgery.
- Face masks, purchased from AlphaProTech, Inc. (Salt Lake City, UT), were worn while using chemicals and handling animals.
- Gauze (3 in x 3 in), purchased from Tyco Healthcare (Mansfield, MA), were used to suppress bleeding and clean-up incision sites during animal surgeries.
- Insulin syringe (1 mL, sterilized), purchased from Becton Dickinson & Co. (Franklin Lakes, NJ), were used for administration of anesthesia agents during animal experiments.
- Membrane filters (47 mm, 0.45 μ m, hydrophilic polypropylene, Pall Corp., Ann Arbor, MI) were used to filter mobile phase for LC-MS/MS analysis.
- Microcentrifuge tubes (clear), purchased from VWR (West Chester, PA), were used in sample preparation for microsomal incubations and LC-MS/MS analysis.
- Nylon 2/0 and 3/0 surgical sutures, purchased from Henry Schein Inc. (Melville, NY), were used during animal surgery to close incisions and secure the jugular vein cannula.
- Pipette tips (10 μ L, 20 μ L, 250 μ L, and 1000 μ L), purchased from Rainin Instrument (Oakland, CA), were used along with the appropriate mechanical pipettes for volumetric transfer of liquids.
- Polyethylene tube (I.D. 0.023”, O.D. 0.038”), purchased from Becton Dickson Intramedic & Co. (Franklin Lakes, NJ), were used for blood sampling via jugular vein cannula

- Powder-free latex examination gloves, purchased from VWR (West Chester, PA), were worn during all laboratory and animal experiments.
- Standard silicone tubing (I.D. 0.025", O.D. 0.047"), purchased from HelixMark (Carpinteria, CA), were used as the soft front of the polyethylene tubing.
- Syringe filters (0.45 µm, HPLC certified), purchased from VWR (Radnor, PA), were used to sterilize anesthesia cocktail.
- Syringes (1 ml, sterilized, single use), purchased from Becton Dickson & Co. (Sparks, MD), were used for blood sampling.

3.7.3 Equipment, Apparatus and Software

- Analyst® software v1.6.2, purchased from SCIEX (Foster City, CA), was used to control and acquire data from the LC-MS/MS system.
- Electronic Weighing Balances (AB204-S and AT261 Delta Range), purchased from Mettler Toledo (Columbus, OH), were used to weigh all solid-state excipients and drugs.
- Eppendorf Centrifuge 5427 R (Enfield, CT) was used to centrifuge samples and working solutions to enable collection of supernatants.
- Gastight glass syringe, purchased from Hamilton Company (Reno, NV), was used to tune the mass spectrometer parameters for OJT010 and IS.
- Sigma Plot v11.0, purchased from Graph Pad Software Inc. (La Jolla, CA), was used to generate plots and for statistical analysis of data.

- LC-MS/MS system consisting of the following was used for the quantification of OJT010
 - 6500+ Triple Quad LC-MS/MS system purchased from SCIEX (Foster City, CA)
 - ABN2ZA Tri Gas Generator purchased from Peak Scientific (Billerica, MA)
 - ExionLC AD UHPLC system (Sciex, Redwood City, CA).
 - Kinetex PS C₁₈ column (100 x 2.1 mm, 2.6 μm, 80 Å, Phenomenex Inc., Torrance, CA, USA)
- Phoenix WinNolin® 8.3, purchased from Certara (St. Louis, MO), was used to estimate pharmacokinetic parameters from rat data.
- Pipettes, purchased from Rainin Instrument (Oakland, CA) and Eppendorf (Hamburg, Germany), were used for volumetric measurements.
- Syringe Pump 11 PLUS, purchased from Harvard Apparatus (Holliston, MA), was used to tune the mass spectrometer parameters for OJT010 and IS.
- Vortex machines (Vortex-Genie® 2), purchased from Scientific Industries (Bohemia, NY), were used mix sample preparations.

3.7.4 Animals

The animal protocol (ES-IACUC-00) used in this work was reviewed and approved by the Institutional Animal Care and Use Committee (IACUC) at Texas Southern University. Additionally, all animal studies were conducted in compliance with the National Institute of Health “Guide for the Care and Use of Laboratory Animals, 8th Edition”. Experiments were carried out using adult male Sprague-Dawley rats (body weight 300 – 350 g) purchased from Envigo RMS, LLC, Alice, TX. Upon arrival, the animals were housed under normal conditions which includes free access to food and water, a room temperature environment with 12-hour light-dark cycles from 6 am to 6 pm daily.

These conditions were maintained for one week before starting animal experiments to allow for adequate acclimatization of the animal. The animals were implanted with a cannula tube in the left jugular under anesthesia and allowed to recover for 24 hours before initiating dosing.

3.8 Methods for Pharmacokinetic Study

3.8.1 LC-MS/MS Assay Development

A LC-MS/MS analytical method was developed to quantitate the concentrations of OJT010 in plasma and urine samples collected from pharmacokinetic studies of OJT010 in rats. The development of the method involved optimizing the mass-spectrometric settings to get the optimum signal-to-noise ratio, as well as optimizing the chromatographic conditions to assure the best selectivity and reduce matrix effect caused by interference in the biological matrix.

3.8.2 Chromatography

The liquid chromatography analysis was performed on the ExionLC™ AD UHPLC system (Sciex, Redwood City, CA). The chromatographic separation was achieved using a Kinetex PS C₁₈ column (100 x 2.1 mm, 2.6 μm, 80 Å, Phenomenex Inc., Torrance, CA, USA) with a gradient mobile phase at flow rate of 0.4 mL/min. The sample injection volume was 2 μL, and the mobile phase consisted of a gradient composition of water (0.5 mM ammonium acetate) (A) and acetonitrile (B). The time program of the gradient was as follows: Mobile Phase B was initially kept at 20% for 0.2 min, increased from 20% to 70% in the following 2.3 min, then kept at 70% for 1 min, increased from 70% to 98% in 0.5 min and kept at 98% for 0.5 min, then decreased from 98% to 20% in 0.2 min and kept stably at 40% for 0.8 min. (Table 4)

3.8.3 MS/MS Detection

The MS/MS analysis was performed on a 6500+ Triple Quad quadrupole mass spectrometer system equipped with a Turbo Ion Spray ion source (Sciex, Redwood City, CA). The hybrid triple quadrupole LIT (linear ion trap) mass spectrometer is equipped with a Turbo V™ ion source. Pure nitrogen used as curtain gas, and source and exhaust gases were generated by a Peak Scientific (GENIUS ABN2ZA) Tri Gas Generator. OJT010-d5 was used as internal standard (IS). The quantification was performed using multiple-ion reaction monitoring (MRM) in positive mode, with the transitions of m/z 379 \rightarrow 264 for OJT010 and m/z 384 \rightarrow 264 for IS. The source parameters were set as follows: ion spray voltage, 5200 V; ion source temperature, 550°C; nebulizer gas, 70 psi; heater gas, 70 psi; curtain gas, 45 psi; and the collision gas 11. The compound-dependent parameters for OJT010 and IS were optimized with entrance potential (EP), 5 V and 5 V; declustering potential (DP), 60 V and 60 V; collision energy (CE), 27 V and 30 V; and collision cell exit potential (CXP), 5 V and 5 V, respectively. Analyst® Software 1.6.3 (Redwood City, CA, USA) was used to control the LC-MS/MS system and analyze the data. the compound dependent electronic parameters for the MS/MS acquisition of OJT010 and IS are summarized in Table 5.

Table 1: Electronic Parameters for MS/MS Acquisition of OJT010 and IS

Parent	Transition (m/z)	Dwell Time (msec)	DP (V)	CE (V)	EP (V)	CXP (V)
OJT010	379 → 264	200	60	27	5	5
IS	384 → 264	200	60	30	5	5

3.8.4 Standard and Quality Control Samples

The stock solution of OJT010 was prepared by dissolving the solid compound in 100% methanol at a concentration of 1 mg/mL and was stored at $-20\text{ }^{\circ}\text{C}$ until it was used. The IS was prepared by dissolving OJT010-d5 in acetonitrile at the concentration of 1 mg/mL. The OJT010 working solutions were prepared by diluting the stock solution in 100% acetonitrile final concentrations of 10, 5, 1, 0.5, 0.10, 0.05, 0.025, .001, and 0.005 $\mu\text{g/mL}$. The IS working solution was prepared by diluting the 1 mg/mL stock solution with 100% acetonitrile to obtain a concentration of 10 ng/mL. A series of standard samples were prepared by spiking the working solutions (5 μL) into blank rat plasma or urine (45 μL) to obtain the following concentrations of OJT010: 0.05, 0.1, 2.5, 5, 10, 50, 100, 500, and 1000 ng/mL. The mixture was vortexed for 60 seconds and then centrifuged at 14,000 rpm for 20 minutes. The resulting supernatant was then transferred to an auto-sampler vial for LC–MS/MS analysis.

3.8.5 Plasma and Urine Sample Preparation

Plasma samples stored at -80°C were thawed at room temperature. An aliquot (50 μL) of plasma was extracted for OJT010 using protein precipitation by adding 250 μL of acetonitrile containing the internal standard (10 ng/mL). The mixture was vortexed for 60 s and centrifuged at 14,000 rpm for 20 min at 4°C . An aliquot of the supernatant was injected into the LC-MS/MS for quantitative analysis. The lung tissue samples were prepared by cutting whole lung into small pieces. The lung tissue pieces were weighed. Then 3 mL of water was added per gram of lung and homogenized using a handheld homogenizer. Lung samples were processed by taking an aliquot (50 μL) and extracted using protein precipitation by adding 250 μL of acetonitrile containing the internal standard (10 ng/mL).

3.9 Pharmacokinetic Studies

3.9.1 General Animal Procedures

Jugular vein cannulation was performed under anesthesia using an aqueous anesthetic cocktail composed of ketamine: acetopromazine: xylazine (50:3.3:3.3 mg/Kg) at a dose of 1 mL/Kg the day before the study. A cannula, composed of silicone elastic tubing (0.02" I.D. and 0.037" O.D.) was inserted into the right jugular vein, secured with a silk suture tunneled subcutaneously and exteriorized in the dorsal infrascapular area. The surgical incision was closed with surgical sutures. Cannula patency was maintained

by flushing the cannula line daily with 0.5 mL of sterile heparinized saline solution (100 units/mL).

3.9.2 Evaluation of Oral Bioavailability

A cross-over design was used in this study to evaluate the oral bioavailability of OJT010. Adult male SD rats (n=3) weighing 300 – 350 g were cannulated through the jugular vein under anesthesia one day before the study. Each rat received a 50 mg/kg intravenous dose of OJT010. Serial blood samples (100 μ L each) were collected from each rat before dose and at 0, 2, 5, 15, 30, 60, 90 minutes, and 2, 3, 4, 6, 10, 24, 28, 32 and 48-hours post dose. After blood centrifugation at 13,000 rpm for 3 minutes, the plasma supernatants were collected, and immediately stored in -80°C and analyzed within 14 days. We also collected urine samples up to 24 hours post dose and immediately stored in -80°C and analyzed within 14 days. Following a two-week washout period, the rats were fasted overnight and for four hours after receiving a 250 mg/kg oral dose of OJT010. Water was always available to the rats. Again, serial blood samples were collected before dose and at 0, 5, 15, 30, 45, 60, 90 minutes, and 2, 4, 6, 8, 10, and 24-hours post dose. Blood samples were centrifuged at 13,000 rpm for 3 minutes, and the supernatants were collected. Urine samples were collected up to 24 hours after dose. Urine and plasma samples were stored at -80°C and analyzed by LC-MS/MS analysis within 14 days. Under anesthesia rats were sacrificed and lung was collected at 24 hours post dose. Lung samples were stored at -80°C until analysis.

A multiple dosing design was used in this study to evaluate the oral steady-state concentrations of OJT010. Adult male SD rats (n=6) weighing 300 – 350 g were cannulated through the jugular vein under anesthesia one day before the study. Six Sprague-Dawley rats were randomly distributed into two OJT010 treatment groups; (a) 250 mg/kg and (b) 400 mg/kg. The rats in each group were administered a single oral dose of 250 mg/kg/day and 400 mg/kg/day, respective, consecutively for five days. Rats were fasted for at least 12 hour before and 4 hours after the last dose on Day 5. Serial pre-determined blood samples were collected at various time points as described in the previous single dose studies. Urine samples were collected up to 24 hours post dose. Serial blood samples (100 μ L each) were collected from each rat before dose and at 0, 5, 15, 30, 45 minutes, and 1, 1.5, 2, 4, 6, 8,10, 24 hours post last dose. After blood centrifugation at 13,000 rpm for 3 minutes, the plasma supernatants were collected, and immediately stored in -80oC and analyzed within 14 days. We also collected urine samples up to 24 hours post-dose and immediately stored in -800C and analyzed them within 14 days. LC-MS/MS analysis within 14 days. Under anesthesia rats were sacrificed and lung was collected at 24 hours post-dose. Lung samples were stored at –80 °C until analysis.

3.9.3 Pharmacokinetic Analysis

Plasma OJT010 concentration versus time data were analyzed for each rat using a non-compartmental model (WinNonlin 8.1, Pharsight Corp, Mountain View, CA). The

non-compartmental pharmacokinetic parameters derived after intravenous administration were maximum plasma concentration (C_0), terminal elimination half-life ($T_{1/2}$), systemic plasma clearance (Cl), volume of distribution (V_d), the total area under the plasma drug concentration-time curve from 0 to last sampled point (AUC_{Last}), the total area under the plasma drug concentration-time curve from 0 to infinity ($AUC_{0-\infty}$), mean residence time (MRT) as described below in detail:

- AUC_{Last} – The area under the plasma drug concentration-time curve from time zero to the last sampling time point was calculated using the trapezoidal method
- $AUC_{0-\infty}$ - The area under the concentration-time curve from time zero to infinity was calculated using the trapezoidal method from the plasma drug concentration vs time data from time zero to the last experimental time plus the excess area (from last experimental time to infinity).
- C_0 - Estimated initial plasma concentration of drug was determined by back extrapolation of plasma drug concentration at time 0 following intravenous drug administration.
- C_{max} - Maximum observed concentration, occurring at T_{max} . It is determined by observation of the plasma- concentration time profile following oral drug administration.
- T_{max} - Time of maximum observed concentration following oral drug administration. It is determined by observation of the entire concentration time- profile.

- K - The terminal phase rate constant was determined from the slope of the terminal linear segment of a semilogarithmic plot of plasma drug concentration vs. time.

- $T_{1/2}$ – The terminal half-life of the drug was calculated as

$$T_{1/2} = 0.693/K$$

- V_d - Volume of distribution was calculated as

$$V_d = \text{Dose} / (K \times \text{AUC}_{0-\infty})$$

- Cl – The total systemic clearance was calculated as

$$\text{Cl} = \text{Dose} / \text{AUC}_{0-\infty}$$

- MRT- The mean residence time was calculated using moment analysis according to the equation

$$\text{MRT} = \text{AUMC}_{0-\infty} / \text{AUC}_{0-\infty}$$

where $\text{AUMC}_{0-\infty}$ is the area under the first moment curve extrapolated to infinity and $\text{AUC}_{0-\infty}$.

- V_{ss} - The volume of distribution at steady state was calculated according to the following equation

$$V_{ss} = \text{Cl} \times \text{MRT}$$

- After extravascular administration, the following pharmacokinetic parameters were calculated using phoenix WinNonlin non-compartmental analysis:

- F - The absolute oral bioavailability was estimated according to the following equation:

- $$F\% = \frac{\text{AUC}_{\text{po/Oral dose}}}{\text{AUC}_{\text{iv/IV dose}}} \times 100\%$$

CHAPTER 4

RESULTS AND DISCUSSION

4.1 Effects of OJT010 and OJT009 on rhACE2 and Spike (RBD) Protein Interaction

The interaction between the human ACE2 and receptor-binding domain of SARS-CoV-2 spike protein is a crucial first step in the entry process required for the viral infectivity (Wrapp et al., 2020). Using an adapted *in vitro* enzyme-linked immunosorbent assay (ELISA) (RayBiotech, 2022), we evaluated the effect of OJT010 and OJT009 on the binding affinity of rhACE2 and RBD of S protein at concentrations ranging from 100 μ M to 100 nM. Prism graph pad version 8.4.3 was used to generate dose-response curves. We observed a unique bell shape curve for both compounds when fitted using a special bell-shaped curve model. OJT010 was more potent at disrupting the interaction between ACE2 and RBD than OJT009.

Surprisingly, the percent inhibition was greater at low concentrations of OJT010 than at high values. On the other OJT009, we observed an unexpected bell-shaped curve with activation and inhibition at opposite ends. OJT009 increased the binding of ACE2 and RBD at high concentrations of 100 and 50 μ M but blocked the interaction at low concentrations.

For both drugs, the bell-shaped model predicted two IC_{50} values. The dose-response curves for OJT009 and OJT010 are shown in Figures 8 and 9. Table 2 displays the IC_{50} values for each drug obtained in this assay.

Like our results in the presence of OJT009, Bradfeut al. observed a dose-dependent increase in cellular fusion. On the other hand, treatment with 50 μ M of OJT010 resulted in mild inhibition of SARS-CoV-2 activity but did not cause any enhancement in cellular fusion (SB et al., 2020). Honrich et al. also reported mild inhibition of SARS-CoV-2 replication with OJT010 (BF et al., 2021).

The findings of our study suggest that OJT010's mechanism action against SARS-CoV-2 comes from a direct antiviral effect rather than its predicted effects on TMPRSS2. Even though OJT009 and OJT010 are classed as TMPRSS2 inhibitors, current research has revealed that these two drugs do not directly block the TMPRSS2 activity (Shrimp et al., 2020). One plausible mechanism for antiviral action of OJT010 in SARS-CoV-2 could be inhibition of the interaction between ACE2 and the Spike protein, as reported by our study. More research is needed to understand the role of OJT010 in SARS-CoV-2.

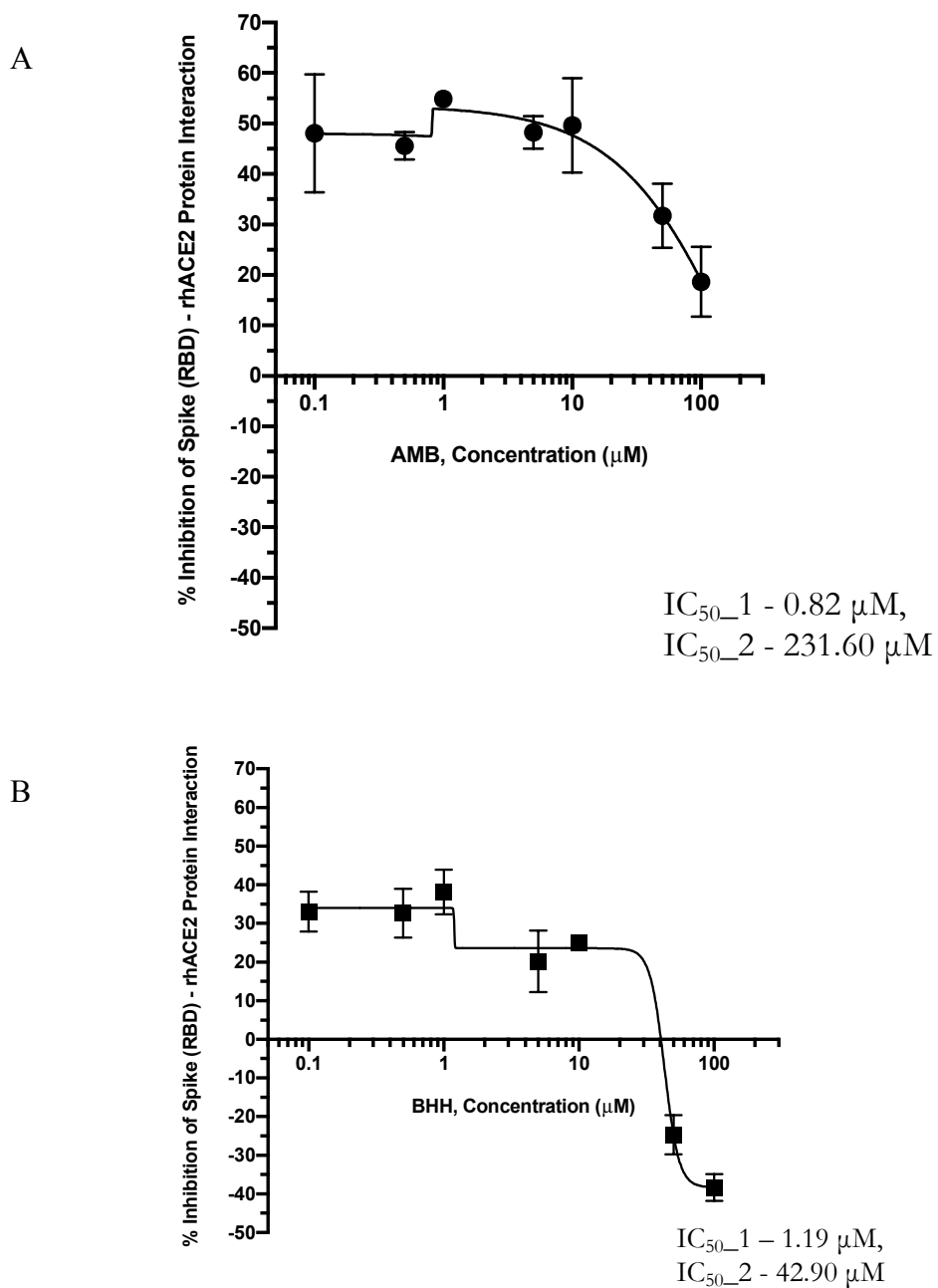


Figure 8. Effect of OJT010 and OJT009 on the interaction of rhACE2 and SARS-CoV-2 Spike (RBD) protein. A. OJT010 and B. OJT009

Table 2: Effect of OJT010 & OJT009 on the Binding of rhACE2 & RBD of Spike

Estimated Relative IC₅₀ against rhACE2 and RBD Interaction Assay		
Inhibitor ID	IC_{50_1} (μM)	IC_{50_2} (μM)
OJT010	0.82	231.6
OJT009	1.19	42.9

4.2 Effects of OJT010 and OJT009 on Exopeptidase Activity of ACE2

To further understand our RBD-ACE2 interaction assay results, we decided to investigate the role of both drugs on the exopeptidase activity of ACE2. ACE2 exopeptidase activity is vital for normal physiology, and long-term inhibition of ACE2 could be detrimental to cardiovascular health (Ni et al., 2020). Therefore, to rule out ACE2 inhibition by our drugs we determined the effect of OJT010 and OJT009 on the exopeptidase activity of rhACE2 using an adapted fluorometric assay (BPSBioscience, 2022). We found that OJT010 doesn't inhibit the exopeptidase activity of rhACE2 even at a very high concentration. On the other hand, OJT009 completely inhibited the exopeptidase function of ACE2 at high concentrations from 50 μM to 500 μM with an IC₅₀ value of 25.98. Surprising at a low concentration from 0.1nm to 10 μM, OJT009 had no activity against ACE2. To our knowledge, these results revealed for the first time that OJT010 doesn't

inhibit the exopeptidase activity rhACE2, while OJT009 inhibits its function at high and. Figure 9 shows the dose-response curve for OJT010 and OJT009 against ACE2 activity.

The behavior of OJT009 in the two biochemical assays; ACE2 exopeptidase activity and rhACE2 and RBD interaction shed light on their mechanism of action. At a high concentration (above 50 μ M), OJT009 inhibits the ACE2 activity but enhances the binding of ACE2 with RBD. While at a low concentration, it does not affect ACE2 activity but disrupts the interaction of ACE2 and RBD. According to these findings interactions of these compounds with ACE2 modulate the extent of binding between ACE2 and RBD.

ACE2 has a bound chloride ion in its structure, which plays an essential role in substrate hydrolysis by ACE2 (Vickers et al., 2002). The presence of chloride and fluoride ions activate ACE2 and enhances its exopeptidase activity. Furthermore, chloride ion determines the confirmation of the enzyme in native and inhibitor bound form (Towler et al., 2004).

OJT010 is known to increase chloride conductance in cystic fibrosis. In our ACE2 exopeptidase assay in the presence of OJT010, we saw an enhancement in the exopeptidase activity. However, activation of ACE2 by OJT010 was not dose dependent. More research is needed to prove the results obtained in our study.

Additional ions play an important role in determining the strength and stability of RBD and ACE2 binding. It may be possible that OJT010 and OJT009 work by modulating ions concentrations which cause conformational changes in the structure of ACE2 and make it less receptive for RBD binding. However, this is just a hypothesis, and further X-ray crystallography studies are needed to understand the exact mechanism of action. Nevertheless, our findings reveal a new pharmacologic mode of action and novel target for OJT010 and OJT009.

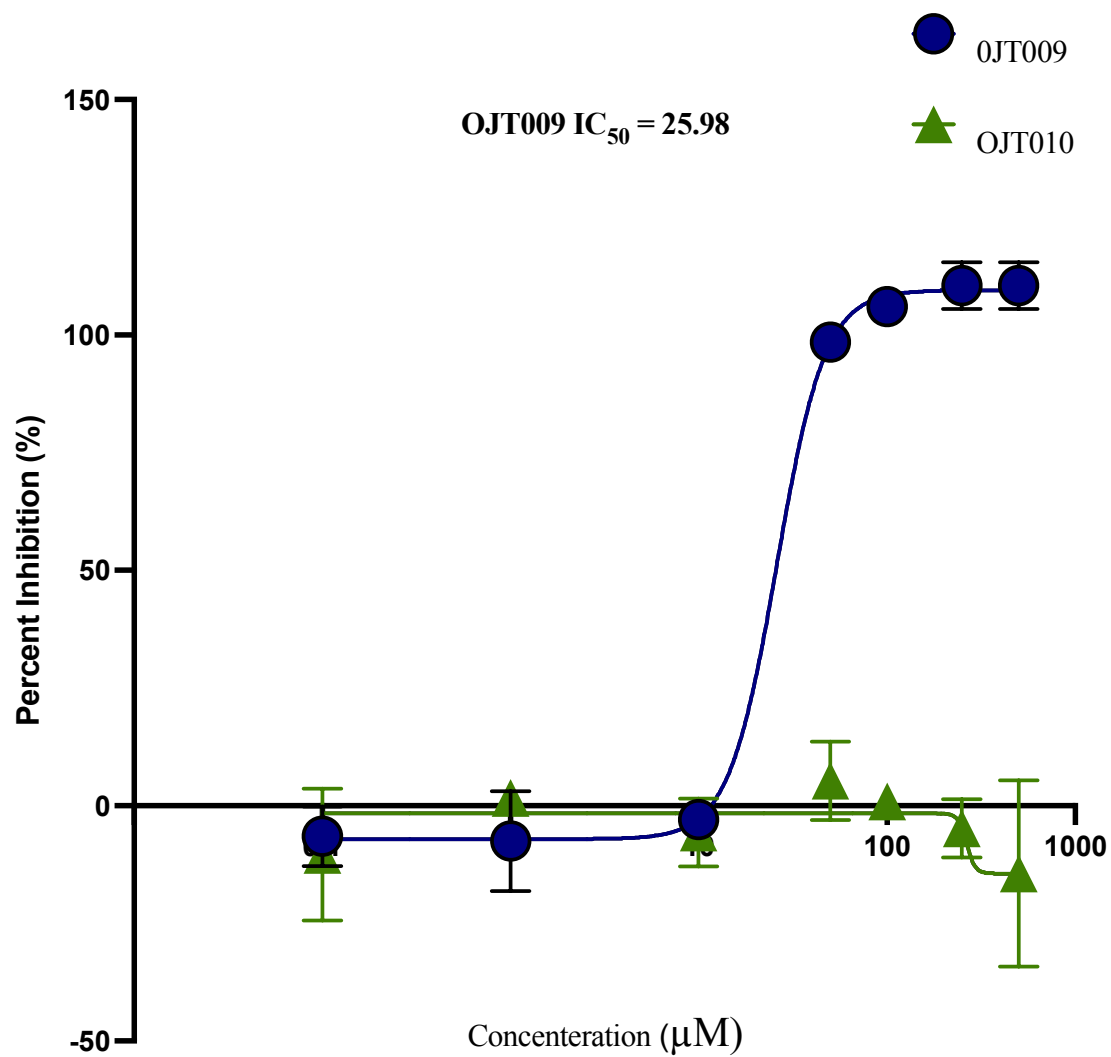


Figure 9: Effect of OJT010 and OJT009 on the Exopeptidase Activity of ACE2.

4.2 Effects of OJT010 on Exopeptidase Activity of ACE

Earlier in the pandemic, many controversial reports came out concerning the role of ACE inhibitors (ACEIs) in COVID-19. Many believed that ACEIs will lead to overexpression of ACE2, which will result in more severe infection. Conversely, observational data from COVID-19 patients showed better outcomes with ACEIs, leading to speculations that they will prevent Ang II-mediated pulmonary inflammation and reduce acute lung injury. To determine if OJT010 interacts with ACE, we examined the role of OJT010 on the exopeptidase activity of ACE. Like the findings of the ACE2 assay, OJT010 does not inhibit the activity of ACE. Even in the presence of very high concentrations of OJT010 such as 500 μM , ACE was 100% active.

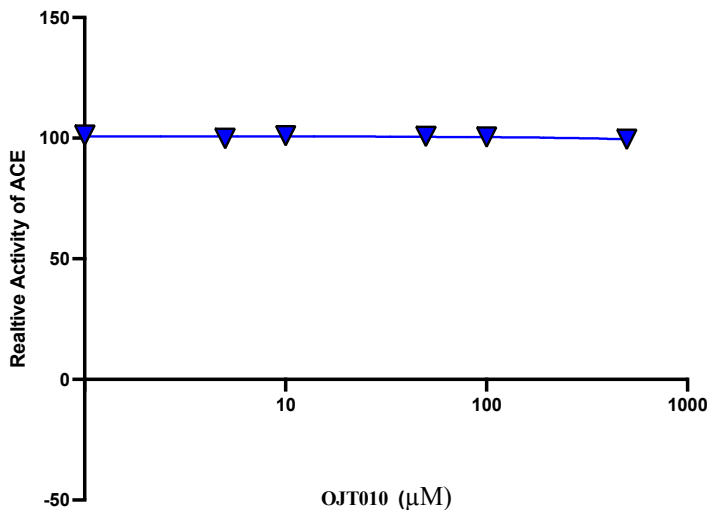


Figure 10: Effect of OJT010 on the Exopeptidase Activity of ACE

4.3 Efficacy of OJT010 against SARS-CoV-2 and Spike (B.1.617.2 Delta Variant) in a Pseudo virus assay

Based on the behavior of two drugs in the biochemical assays, we decided to move forward with OJT010 for two reasons. First, it prevents the binding of spike protein with RBD and doesn't enhance ACE2 and RBD binding as seen with OJT009. Second, it has no inhibitory activity against host receptor ACE2.

Therefore, we assessed whether OJT010 can block the infection of cells with spike Pseudotyped Lentivirus particles. A preliminary screen was done with four concentrations ranging from 10 μ M to 100 μ M. Interestingly OJT010 effectively blocked the entry of pseudo spike protein into the cells. We saw a dose-dependent neutralization of viral particles with increasing concentrations. OJT010 at 50 μ M showed a close to 50% reduction of the viral entry (Table 3). This assay further validates the results from biochemical assays that the interaction of OJT010 with ACE2 and RBD is part of its mechanism of action for SARS-CoV-2 neutralization.

Next, we evaluated the efficacy of OJT010 to neutralize the B.1.617.2 Delta Variant of SARS-CoV-2. A similar assay was performed with spike pseudo-type lentiviral particle-containing B.1.617.2 Delta Variant gene. Interestingly at the concentrations tested, OJT010 retained similar potency as of wild type SARS-CoV-2. OJT010 blocked the entry of viral particles by 50% at 50 μ M and 100% at 100 μ M. Surprisingly, OJT010 was

slightly more potent against the delta variant of SARS-CoV-2 than the wild-type virus (Table 3).

Given that Pseudotyped assay only measures the effect of the compound on preventing the entry of spike protein into the cells, it further substantiates our hypothesis that OJT010 interacts with the entry receptors. Further studies are needed to identify the actual target of OJT010 in the SARS-CoV-2 inhibition pathway. To our knowledge, this is the first study revealing a new mechanism of action for OJT010 in regards to ACE2-RBD interaction in SARS-CoV-2 pathogenesis.

Table 3: Effect of OJT010 on the SARS-CoV-2 and Delta Variant Pseudo typed Lentivirus Infection in ACE2 HEK-293 cells

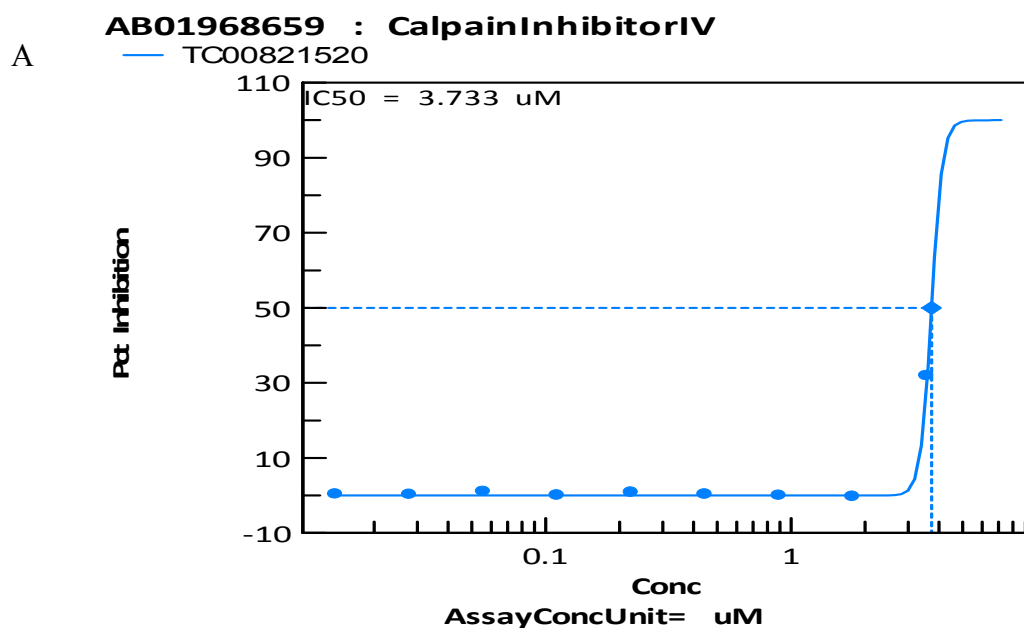
Percent (%) Inhibition of Pseudo virus Entry in HEK293 Kidney Cells		
Percent Inhibition	SARS-CoV-2	B.1.617.2 Delta Variant
Conc (μ M)	OJT010	OJT010
100	89	95
50	46	48
25	12	19
10	2	6

4.4 Efficacy of OJT010 against SARS-CoV-2 Infection-Induced Cytopathic Effect (CPE) in Vero E6 cells

To determine whether the results obtained in biochemical, and Pseudo typed assay also apply to SARS-CoV-2 infection *in vitro*. We evaluated the antiviral activity of OJT010 using a standard luminescent-based high-throughput screening (HTS) platform for SARS-CoV-2 infection-induced CPE in African Green Monkey Kidney Vero E6 cells (CB et al., 2008; WE et al., 2007). As expected, the treatment with OJT010 inhibited SARS-CoV-2 infection-induced CPE *in vitro* with a 50% Inhibitory Concentration (IC₅₀) value at about ~150 µM. The IC₅₀ obtained in this assay is almost two-fold higher than the IC₅₀ in the Pseudotyped assay. One reason for the variability in IC₅₀ values is the use of different cell lines. In the Pseudo virus assay, we used HEK293 kidney cells, While VeroE6 cells were used in the CPE assay. Moreover, Pseudotyped lentiviral assay only measures the entry of the spike particles into the cell. It doesn't quantify viral replication and other viral factors essential in the SARS-CoV-2 infection pathway. Even though VeroE6 cells are often used for SARS-CoV-2 infection and propagation, they were originally obtained from the African green monkey kidney and hence did not represent an ideal model for SARS-CoV-2 infection because it targets mainly the respiratory cells from the human lung. Moreover, the CPE assay is an indirect measure for viral replication by determining cell viability after the infection.

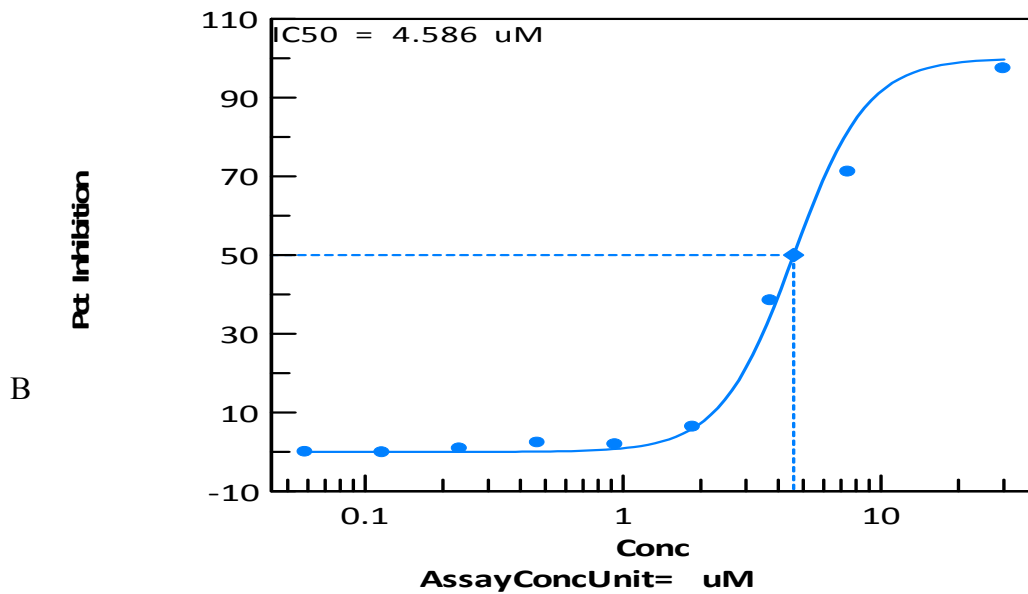
In addition to OJT010, we evaluated the antiviral activity of four known inhibitors SARS-CoV-2 as positive controls for the current assay: Calpain Inhibitor IV,

Chloroquine, Remdesivir, and Aloxistatin. The IC_{50} values for most of the reference compounds (Calpain Inhibitor IV (3.73 μM), Chloroquine (8.85 μM), and Remdesivir (16 μM)) and Aloxistatin (4.58 μM) were significantly lower than the IC_{50} values for OJT010. The IC_{50} values for the reference substances obtained in our assay were like previously reported IC_{50} (Chen et al., 2020; OA et al., 2021; M. Wang et al., 2020). Figure 10 shows the dose-response curve for OJT010 and reference compounds against SARS-CoV-2 infection-induced cytopathic effect. Table 4 shows the structure and effective concentration for the reference compounds.

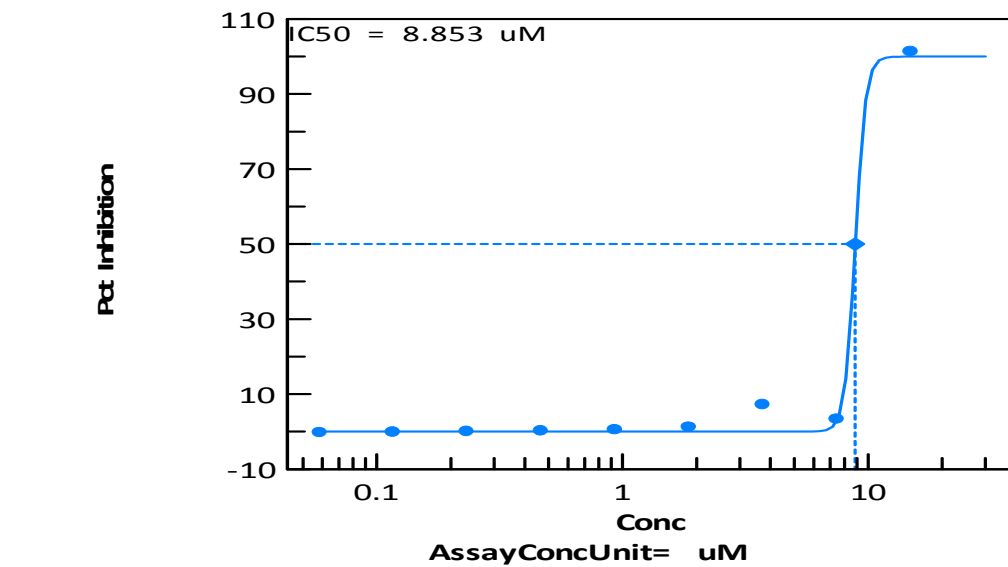


AB01955411 : E64d (Aloxistatin)

— TC00821520

**AB00053436 : Chloroquine**

— TC00821520



D

AB01952209 : Remdesivir

— TC00821520

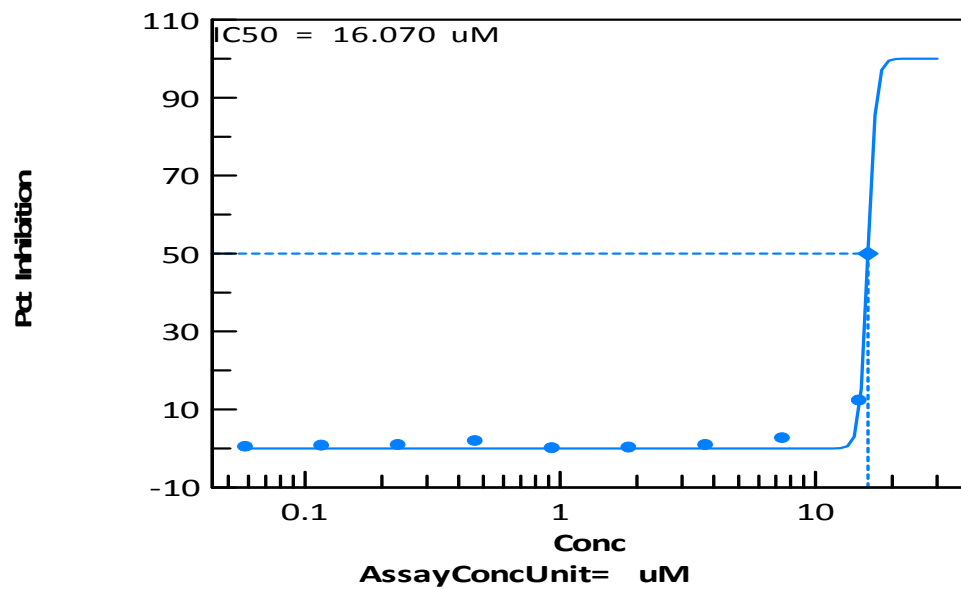


Figure 11: Efficacy of Reference Inhibitors against SARS-CoV-2 Induced Cytopathic Effect (CPE) in Vero E6 cells: A Calpain Inhibitor IV, B, Chloroquine, C.E64d (Aloxistatin), D. Remdesivir.

Table 4: Activity of OJT010 and Reference Compounds against SARS-CoV-2 Induced Cytopathic Effect in Vero E6 Cells

Inhibitor ID	IC ₅₀ (μM)	Maximum Inhibition (%)	Concentration at Maximum % Inhibition (μM)
OJT010	>150	49.87	150
CalpainInhibitorIV	3.73	115.91	7.17
E64d (Aloxistatin)	4.59	130.81	15
Chloroquine	8.85	114.51	30
Remdesivir	16.07	120.89	30

4.5 Cytotoxicity Effects of OJT010 in Vero E6 cells

We measured the cytotoxicity of OJT010 and reference compounds using a Cell Titer-Glo Luminescent Cell Viability Assay (WE et al., 2007) in Vero E6 cells and observed the 50% cytotoxic concentration (CC_{50}) of OJT010 was 183.71 μ M. At the concentration of 300 μ M, the percent viability was 0.55%, while maximum viability of 96 % was seen at a low concentration of 0.59 μ M. The CC_{50} values were also obtained for the reference compounds. For reference compounds, the maximum tested concentration was 30 μ M. Figure 11 shows the cytotoxicity of OJT010 in VeroE6 cells, and Table 5 represents the cytotoxicity and percent viability of cells for OJT010 and reference compounds.

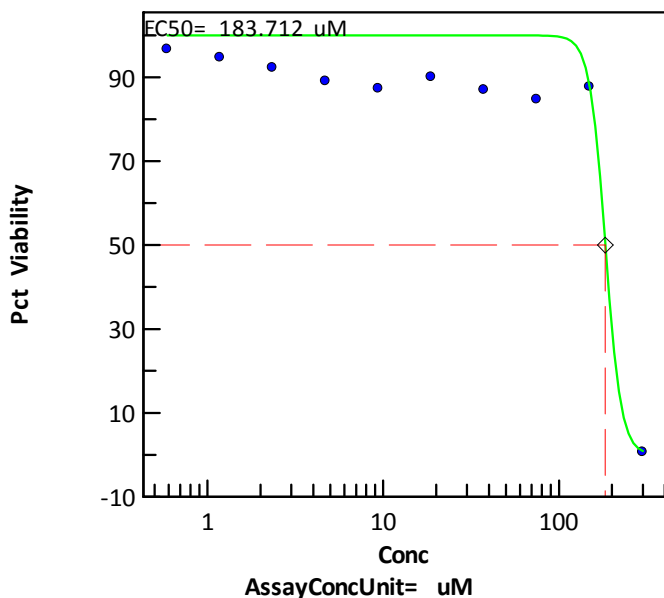


Figure 12: Cytotoxicity of OJT010 in VeroE6 cells

Table 5: Cytotoxicity of OJT010 in Vero E6 Cells, in Comparison to Reference Inhibitors of SARS-CoV-2

Inhibitor ID	Cytotoxicity CC ₅₀ (μM)	Minimum Viability (%)	Concentration at Minimum % Viability (μM)	Maximum Viability (%)	Concentration at Maximum % Viability (μM)
OJT010	183.71	0.55	300	96.64	0.59
CalpainInhibitorIV	>7.17	99.77	0.028	106.84	0.056
E64d (Aloxistatin)	>30.00	93.02	0.117	106.71	0.234
Chloroquine	>30.00	90.50	3.750	99.66	0.469
Remdesivir	>30.00	91.15	0.117	100.73	3.750

4.6 Effect of OJT010 on the Replication of SARS-CoV-2 Nanoluciferase Reporter

Virus Assay 549 cells

After determining the IC_{50} in CPE, we measured the potency of OJT010 in inhibiting the viral replication in A549 cells using Nanoluciferase Reporter Virus Assay (NLRV). A549 cells are human epithelial lung cells that are optimized to express AEC2. Unlike CPE, Nanoluciferase assay is a direct measure of viral replication, and efficacies were evaluated by quantifying the viral level in the cells. Moreover, CPE assay is done veroE6; in contrast, NLRV is done A549 lung cell line, representing a closer model for SARS-CoV-2 infection *in vivo*.

In the NLRV assay, the EC_{50} of OJT010 is 47 μ M compared to 150 μ M in the CPE assay. The EC_{50} obtained by the NLRV assay is very close to what we have seen in the Pseudotyped lentiviral assay. In addition to OJT010, we also evaluated the antiviral activity of other inhibitors SARS-CoV-2 as positive controls for the current assay: Calpain Inhibitor IV, Chloroquine, Remdesivir, Paxlovid, and Molnupiravir. Similar to OJT010, reference compounds were also more potent in this assay compared to the CPE assay. The IC_{50} values for most of the reference compounds (Calpain Inhibitor IV (.0005 μ M), Chloroquine (3.3 μ M), and Remdesivir (3.3 μ M), Paxlovid (0.05 μ M), and Molnupiravir (4.2 μ M) were significantly lower than the IC_{50} values for OJT010. Figure 12, and 13 shows the dose-response curve for OJT010 and reference compounds against SARS-CoV-2 replication Nanoluciferase Reporter Virus Assay 549 cells. Table 6 shows the IC_{50} value of OJT010 in comparison to reference compounds.

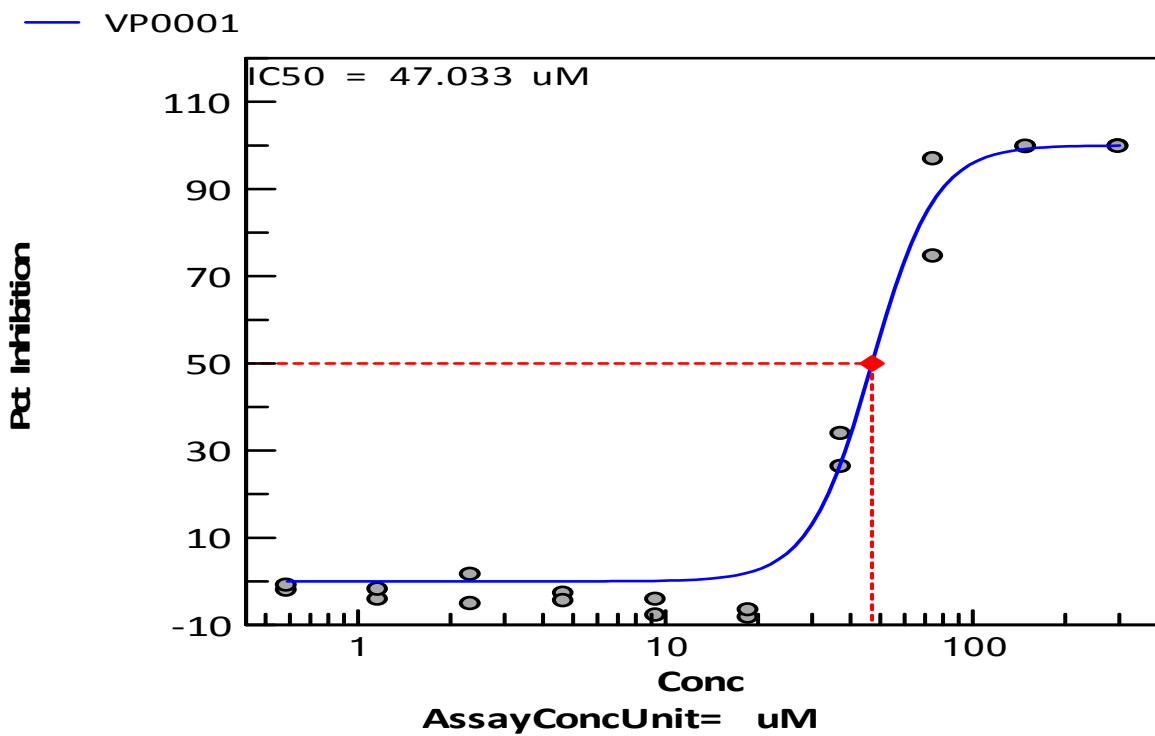
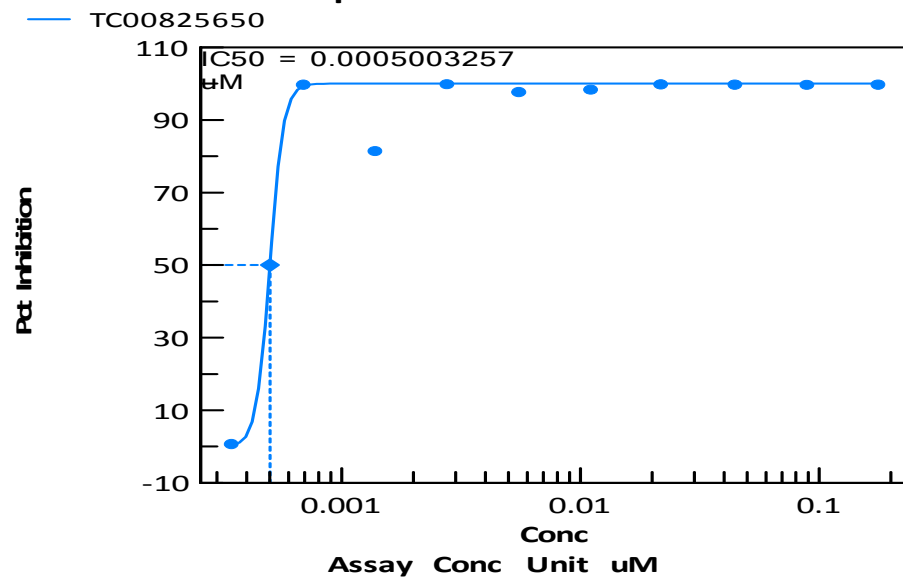
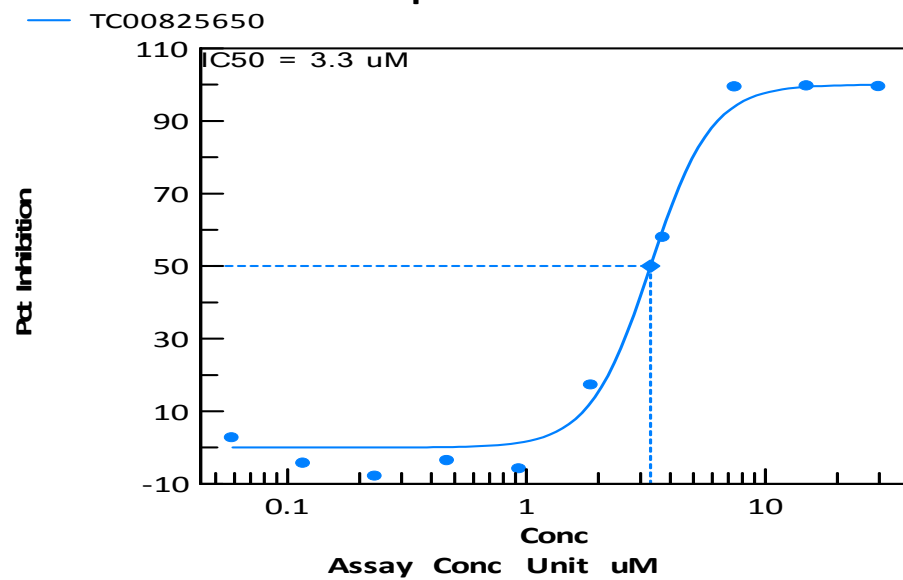
AB01973869 : OJT2101

Figure 13: Efficacy of OJT010 against SARS-CoV-2 in Nanoluciferase Reporter Assay in A549 cells

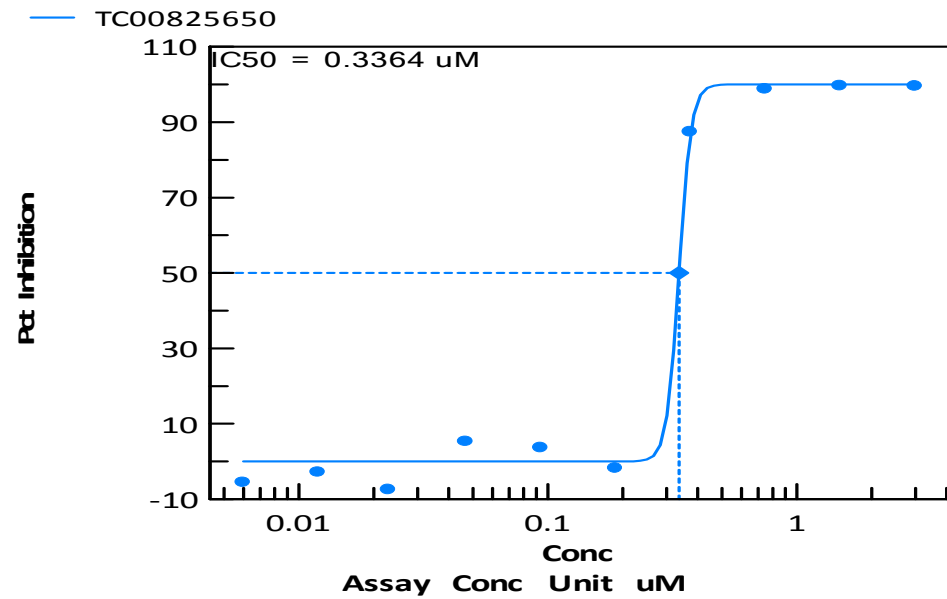
A

AB01968659 : CalpainInhibitorIV

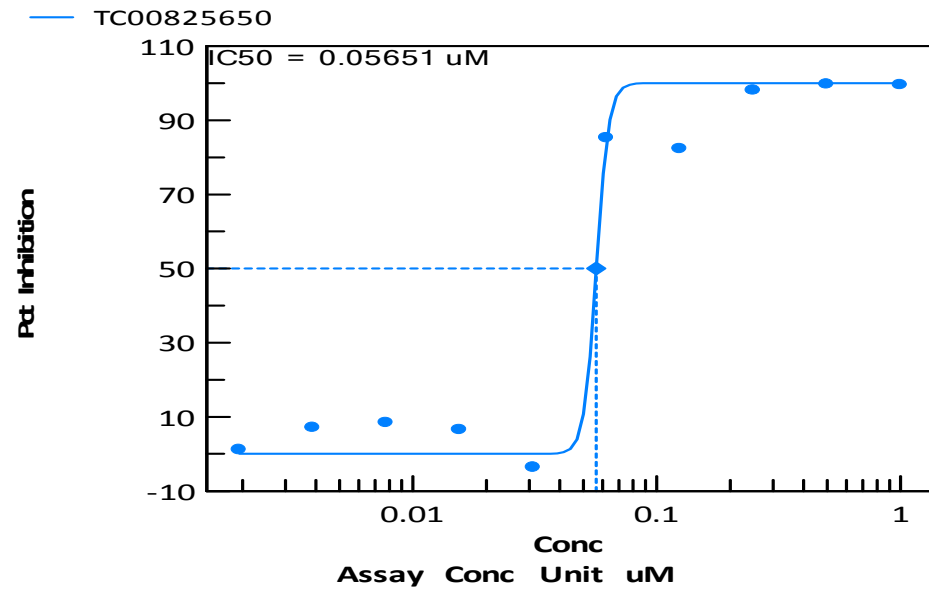
B

AB00053436 : Chloroquine

C

AB01952209 : Remdesivir

D

AB01973774 : PF-07321332

E

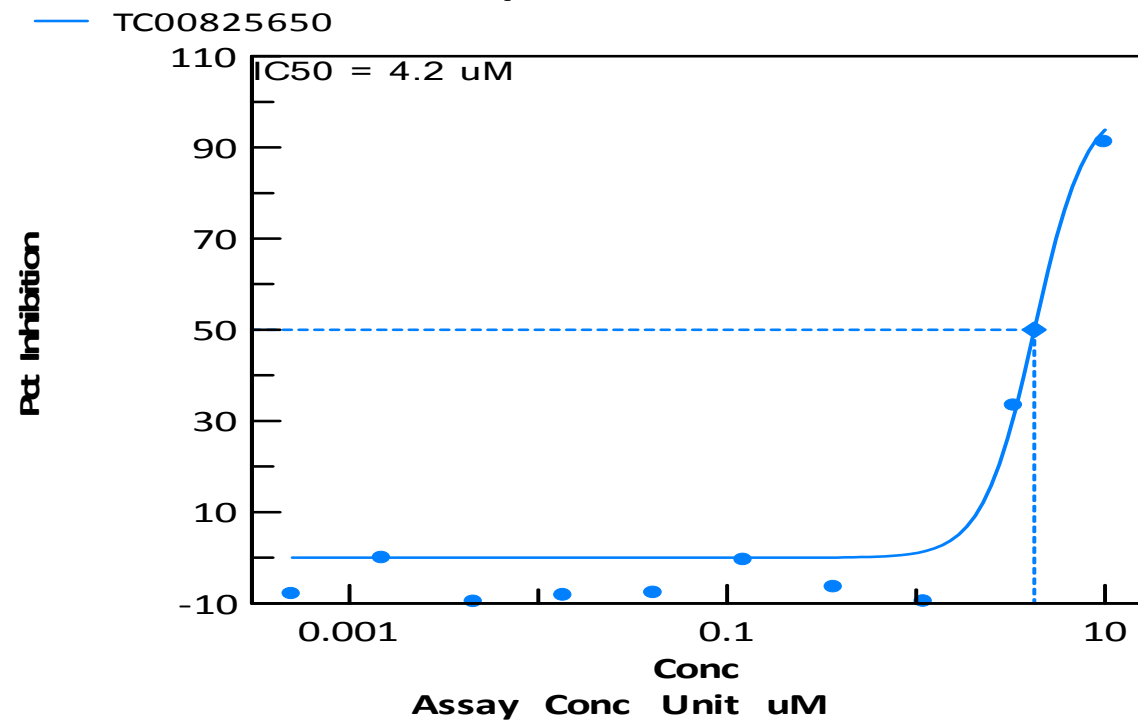
AB01973775 : Molnupiravir

Figure 14: Efficacy of Reference Inhibitors against SARS-CoV-2 NLRV in Vero E6 cells: A CalpainInhibitorIV, B, Chloroquine, C. Remdesivir, D. Paxlovid, E. Molnupiravir

Table 6: Activity of OJT010 and Reference Compounds against SARS-CoV-2 infection using NLRV assay in A549 lung cells

Inhibitor ID	IC ₅₀ (μ M)	Maximum Inhibition (%)	Concentration at Maximum % Inhibition (μ M)
OJT010	47.33	99.73	300
CalpainInhibitorIV	0.0005	99.56	.0028
PF-07321332	0.057	99.67	0.5
Chloroquine	3.3	99.53	15
Remdesivir	0.336	99.58	1.5
Molnupiravir	4.2	91.12	10

4.7 Cytotoxicity of OJT010 in A549 lung Cells using NLRV Assay

We also obtained the CC_{50} for OJT010 and reference compounds in A549 cells. The cytotoxic concentration obtained in this assay was 137.18 μM a little less than the CPE assay. However, it was still very high compared to the reference compounds. At 300 μM , only 0.14% of cells were viable. Cytotoxicity for OJT010 and reference compounds are shown in Table 6. Figure 14 shows a graph for CC_{50} of OJT010 in A549 cells

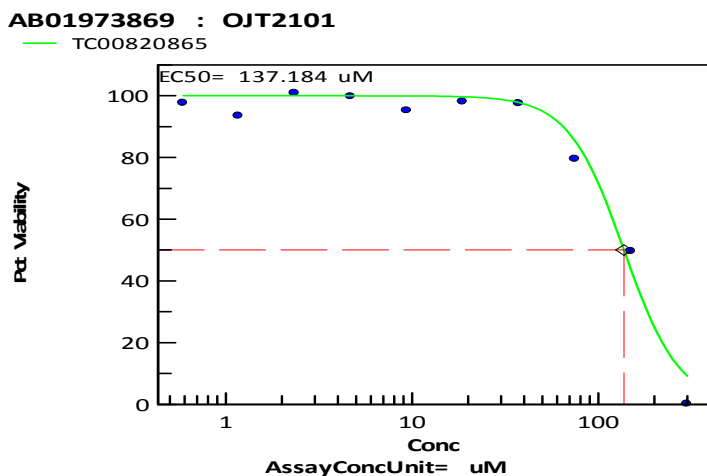


Figure 15: Cytotoxicity of OJT010 in A549 Lung Cells

Table 7: Cytotoxicity of OJT010 in A549 Cells, in comparison, to Reference Inhibitors of SARS-CoV-2

Inhibitor ID	Cytotoxicity CC ₅₀ (μM)	Minimum Viability (%)	Concentration at Minimum % Viability (μM)	Maximum Viability (%)	Concentration at Maximum% Viability (μM)
OJT010	137.44	0.14	300	100	2.34
CalpainInhibitorIV	>0.179	77.49	.0056	94.37	.090
Chloroquine	18.37	9.11	30	117.48	.023
Remdesivir	>3	84.65	0.094	95.46	.006
Paxlovid	>1	89.51	0.004	101.24	1
Molnupiravir	>10	88.88	0.014	98.56	.002

4.8 Efficacy of OJT010 against B.1.617.2 Delta Variant Infection-Induced Cytopathic Effect (CPE)

To validate the preliminary results of the Pseudotyped delta virus assay, we assessed the efficacy of OJT010 in inhibiting delta viral replication in CPE assay. A luminescent-based high-throughput screening (HTS) platform was used to evaluate the antiviral activity of OJT010 against delta variant of SARS-CoV-2 infection-induced CPE in African Green Monkey Kidney Vero E6 cells. We found that OJT010 inhibited B.1.617.2 Delta Variant infection-induced CPE *in vitro* with a 50% Inhibitory Concentration (IC₅₀) value at about 98 µM. The results were similar to what we saw earlier in the Pseudotyped assay. OJT010 is more potent against B.1.617.2 Delta Variant than wild typed SARS-CoV-2. In addition, to OJT010, we also tested the antiviral activities of known SARS-CoV-2 inhibitors as reference compounds: The IC₅₀ values for the majority of the reference compounds (Calpain Inhibitor IV (0.124 µM), Chloroquine (8.3 µM), PF-07321332+EI (0.029 µM), Remdesivir+Pfz EI (0.17 µM), PF-07321332 (1.98 µM), E64d (Aloxistatin) (9.84 µM) and Remdesivir (8.24 µM) were lower than the IC₅₀ values for OJT010. Figure 15 and 16 shows the IC₅₀ dose-response curve for OJT010 and reference compounds respectively. Table 8 shows the efficacy of OJT010 in comparison to reference compounds.

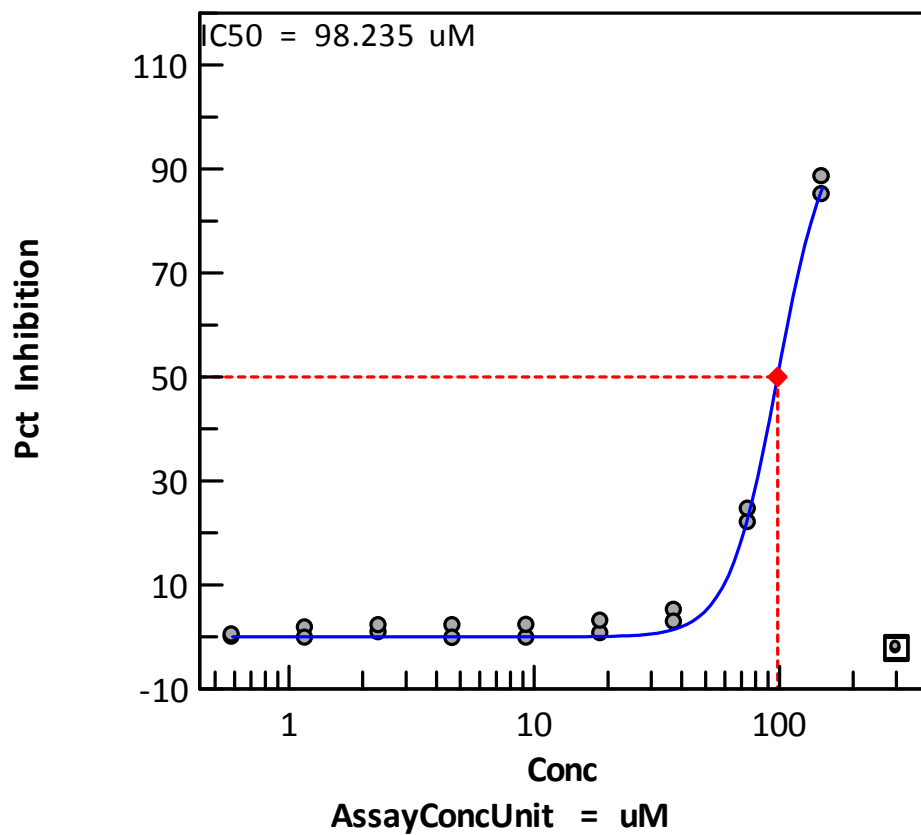
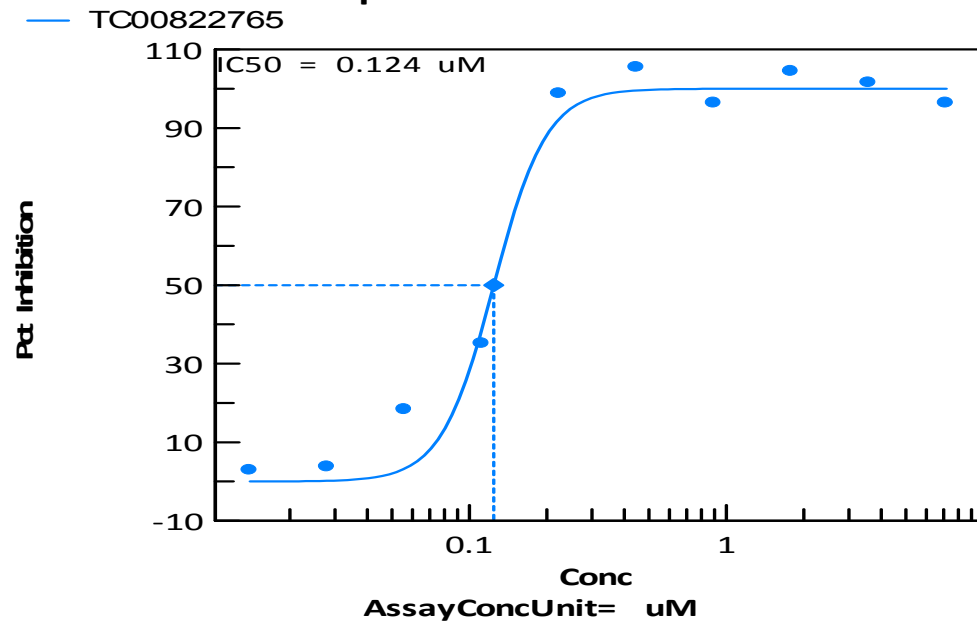
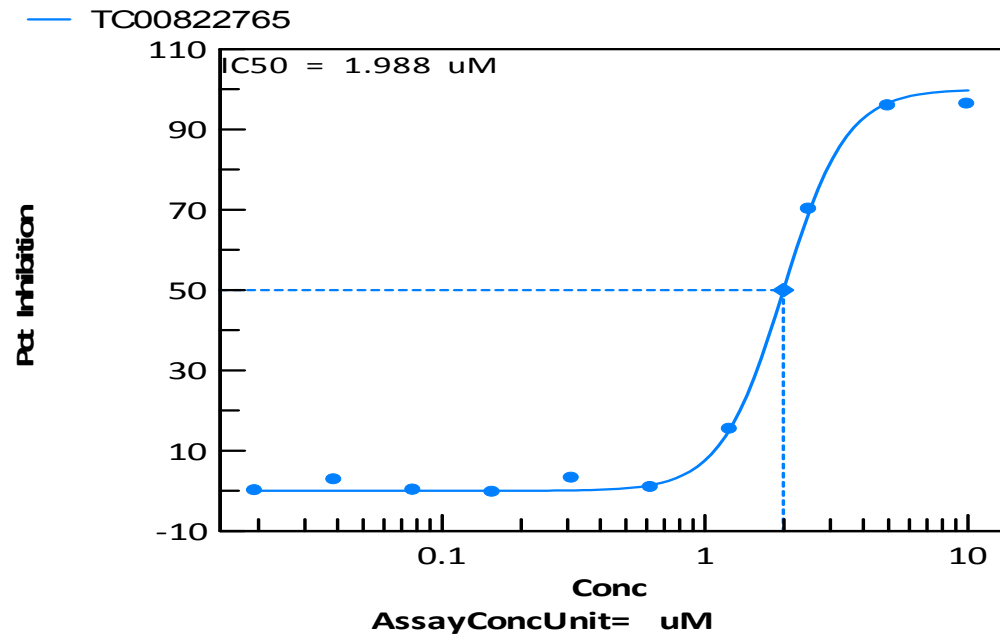


Figure 16: Efficacy of OJT010 against Delta Variant of SARS-CoV-2 in Infection Induced Cytopathic Effect (CPE) assay

A

AB01968659 : CalpainInhibitorIV

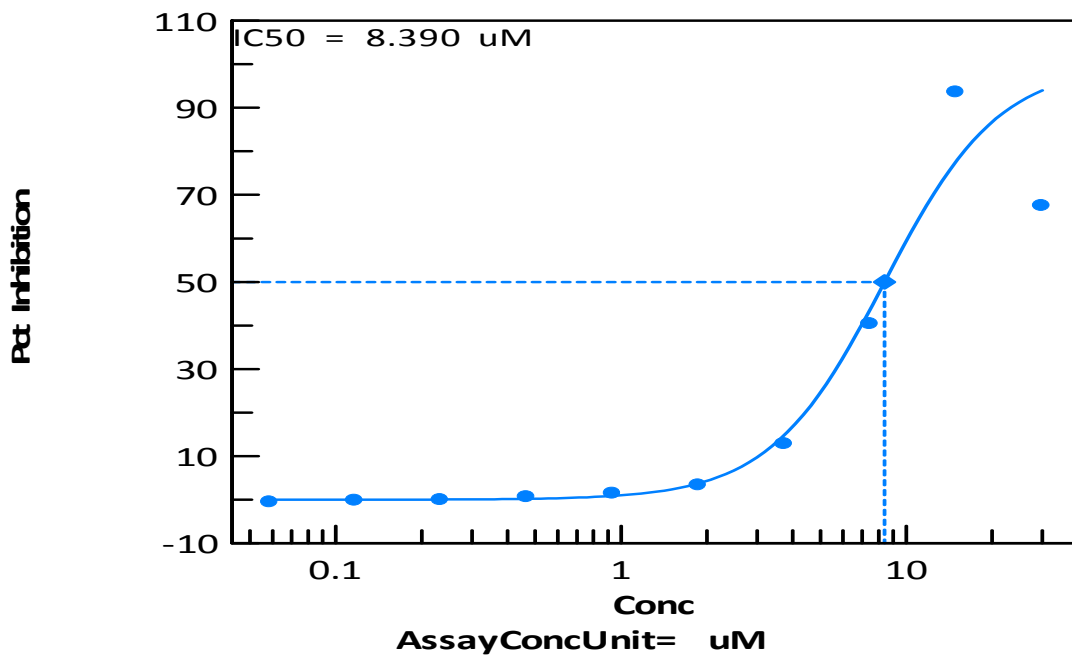
B

AB01973774 : PF-07321332

C

AB00053436 : Chloroquine

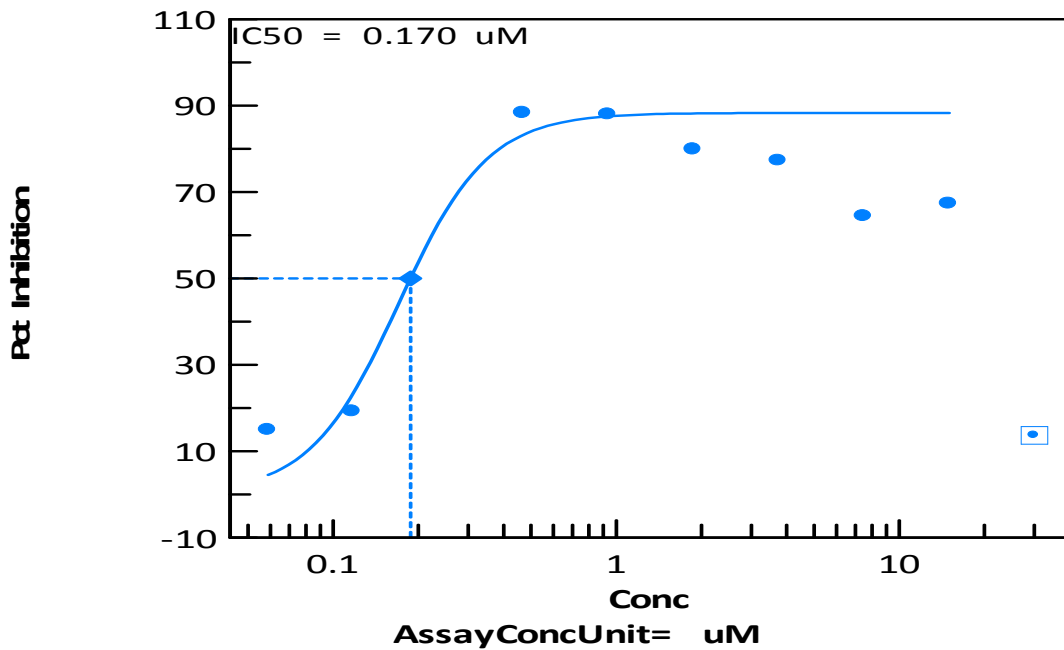
— TC00822765



D

AB01952209 : Remdesivir+Pfz EI (6)

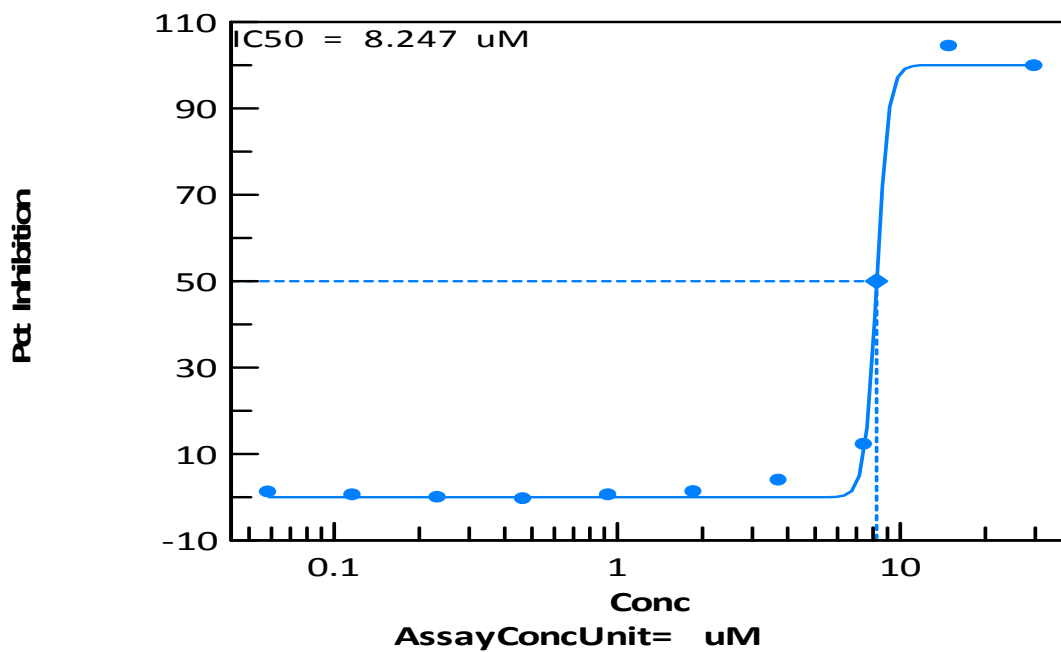
— TC00822765



E

AB01952209 : Remdesivir

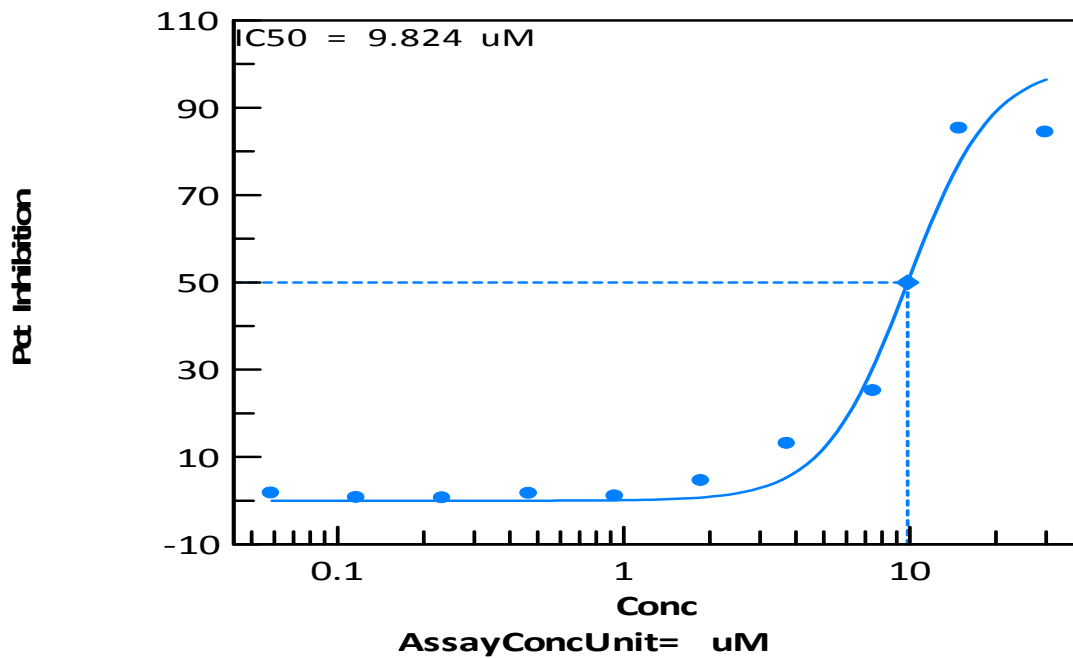
— TC00822765



F

AB01955411 : E64d (Aloxistatin)

— TC00822765



G

AB01973773 : PF-07321332+EI

— TC00822765

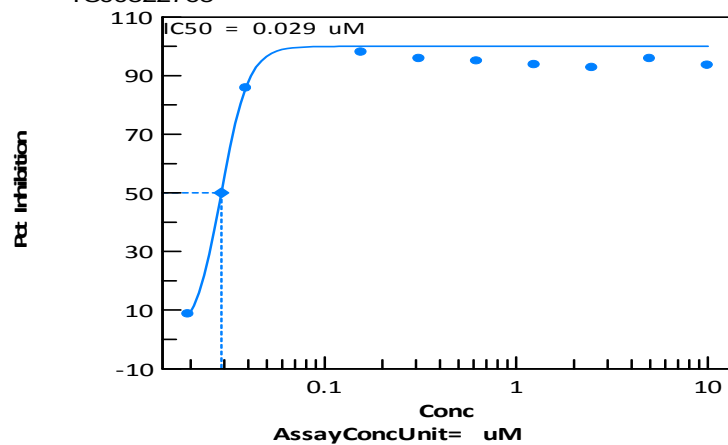


Figure 17: Efficacy of Reference Inhibitors against Delta SARS-CoV-2 CPE in Vero E6 cells: A CalpainInhibitorIV, B, PF-07321332, C. Chloroquine, D. Remdesivir+Pfz EI, E. Remdesivir, F E64d (Aloxistatin), G PF-07321332+EI

Table 8: Activity of OJT010 and Reference Compounds against Delta Variant of SARS-CoV-2 in CPE assay

Inhibitor ID	IC ₅₀ (μM)	Maximum Inhibition (%)	Concentration at Maximum % Inhibition (μM)
OJT010	98.23	88.38	150
CalpainInhibitorIV	0.124	105.43	0.45
PF-07321332	1.98	96.28	10
Chloroquine	8.3	993.48	15
Remdesivir	8.24	104.26	15
PF-07321332 + EI	0.029	116.90	.08
Remdesivir + Pfz EI	0.170	88.29	.47
E64d (Aloxistatin)	9.82	85.17	15

4.9 Effect of Combination of Remdesivir and OJT010 on the Replication of SRAS-CoV-2 in NLRV assay

We determine the effect of the combination of OJT010 and Remdesivir on SARS-CoV-2 replication at the same concentration as monotherapy. We used the Zero interaction potency (ZIP) model to characterize the interactions between the two drugs. This model evaluates drug response by comparing drug response curves between individual drugs and their combination. A synergy score obtained in this assay ranges from -10 to 10. It can be interpreted as an average increase in drug response due to drug interaction. For example, a synergy score of 10 corresponds to a 10% response beyond expectations. Based on the score obtained, drugs are classified as antagonist, additive and synergistic. Three major score windows; (A) Score of (-10) represent antagonistic behaviour, (b) Scores between -10 to 10 are likely due to being an additive effect of drugs on each other, while (3) Scores greater than 10 represents synergism between the two compounds.

In our study, we obtained a combined score of 0.37. This means that drugs are showing an additive effect on each other. We observed an additive effect of remdesivir on OJT010. Increasing concentrations of remdesivir (0-.2 μM) potentiated the effect of OJT010 seen at 37.5 and 75 μM . Remdesivir alone at these concentrations (0 to 0.2 μM) had no activity of its own against SARS-CoV-2.

Interestingly addition of OJT010 decreases the potency of remdesivir. At 0.4 μM , remdesivir had a percent inhibition of 94, but when increasing concentrations of OJT010 are added, there is a drop in the percent inhibition by remdesivir. The paradoxical behavior of OJT010 couldn't be explained based on the finding of this assay. Further studies are needed to understand the unique relationship between these drugs.

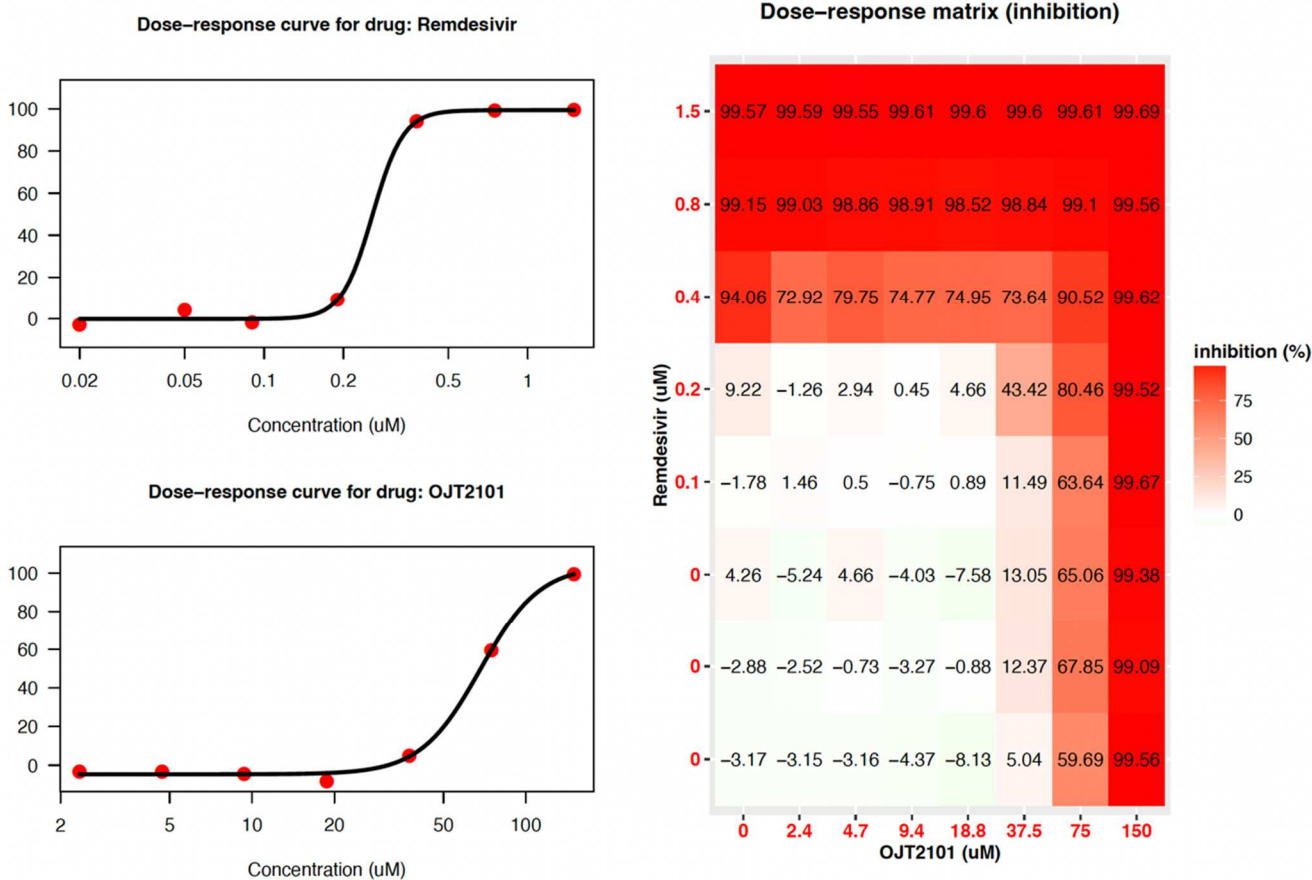


Figure 18: Effect of Combination of OJT010 and Remdesivir on SARS-CoV-2 Replication in NLRV assay

Drug combinations:**Drug combination Synergy score Most synergistic area score Method**

OJT2101 - Remdesivir	0.37	7.45	
----------------------	------	------	--

4.10 Inhibitory Mechanism of OJT010 as Potent Blockers of Molecular Interaction between SARS-CoV-2 Spike protein and Human Angiotensin-converting Enzyme-2

We used computational tools to investigate the inhibitory potentials of OJT010 as potent blockers of the molecular interactions between the ACE2 and RBD of SARS-CoV-2 and Delta Variant. We examined how the binding of OJT010 at the RBD site of the spike protein and the exopeptidase site of hACE-2 affected the binding affinity and molecular interactions between RBD and ACE2 Complex. The binding energies (G_{bind}) between the two proteins were calculated using the molecular mechanics/generalised born surface area (MMGBSA) computational approach. Table 1.0 shows the binding affinity of the two proteins before and after the medicines bind to the Spike protein's RBD site.

First, we identified the binding energies for the ACE2 and RDB complex and then evaluated the change in binding energy after OJT010 binds to the RBD of the spike protein. The results showed high binding energy of -64.856 Kcal/mol for ACE2 and RBD complex in the absence of any drugs (unbound complex). We saw no significant difference in the binding energy of the ACE2 and RBD complex after docking OJT010 on the RBD site.

Table 1 shows the binding affinity of ACE2 and RBD complex alone (-64.856 Kcal/mol) and in OJT010 bound state (-62.442 Kcal/mol). This indicates that the binding of OJT010 to the spike RBD does not affect the complex's binding affinity or molecular interaction.

Further analysis of the binding energies of OJT010 at the RBD site of spike protein revealed that it has comparatively modest binding energies at the RBD site of spike protein (Table 2). This explains why OJT010 had such a small impact on the binding affinities of the complex.

Next, we examined the impacts of the binding of OJT010 at the exopeptidase site of hACE-2 on the binding affinity and molecular interactions between ACE2 and RBD complex for wild type and Delta variant SARS-CoV-2. The binding of OJT010 at the exopeptidase site significantly reduced the binding energies for the complex (Table 3). A decrease in binding affinity was more significant with Delta variant compared to the wild type. These findings imply that the binding of OJT010 to the exopeptidase site of hACE-2 reduces the binding affinity for the formation of ACE2 and RBD complex.

These promising results prompted further analysis into the binding energies of OJT010 at the hACE-2 exopeptidase site (Table 4.0). The results revealed that OJT010 has greater binding energies at the hACE-2 exopeptidase site than at the RBD site. Taken together with findings of our study show that the binding of OJT010 at the exopeptidase site of hACE-2 lowers the binding affinity for the formation of ACE2 and RBD complex.

Table 9: Thermodynamic Binding Free Energy Profiles for the Spike RBD towards hACE2 before and after ligands binding at RBD-hACE2

Energy Components (kcal/mol)					
Complex	ΔE_{vdW}	ΔE_{elec}	ΔG_{gas}	ΔG_{solv}	ΔG_{bind}
Spike RBD					
hACE-2	-97.11 ± 7.20	-633.80 ± 32.28	-730.92 ± 33.67	666.06 ± 30.00	-64.85 ± 10.19
hACE-2 (OJT010)	-101.18 ± 6.2	-640.13 ± 37.29	-741.32 ± 37.29	676.88 ± 36.20	-62.44 ± 8.08

ΔE_{elec} electrostatic energy, ΔE_{vdW} van der Waals energy, ΔG_{bind} total binding free energy, ΔG_{sol} solvation free energy, ΔE_{gas} gas-phase free energy

Table 10: Thermodynamic Binding Free Energy Profiles for the ligands at the hACE2-Spike RBD site

Energy Components (kcal/mol)					
Complex	ΔE_{vdW}	ΔE_{elec}	ΔG_{gas}	ΔG_{solv}	ΔG_{bind}
Spike RBD					
OJT010	-18.85 ± 3.78	-198.96 ± 15.77	$-211.81 \pm$	$198.13 \pm$	$-24.68 \pm$
			17.35	17.35	4.66

ΔE_{elec} electrostatic energy, ΔE_{vdW} van der Waals energy, ΔG_{bind} total binding free energy, ΔG_{sol} solvation free energy, ΔE_{gas} gas-phase free energy

TABLE 11: Results of Binding Energies and Interactions Between ACE2 And SARS-CoV-2 Spike `Before and After Drugs Bind to Exopeptidase Site Of ACE2

	Unbound		OJT010	
	WT	DT	WT	DT
Binding Energy/Affinity	-211.5±23.8	-50.6±6.8	-137.8±21.8	-23.7±3.9
DOCK score	-119.8±0.2	-59.2±6.5	-116.6±3.8	-59.5±6.1
Z-Score	-1.6	-1.4	-1.6	-1.7

KEY: WT-WILD TYPE, DT-DELTA TYPE

Table 12: Thermodynamic Binding Free Energy Profiles for the ligands at the hACE2 binding site of hACE2-Spike RBD

<i>Energy Components (kcal/mol)</i>					
<i>Complex</i>	<i>ΔE_{vdW}</i>	<i>ΔE_{elec}</i>	<i>ΔG_{gas}</i>	<i>ΔG_{solv}</i>	<i>ΔG_{bind}</i>
<i>Spike RBD</i>					
<i>OJT010</i>	<i>-31.797±7.254</i>	<i>-195.455±6.282</i>	<i>-214.784±19.098</i>	<i>177.787±7.899</i>	<i>-42.231±5.324</i>

ΔE_{elec} electrostatic energy, ΔE_{vdW} van der Waals energy, ΔG_{bind} total binding free energy, ΔG_{sol} solvation free energy, ΔE_{gas} gas-phase free energy

4.11 Single Dose Pharmacokinetic Studies Evaluating Oral Bioavailability

We conducted a preliminary study in a rat given 100 mg/kg intravenous bolus administration. After dose, the rat was lethargic but survived; therefore, the amount was reduced by half for future studies. No animal distress was observed at 50 mg/kg, IV bolus dose or at 250 mg/kg oral dose.

Figure 19 shows the mean plasma concentration-time profiles of OJT010 after a 50 mg/kg IV bolus administration to rats. The data showed a tri-exponential profile where OJT010 plasma concentrations decreased rapidly immediately after IV administration, followed by a slower decrease, and further slowed at later points.

Following oral administration, Pharmacokinetic Parameters and Oral Bioavailability of OJT010 after Single Oral Dose Study are summarized in Table 13.

OJT010 has a mean terminal elimination half-life was 7.9 Hours. There was < 1% of unchanged OJT010 excreted in the urine by 24 hours post dose. Following the oral 250 mg/kg administration, OJT010 was absorbed rapidly reaching a mean maximum plasma concentration (C_{max}) of 2,560 ng/mL in 30 mins. OJT010 was well absorbed, with absolute oral bioavailability of 15 ± 5.8 %. Interestingly, after

an oral dose, the mean concentration of OJT010 in the lungs was 317 ng/g at 24 h post-dose, whereas there was only about 20 ng/mL of the drug concentration in plasma at 24 h post-dose. Figure 20 shows the mean plasma concentration-time profiles of OJT010 after a 250 mg/kg oral dose to rats.

Table 13: Pharmacokinetic Parameters and Oral Bioavailability of OJT010

PK Parameters			
Route of Administration	Units	IV (n=3)	P.O. (n=3)
Dose	mg/kg	50	250
T _{max}	hr	-	0.5 - 0.75
C _{max}	ng/mL	19326 ± 3931	2560 ± 709
AUC last	hr*ng/ml	8809 ± 715	6678 ± 1901
V/F	mL/kg	61591 ± 41096	452901 ± 228004
CL/F	ml/hr/kg	5697 ± 478	37752 ± 9097
T _{1/2}	hr	7.2 ± 4.2	7.9 ± 2.4
F	%		15.5 ± 5.8
Average % dose excreted in urine in 24 hours	%	0.32 ± 0.11	0.13 ± 0.3

after Single Oral Dose Study

C_{max} = maximum plasma concentration; AUC last = area under the curve from time 0 to the last dose measured; V/F = apparent volume of distribution; CL/F = apparent systemic clearance; T_{1/2} = elimination half-life; CL = total clearance; Vd = apparent volume of distribution; F = absolute oral bioavailability

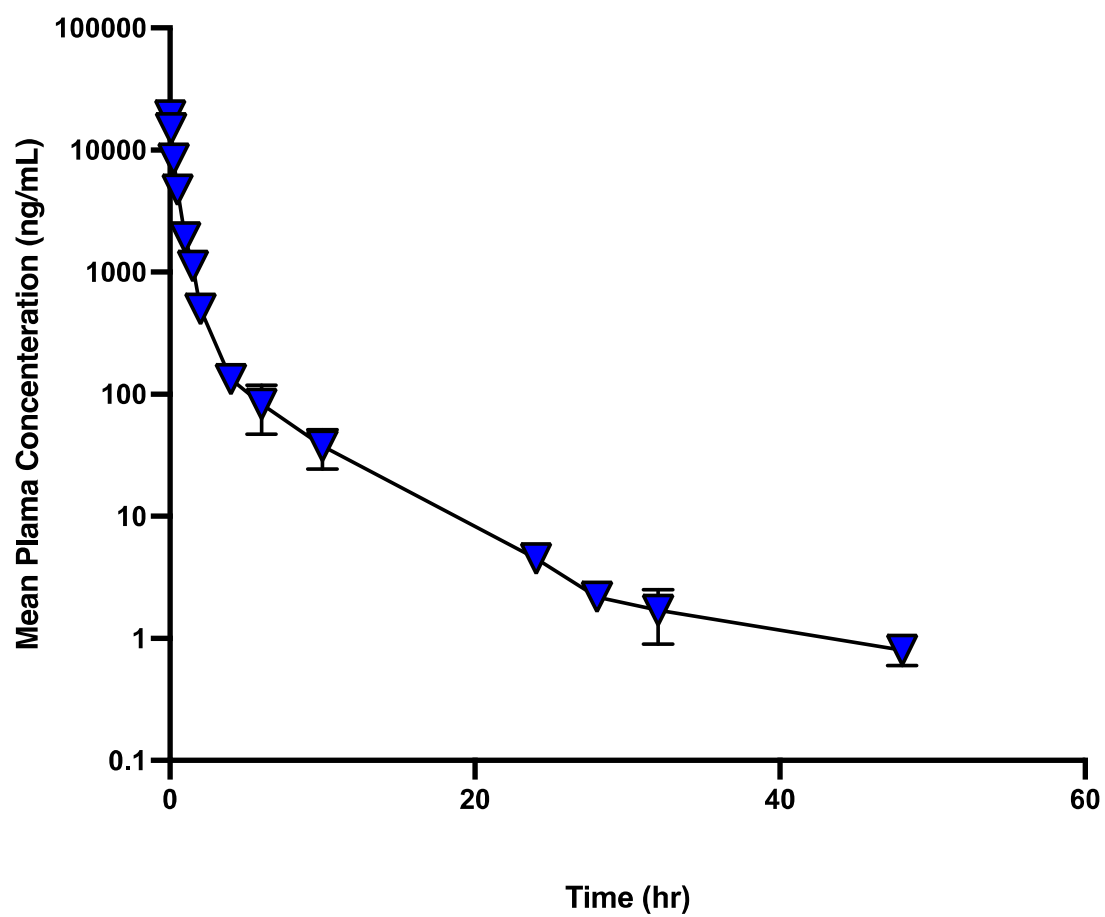


Figure 19: Mean Plasma Concentration-Time Profile of OJT010 following Single IV (50 mg/kg) Dose in Rats

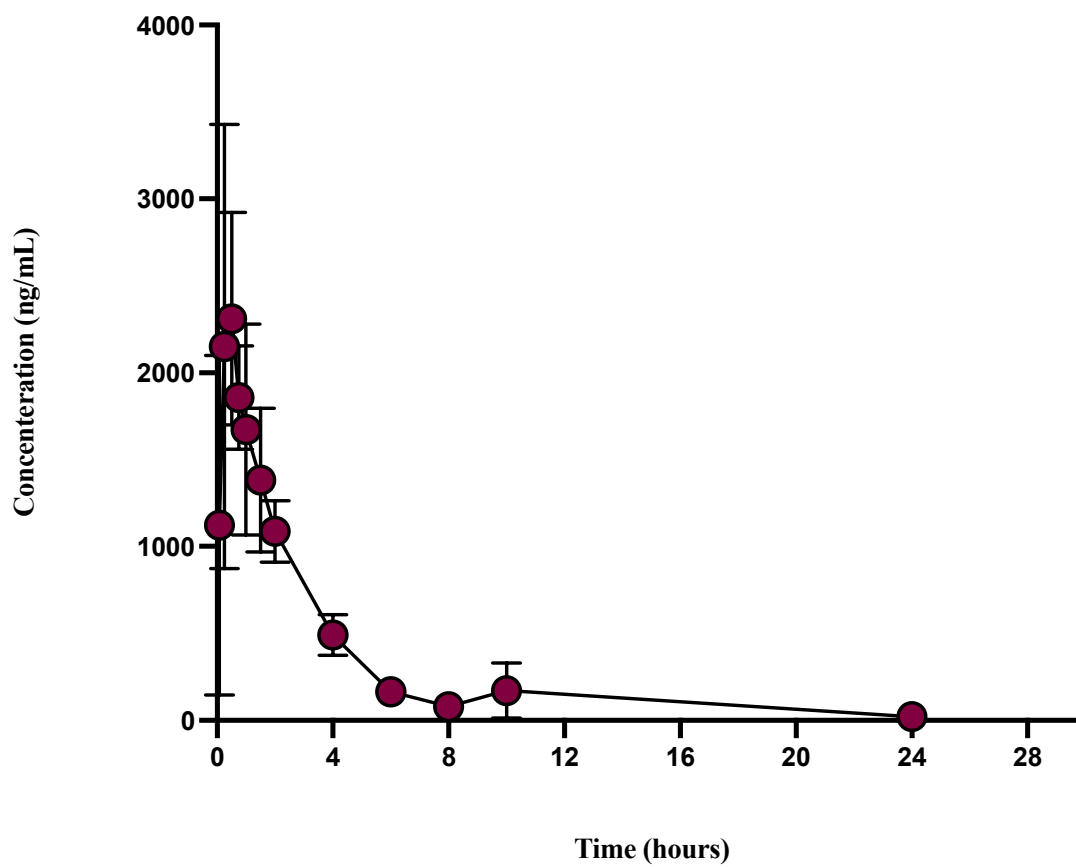


Figure 20: Mean Plasma Concentration-Time Profile of OJT010 following Single oral (250 mg/kg) Dose in Rats

Multiple-dose Pharmacokinetic Study

Six Sprague-Dawley rats were randomly distributed into two OJT010 treatment groups; (a) 250 mg/kg and (b) 400 mg/kg. The rats in each group were administered a single oral dose of 250 mg/kg/day and 400 mg/kg/day, respectively, consecutively for five days. Rats were fasted for at least 12 hours before and 4 hours after the last dose on Day 5. Serial pre-determined blood samples were collected at various time points as described in the previous single dose studies. Urine samples were collected up to 24 hours post dose. Table 2 summarizes mean plasma concentrations observed after multiple doses.

Two-compartmental analyses were used to generate PK parameters for OJT010. Table 3 shows PK parameters after multiple dosing for two-compartmental analysis. Following oral administration, Pharmacokinetic Parameters and Oral Bioavailability of OJT010 after Multiple Oral Dosing Study are summarized in Table 14.

OJT010 has a mean terminal elimination half-life was 10 and 62 hours with 250 mg/kg and 400 mg/kg respectively. There was < 1% of unchanged OJT010 excreted in the urine by 24 hours post dose. Following the oral of 250 mg/kg and 400mg/kg administration, OJT010 was absorbed rapidly reaching a mean maximum plasma concentration (C_{max}) of 826 ng/mL and 1117 ng/ml in 43 and 20 mins respectively. Interestingly, after an oral dose, the mean concentration of OJT010 in the lungs was 20~22-fold higher than in the plasma at 24 h post-dose.

Figure 21 shows the mean plasma concentration-time profiles of OJT010 after a 250 mg/kg and 400 mg/kg oral dose to rats.

The area under the curve for the group was 3354.90 hr*ng/ml and 4812.46 hr*ng/ml with 250mg/kg and 400mg/kg respectively. Table 15 shows the Plasma Concentrations of OJT010 following Oral Administration of Single and Multiple Dose in Rats

Following both single and multiple-dose administration, OJT010 concentration-time profiles were characterized by a rapid absorption phase, with peak plasma concentrations occurring in less than 1 h for all groups. The C_{max} and $AUC_{0-\infty}$ obtained in the multiple-dose study were lower than the single-dose study. The $T_{1/2}$ of multiple-dose with 400 mg/kg dose was significantly higher (60 h) than the single-dose group (12 h).

To study the difference obtained between the PK parameters of multiple-dose and single-dose group we conducted the analysis of variance (ANOVA). Scores obtained showed significant variance in the values of $C_{max}/Dose$ with a p -value of 0.02. A post hoc Tukey test showed that single-dose study vs multi-dose study at 400mg/kg differed significantly with a p -value of 0.03. Although all parameters were lower with multiple dosing compared to the single dosing study, none except dose-normalized C_{max} were statistically significant. The discrepancies in C_{max} could be attributed to a small number of animals used in our study. More studies

with a higher number of animals are needed to rule out obtained differences in our study.

Table 14: Pharmacokinetic Parameters and Oral Bioavailability of OJT010 after Multiple Oral Dose Study

PK Parameters			
Route of Administration	Units	Oral (n=3)	Oral (n=3)
Dose	mg/kg	250 mg/kg	400 mg/kg
C _{max}	ng/mL	826 ± 233	1117 ± 465
T _{1/2ka}	hr	0.34 ± 0.33	0.13 ± 0.14
T _{1/2}	hr	10 ± 3.8	62 ± 46
AUC _{0-∞}	hr*ng/ml	3844 ± 811	7371 ± 3392
Cl _F	L/hr/kg	66 ± 12	66 ± 40
V _{2_F}	L/Kg	2006 ± 2939	2174 ± 1415
V _{1_F}	L/kg	215 ± 138	296 ± 133
T _{max}	hr	0.72 ± 0.31	0.49 ± 0.33
Average % dose excreted in urine in 24 hours	%	0.53 ± 0.05	0.40 ± 0.07

C_{max} = maximum plasma concentration; AUC_{0-∞} = area under the curve from time 0 to the infinity; V_{z_pred} = volume of distribution; Cl_F = apparent systemic clearance; T_{1/2} = elimination half-life; CL = total clearance; V_{2_F} = apparent volume of distribution; F = absolute oral bioavailability

Table 15: Plasma Concentrations of OJT010 following Oral Administration of Single and Multiple Dose in Rats

Rat #	D2	E2	F2	G	H	I	J	K	L
Drug	OJT010								
Loading solution Conc (mg/mL)	20	20	20	35	35	35	35	35	35
Dosage (mg/kg)	250	250	250	250	250	250	400	400	400
Route	P. O	P. O	P. O	P. O	P. O	P. O	P. O	P. O	P. O
	Single dose			Multiple dose (5 days, once daily)			Multiple dose (5 days, once daily)		
Day 1 weight(g)	306	321	260	287	290	299	301	325	302
Day 1 dosing volume (ml)	3.8	4.0	3.2	2.05	2.07	2.14	3.44	3.71	3.45
Day 2 weight (g)				297	307	315	303	324	310
Day 2 Dosing volume (ml)				2.12	2.19	2.25	3.46	3.7	3.54
Day 3 weight(g)				301	309	317	315	323	309
Day 3 Dosing volume (ml)				2.15	2.21	2.26	3.6	3.69	3.53
Day 4 weight(g)				299	312	317	317	320	314
Day 4 Dosing volume (ml)				2.14	2.23	2.26	3.62	3.66	3.59
Day 5 weight (post overnight-fasting) (g)				287	294	297	297	300	297
Day 5 Dosing volume (ml)				2.0	2.0	2.0	3.4	3.4	3.4
0*	<0.5	<0.5	<0.5	104	76.8	82.5	48.9	82.1	80.2
5min	368	775	2225	108	99.7	221	181	397	1110
15min	820	2260	3370	581	476	868	1570	712	1120
30min	1830	2100	3000	889	547	1170	1700	548	847
45min	2050	1515	2010	902	561	875	2220	544	752
1h	1520	1155	2340	1010	401	802	1460	356	516
1.5h	1295	1020	1835	854	328	634	1020	352	414
2h	1030	945	1285	866	462	469	1210	244	276
4h	358	531	581	232	229	244	951	251	201
6h	178	190	124	59.9	48	85.6	226	102	79.4
8h	71.8	65.3	100	65.4	36.5	58.4	115	286	66.8
10h	40.1	126	347	20.4	28.2	41.5	66.3	86.1	55
24h	18.4	25.7	15.9	4.9	19.7	26	26	42.6	55.6
Ratio of C_{lung}/C_{plasma} (Ave.=17.7)	9	18.2	20	24	24.6	14.1	7.6	19.2	22.2
Conc. in Lung at 24h	165.6	468	317.6	117.6	484	366.2	197.8	816	1232

(ng/g)									
Mean \pm SD (ng/g)	317 \pm 151			323 \pm 187			749 \pm 520		
Lung weight (g)	1.6298	1.7356	1.0885	1.3143	1.2373	1.2168	1.2476	1.3916	1.2074
Total amount in lung (ng)	269.89	812.26	345.71	154.56	598.85	445.59	246.78	1135.55	1487.52
Concentration in urine (ng/mL)	4540	11700	6810	26100	35600	32850	22300	72600	48400
Urine volume (mL)	17.5	9	15	13	11	13	18	7	12
Total amount in urine (μ g)	79.5	105.3	102.2	339.3	391.6	427.05	401.4	508.2	580.8

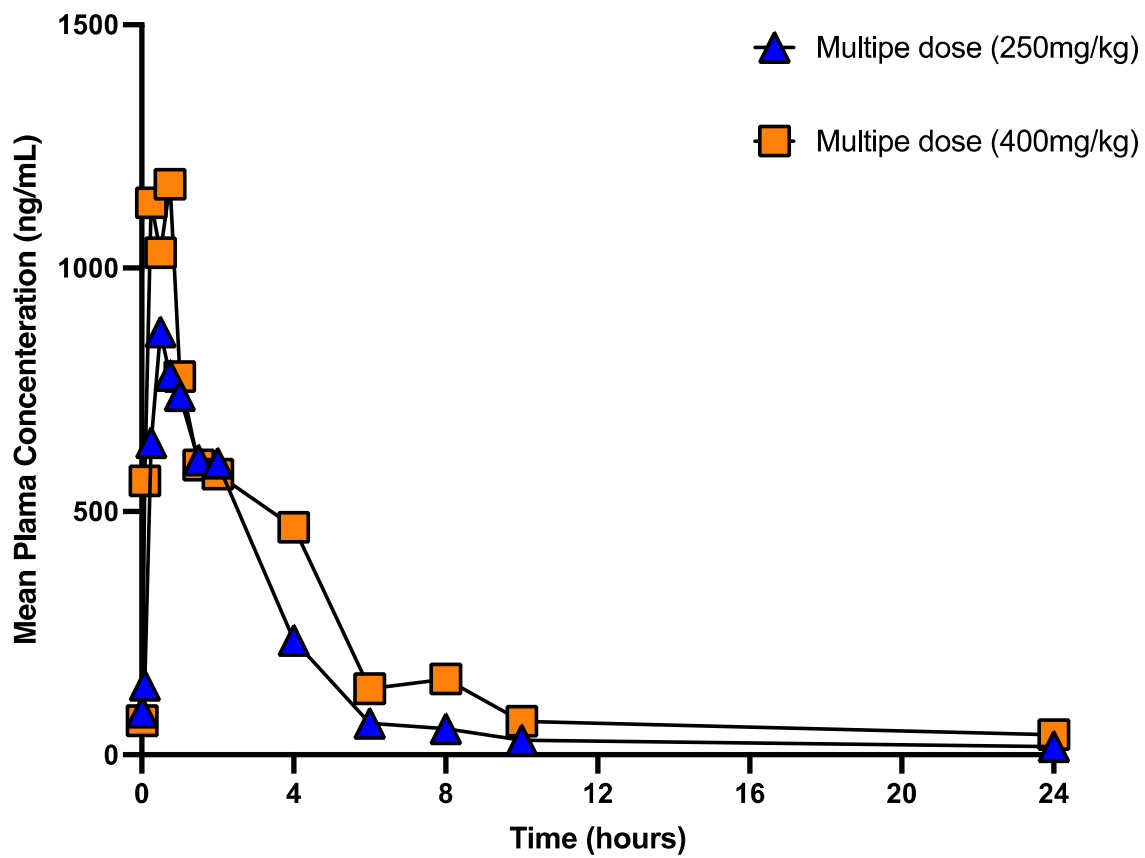


Figure 21: Mean Plasma Concentration-Time Profile of OJT010 following Multiple Oral (2500 and 400 mg/kg) dosing in Rats

CHAPTER 5

SUMMARY AND CONCLUSION

The ongoing pandemic of coronavirus disease (COVID-19) caused by the highly infectious pathogen, severe acute respiratory syndrome coronavirus 2 (SARS-CoV-2), presents a global public health challenge. To contain the pandemic, successful intervention strategies are urgently needed. Effective therapeutic countermeasures against SARS-CoV-2 infection require inhibition of critical viral entry and post-entry pathways targeting viral enzymes or host receptors. The advent of SARS-CoV-2 variants with mutations in the viral genes has made it imperative to discover therapeutics that target the host receptors for COVID-19 treatment. Therefore, our research has focused on targeting the two critical host entry receptor: Angiotensin-converting enzyme-2 for SARS-CoV-2 entry into the human cells.

Small molecule antivirals can inhibit viruses through multiple mechanisms, including preventing viral entry, inhibiting viral and host proteases, inducing or inhibiting autophagy, decreasing inflammatory markers, and improving lung conditions. Several drugs are under evaluation in clinical trials to treat COVID 19.

Through targeted drug discovery efforts for repurposing existing clinically approved drugs for the potential treatment of SARS-CoV-2, here we report the potent antiviral activity of OJT010 against SARS-CoV-2 in human lung epithelial and African green monkey kidney cells. Here we report that OJT010 inhibited SARS-CoV-2 and Delta variant and improved viability of VeroE6 kidney cells. Furthermore, it inhibited viral replication in Nano luciferase reporter assay at micromolar concentrations. Additionally, it also prevented the entry of Pseudotyped spike particles into VeroE6 cells.

Our study noted that EC_{50} values of OJT010 were high against SARS-CoV-2. However, clinical concentrations approaching 100 μ M are safe in long-term use in Parkinson's disease, Gaucher disease, and pregnant women (H et al., 2022; M & B, 2008; Magalhaes et al., 2018; S et al., 2020; Y et al., 2022). Furthermore, OJT010 at high doses has been demonstrated to reduce inflammatory cytokines (TNF- α and IL-1, IL-6, Nf- κ B) (D et al., 1994; KM et al., 2008). Additionally, at high doses, OJT010 improves oxygenation (PaO₂/FiO₂ ratio, Po₂, and SaO₂) while lowering inflammatory markers in Acute respiratory distress patients, which would be highly desirable in COVID 19 patients (D et al., 1994).

We also investigated the ability of OJT010 and its progenitor drug OJT009 to modulate the critical interaction between the RBD of SARS-CoV-2 spike protein and human ACE2. Here we show that OJT010 inhibits the interaction of SARS-CoV-2 spike protein receptor-binding domain (RBD) with human recombinant ACE2 (rhACE2) in nano to the micromolar range, thereby blocking its entry into human cells.

In this study, we explored the possibility of OJT010 and OJT009 as potential effectors of exopeptidase activity of ACE2. Using a fluorogenic assay, we found that OJT010 has no effects on the exopeptidase activity of ACE2, while OJT009 inhibits the exopeptidase activity of ACE2 at high concentrations. ACE2, a membrane-bound metalloprotease and an essential component in the Renin-Angiotensin system converting Angiotensin II (Ang II) to Angiotensin 1-7, a potent vasopressor. Although ACE2 facilitates viral entry, it protects against acute lung damage, implying that the ACE2/Ang 1-7 pathway must be carefully manipulated to reduce SARS-CoV-2 induced lung injuries. ACE2 counteracts ACE negative effects in the lungs by decreasing Ang II levels. Downregulation of ACE2 by SARS-CoV-2 creates an imbalance of ACE2 and ACE in the lungs. This further aggravates lung inflammation by increasing capillary permeability and leading to pulmonary edema. This further activates the releases of inflammatory markers, which eventually lead to cytokines storm (D. P et al., 2020).

To further investigate the mechanism of action of OJT010 in SARS-CoV-2 inhibition, we used artificial intelligence to evaluate the binding parameters of OJT010 with RBD of Spike protein and ACE2. Using molecular docking techniques, we also assessed the effect of OJT010 on the molecular interaction between RBD and ACE2. We discovered that the binding of the OJT010 at the RBD-ACE-2 site does not alter the binding affinity and molecular interaction between RBD and ACE2. Whereas the binding of OJT010 at the exopeptidase site of ACE2 considerably lowered the binding affinities between the proteins compared to the unbound, ACE2-RBD complex. The result further showed that OJT010 has a good affinity at the exopeptidase site of ACE2.

Interestingly the binding energies of the Delta variant with ACE2 were greater than wild type SARS-CoV-2, and hence more significant disruption of the complex was obtained. These findings validate the *in vitro* efficacies of OJT010 obtained in CPE, NLRV, and Pseudo virus assay.

Our study shows multiple lines of evidence that OJT010 mediated inhibition of SARS-CoV-2 entry through its interactions with ACE2. Our findings suggest that OJT010 binding to rhACE2 may preserve its physiological function and will prevent non-target cardiac toxicities observed in other ACE2 modulating drugs. To our knowledge, this is the first experimental study revealing this class of compounds as potent effectors of ACE2 exopeptidase activity. This study provides strong evidence that OJT010 could serve as a promising lead for developing SARS-CoV-2 inhibitors and potential COVID-19 therapeutics.

In addition to the anti-SARS-CoV-2 activity of OJT010, it protects against infections in multiple ways. As discussed earlier, OJT010 is a potent anti-inflammatory and antioxidant agent. It provides a defense against acute and chronic respiratory diseases (KM et al., 2008). Moreover, it has been shown that administration of OJT010 could significantly lessen the extent of ventilation induce lung injury in rats (DW et al., 2019). Furthermore, it increases lung levels of other antibiotics and potentiates their different antibiotics activity (V & GS, 2019).

Additionally, OJT010 has shown efficacy against SARS-CoV-2, rhinovirus, and influenza virus in cells. In animal models of rhinovirus infection, OJT010 effectively improved the survival rate of mice by suppressing virus multiplication (C et al., 2020; M et al., 2014). It has a wide range of actions with minimum adverse events and a favorable safety profile (M & B, 2008). These unique characteristics indicate that OJT010 could be a novel therapeutic agent for treating SARS-CoV-2.

To guide the design of efficacy studies in a hamster model of SARS-CoV-2 infection and further develop for Phase I/Phase II clinical trials, we investigated pharmacokinetics parameters of OJT010 in healthy rats. In the study, we determined the oral bioavailability of OJT010 and obtained steady-state concentration. In rats' oral bioavailability of OJT010 was ~15%. The maximum plasma drug concentration (2560 ng/ml) following a single oral dose of 250 mg/kg reached between 30-45 minutes. High penetration of OJT010 was observed in the lungs ranging from 15~20 fold higher than plasma. High drug concentrations were highly safe, and adverse events were reported.

Given the urgency to find treatment for COVID-19, drug repurposing is the most promising approach to identified inhibitors of SARS-CoV-2. Inhibiting the critical viral entry pathways into host cells is a promising therapeutic possibility to combat SARS-CoV-2 infection. An ideal therapeutic intervention to combat SARS-CoV-2 infection might inhibit the viral RBD attachment to its receptor ACE2 without blocking the

catalytic activity of ACE2, thereby preventing viral spread and dissemination into the host system. Therefore, compounds such as OJT010 with potent efficacy, excellent safety, and pharmacologic profile represent a promising pharmacophore candidate for drug repurposing as possible prophylactic or treatment options against COVID-19 infection. If proven effective, this will allow rapid and cost-effective intervention to combat SARS-CoV-2 worldwide.

REFERENCES

- @JohnsHopkins. (2022). *COVID-19 Map - Johns Hopkins Coronavirus Resource Center*.
@JohnsHopkins. <https://coronavirus.jhu.edu/map.html>
- @US_FDA. (2020). Coronavirus (COVID-19) Update: FDA Authorizes Monoclonal Antibodies for Treatment of COVID-19 | FDA. <https://www.fda.gov/news-events/press-announcements/coronavirus-covid-19-update-fda-authorizes-monoclonal-antibodies-treatment-covid-19>
- @US_FDA. (2022a). Coronavirus (COVID-19) | Drugs | FDA. <https://www.fda.gov/drugs/emergency-preparedness-drugs/coronavirus-covid-19-drugs>
- @US_FDA. (2022b). Coronavirus (COVID-19) Update: FDA Limits Use of Certain Monoclonal Antibodies to Treat COVID-19 Due to the Omicron Variant | FDA. <https://www.fda.gov/news-events/press-announcements/coronavirus-covid-19-update-fda-limits-use-certain-monoclonal-antibodies-treat-covid-19-due-omicron>
- A, B., C, Q., F, R., M, S., A, H., S, N., & JP, L. (2020). Drug repositioning in neurodegeneration: An overview of the use of ambroxol in neurodegenerative diseases. *European journal of pharmacology*, 884. <https://doi.org/10.1016/j.ejphar.2020.173446>
- A, C., B, G., M, H., S, P., N, H., MJ, E., M, K., J, K., KA, B., & E, G. (2021). Inhibition of acid sphingomyelinase by ambroxol prevents SARS-CoV-2 entry into epithelial cells. *The Journal of biological chemistry*, 296. <https://doi.org/10.1016/j.jbc.2021.100701>
- A, M., M, F., G, G., U, F., A, A., M, M., G, R., G, C., A, G., & V, C. (1987). Ambroxol in the treatment of idiopathic respiratory distress syndrome. An interim report on a controlled double-blind multicenter study versus placebo. *Respiration; international review of thoracic diseases*, 51 Suppl 1. <https://doi.org/10.1159/000195276>
- Agostini, M. L., Andres, E. L., Sims, A. C., Graham, R. L., Sheahan, T. P., Lu, X., Smith, E. C., Case, J. B., Feng, J. Y., Jordan, R., Ray, A. S., Cihlar, T., Siegel, D., Mackman, R. L., Clarke, M. O., Baric, R. S., & Denison, M. R. (2018). Coronavirus Susceptibility to the Antiviral Remdesivir (GS-5734) Is Mediated by the Viral Polymerase and the Proofreading Exoribonuclease. *mBio*, 9(2). <https://doi.org/10.1128/mBio.00221-18>
- Aldrich, S. (2022). *ACE1 Inhibitor Screening Kit (Colorimetric) sufficient for 100 colorimetric tests | Sigma-Aldrich*. <http://www.sigmaaldrich.com/>
- Andrew Hill, L. E., Junzheng Wang, Toby Pepperrell. (2022). Prices versus costs of production for molnupiravir as a COVID-19 treatment. <https://doi.org/10.21203/rs.3.rs-1169509/v1>
- B, N., A, G., K, G., R, H., N, N., A, G.-D., & O, C. (2021). The interaction of the severe acute respiratory syndrome coronavirus 2 spike protein with drug-inhibited

- angiotensin converting enzyme 2 studied by molecular dynamics simulation. *Journal of hypertension*, 39(8). <https://doi.org/10.1097/HJH.0000000000002829>
- B, Y., DF, Y., M, O., M, I., M, Y., Y, O., & H, K. (2002). Ambroxol suppresses influenza-virus proliferation in the mouse airway by increasing antiviral factor levels. *The European respiratory journal*, 19(5). <https://doi.org/10.1183/09031936.02.00253302>
- B, Y., K, W., T, A., & J, T. (2015). Searching for Drug Synergy in Complex Dose-Response Landscapes Using an Interaction Potency Model. *Computational and structural biotechnology journal*, 13. <https://doi.org/10.1016/j.csbj.2015.09.001>
- Baden, L. R., El Sahly, H. M., Essink, B., Kotloff, K., Frey, S., Novak, R., Diemert, D., Spector, S. A., Roupheal, N., Creech, C. B., McGettigan, J., Khetan, S., Segall, N., Solis, J., Brosz, A., Fierro, C., Schwartz, H., Neuzil, K., Corey, L., . . . Group, C. S. (2021). Efficacy and Safety of the mRNA-1273 SARS-CoV-2 Vaccine. *N Engl J Med*, 384(5), 403-416. <https://doi.org/10.1056/NEJMoa2035389>
- Basconi, J. E., & Shirts, M. R. (2013). Effects of Temperature Control Algorithms on Transport Properties and Kinetics in Molecular Dynamics Simulations [research-article]. <https://doi.org/10.1021/ct400109a>
- Bernal, A. J., Silva, M. M. G. d., Musungaie, D. B., Kovalchuk, E., Gonzalez, A., Reyes, V. D., Martín-Quirós, A., Caraco, Y., Williams-Diaz, A., Brown, M. L., Du, J., Pedley, A., Assaid, C., Strizki, J., Grobler, J. A., Shamsuddin, H. H., Tipping, R., Wan, H., Paschke, A., . . . Anda, C. D. (2021). Molnupiravir for Oral Treatment of Covid-19 in Nonhospitalized Patients [research-article]. <https://doi.org/10.1056/NEJMoa2116044>. <https://doi.org/NJ202202103860605>
- Bernal, J. L., Andrews, N., Gower, C., Gallagher, E., Simmons, R., Thelwall, S., Stowe, J., Tessier, E., Groves, N., Dabrera, G., Myers, R., Campbell, C. N. J., Amirthalingam, G., Edmunds, M., Zambon, M., Brown, K. E., Hopkins, S., Chand, M., & Ramsay, M. (2021). Effectiveness of Covid-19 Vaccines against the B.1.617.2 (Delta) Variant [research-article]. <https://doi.org/10.1056/NEJMoa2108891>. <https://doi.org/NJ202108123850705>
- BF, G., W, S., IB, V., P, B., U, B., HH, W., & G, Z.-K. (1999). Ambroxol inhibits the release of histamine, leukotrienes and cytokines from human leukocytes and mast cells. *Inflammation research : official journal of the European Histamine Research Society ... [et al.]*, 48(2). <https://doi.org/10.1007/s000110050421>
- BF, H., AK, G., S, S., M, T., H, K.-W., F, N., C, S.-H., & AS, H. (2021). SARS-CoV-2 and SARS-CoV Spike-Mediated Cell-Cell Fusion Differ in Their Requirements for Receptor Expression and Proteolytic Activation. *Journal of virology*, 95(9). <https://doi.org/10.1128/JVI.00002-21>
- Bioscience, B. (2022). Pseudoviruses for SARS-CoV-2 Research. <https://bpsbioscience.com/pseudoviruses-sars-cov-2-research>
- Boehm, M., & Nabel, E. G. (2002). Angiotensin-converting enzyme 2--a new cardiac regulator. *N Engl J Med*, 347(22), 1795-1797. <https://doi.org/10.1056/NEJMcibr022472>
- BPSBioscience. (2022). ACE2 Inhibitor Screening Assay Kit. <https://bpsbioscience.com/ace2-inhibitor-screening-assay-kit-79923>

- Bugin, K., & Woodcock, J. (2021). Trends in COVID-19 therapeutic clinical trials. *Nat Rev Drug Discov*, 20(4), 254-255. <https://doi.org/10.1038/d41573-021-00037-3>
- Burki, T. K. (2022). Omicron variant and booster COVID-19 vaccines. *Lancet Respir Med*, 10(2), e17. [https://doi.org/10.1016/S2213-2600\(21\)00559-2](https://doi.org/10.1016/S2213-2600(21)00559-2)
- C, D., PV, G., L, L., & FF, R. (1997). Antenatal ambroxol treatment does not prevent the respiratory distress syndrome in premature infants. *European journal of pediatrics*, 156(5). <https://doi.org/10.1007/s004310050622>
- C, W., K, D., & M, S. (2020). Comparative in vitro analysis of inhibition of rhinovirus and influenza virus replication by mucoactive secretolytic agents and plant extracts. *BMC complementary medicine and therapies*, 20(1). <https://doi.org/10.1186/s12906-020-03173-2>
- C, X., Y, W., C, L., C, Z., W, H., X, H., Y, W., Q, H., S, W., Q, Z., Y, W., Y, Y., K, C., W, Z., L, K., F, W., Q, Z., Z, H., & Y, C. (2021). Conformational dynamics of SARS-CoV-2 trimeric spike glycoprotein in complex with receptor ACE2 revealed by cryo-EM. *Science advances*, 7(1). <https://doi.org/10.1126/sciadv.abe5575>
- Cantuti-Castelvetri, L., Ojha, R., Pedro, L. D., Djannatian, M., Franz, J., Kuivanen, S., Meer, F. v. d., Kallio, K., Kaya, T., Anastasina, M., Smura, T., Levanov, L., Szivoczka, L., Tobi, A., Kallio-Kokko, H., Österlund, P., Joensuu, M., Meunier, F. A., Butcher, S. J., . . . Simons, M. (2020). Neuropilin-1 facilitates SARS-CoV-2 cell entry and infectivity [research-article]. <https://doi.org/10.1126/science.abd2985>
- CB, M., L, R., & EL, W. (2008). Adapting Cell-Based Assays to the High Throughput Screening Platform: Problems Encountered and Lessons Learned. *JALA (Charlottesville, Va.)*, 13(3). <https://doi.org/10.1016/j.jala.2008.02.002>
- CH, E., J, J., B, M., K, P., M, S., & P, C. (1987). Influence of ambroxol on tracheobronchial clearance in simple chronic bronchitis. *European journal of respiratory diseases*, 70(3). <https://www.ncbi.nlm.nih.gov/pubmed/3569448>
- Chan, J. F., Lau, S. K., To, K. K., Cheng, V. C., Woo, P. C., & Yuen, K. Y. (2015). Middle East respiratory syndrome coronavirus: another zoonotic betacoronavirus causing SARS-like disease. *Clin Microbiol Rev*, 28(2), 465-522. <https://doi.org/10.1128/CMR.00102-14>
- Chen, C. Z., Shinn, P., Itkin, Z., Eastman, R. T., Bostwick, R., Rasmussen, L., Huang, R., Shen, M., Hu, X., Wilson, K. M., Brooks, B., Guo, H., Zhao, T., Klump-Thomas, C., Simeonov, A., Michael, S. G., Lo, D. C., Hall, M. D., & Zheng, W. (2020). Drug Repurposing Screen for Compounds Inhibiting the Cytopathic Effect of SARS-CoV-2. <https://doi.org/10.1101/2020.08.18.255877>
- Choi, S. W., Gu, Y., Peters, R. S., Salgame, P., Ellner, J. J., Timmins, G. S., & Deretic, V. (2018). Ambroxol Induces Autophagy and Potentiates Rifampin Antimycobacterial Activity [brief-report]. <https://doi.org/10.1128/AAC.01019-18>
- CJ, G., EP, T., RF, S., & M, G. (2021). Molnupiravir promotes SARS-CoV-2 mutagenesis via the RNA template. *The Journal of biological chemistry*, 297(1). <https://doi.org/10.1016/j.jbc.2021.100770>
- Consortium, W. H. O. S. T., Pan, H., Peto, R., Henao-Restrepo, A. M., Preziosi, M. P., Sathiyamoorthy, V., Abdool Karim, Q., Alejandria, M. M., Hernandez Garcia, C., Kieny, M. P., Malekzadeh, R., Murthy, S., Reddy, K. S., Roses Periago, M., Abi

- Hanna, P., Ader, F., Al-Bader, A. M., Alhasawi, A., Allum, E., . . . Swaminathan, S. (2021). Repurposed Antiviral Drugs for Covid-19 - Interim WHO Solidarity Trial Results. *N Engl J Med*, 384(6), 497-511. <https://doi.org/10.1056/NEJMoa2023184>
- Corvol, P., Williams, T. A., & Soubrier, F. (1995). Peptidyl dipeptidase A: angiotensin I-converting enzyme. *Methods Enzymol*, 248, 283-305. [https://doi.org/10.1016/0076-6879\(95\)48020-x](https://doi.org/10.1016/0076-6879(95)48020-x)
- Costantini, V. P., Whitaker, T., Barclay, L., Lee, D., McBrayer, T. R., Schinazi, R. F., & Vinje, J. (2012). Antiviral activity of nucleoside analogues against norovirus. *Antivir Ther*, 17(6), 981-991. <https://doi.org/10.3851/IMP2229>
- Crackower, M. A., Sarao, R., Oudit, G. Y., Yagil, C., Kozieradzki, I., Scanga, S. E., Oliveiras-dos-Santos, A. J., da Costa, J., Zhang, L., Pei, Y., Scholey, J., Ferrario, C. M., Manoukian, A. S., Chappell, M. C., Backx, P. H., Yagil, Y., & Penninger, J. M. (2002). Angiotensin-converting enzyme 2 is an essential regulator of heart function. *Nature*, 417(6891), 822-828. <https://doi.org/10.1038/nature00786>
- Cyril Dominguez, Rolf Boelens, a., & Bonvin*, A. M. J. J. (2003). HADDOCK: A Protein-Protein Docking Approach Based on Biochemical or Biophysical Information [research-article]. <https://doi.org/10.1021/ja026939x>
- D, N., A, A., M, K., P, B., & T, P. (1994). Antioxidant properties of Ambroxol. *Free radical biology & medicine*, 16(4). [https://doi.org/10.1016/0891-5849\(94\)90130-9](https://doi.org/10.1016/0891-5849(94)90130-9)
- D, O., G, Z., G, T., S, D., G, B., G, F., N, C., R, C., E, C., & S, M. (1987). Ambroxol for the prevention of chronic bronchitis exacerbations: long-term multicenter trial. Protective effect of ambroxol against winter semester exacerbations: a double-blind study versus placebo. *Respiration; international review of thoracic diseases*, 51 Suppl 1. <https://doi.org/10.1159/000195274>
- Donoghue, M., Hsieh, F., Baronas, E., Godbout, K., Gosselin, M., Stagliano, N., Donovan, M., Woolf, B., Robison, K., Jeyaseelan, R., Breitbart, R. E., & Acton, S. (2000). A novel angiotensin-converting enzyme-related carboxypeptidase (ACE2) converts angiotensin I to angiotensin 1-9. *Circ Res*, 87(5), E1-9. <https://doi.org/10.1161/01.res.87.5.e1>
- DW, C., MX, H., & XR, Z. (2019). Ambroxol alleviates ventilator-induced lung injury by inhibiting c-Jun expression. *European review for medical and pharmacological sciences*, 23(11). https://doi.org/10.26355/eurev_201906_18092
- E, P., L, R., & J, Z. (1994). [Effect of intravenous ambroxol hydrochloride on lung function and exercise capacity in patients with severe chronic obstructive pulmonary disease]. *Pneumonologia i alergologia polska*, 62(5-6). <https://www.ncbi.nlm.nih.gov/pubmed/7920274>
- Ellul, M. A., Benjamin, L., Singh, B., Lant, S., Michael, B. D., Easton, A., Kneen, R., Defres, S., Sejvar, J., & Solomon, T. (2020). Neurological associations of COVID-19. *Lancet Neurol*, 19(9), 767-783. [https://doi.org/10.1016/S1474-4422\(20\)30221-0](https://doi.org/10.1016/S1474-4422(20)30221-0)
- Fegiz, G. (1991). Prevention by ambroxol of bronchopulmonary complications after upper abdominal surgery: double-blind Italian multicenter clinical study versus placebo. *Lung*, 169(2), 69-76. <https://doi.org/10.1007/BF02714144>

- Feuillet, V., Canard, B., & Trautmann, A. (2021). Combining Antivirals and Immunomodulators to Fight COVID-19. *Trends Immunol*, 42(1), 31-44. <https://doi.org/10.1016/j.it.2020.11.003>
- G, F. (1991). Prevention by ambroxol of bronchopulmonary complications after upper abdominal surgery: double-blind Italian multicenter clinical study versus placebo. *Lung*, 169(2). <https://doi.org/10.1007/BF02714144>
- G, K., HS, H., D, T., C, D., F, S., J, S., L, F., A, S., C, H., & P, C. (2021). Mechanism of SARS-CoV-2 polymerase stalling by remdesivir. *Nature Communications*, 12(1). <https://doi.org/10.1038/s41467-020-20542-0>
- G, V., R, H., H, S., I, O., GM, R., & M, J. (2013). The effect of ambroxol on chloride transport, CFTR and ENaC in cystic fibrosis airway epithelial cells. *Cell biology international*, 37(11). <https://doi.org/10.1002/cbin.10146>
- Gao, Y., Yan, L., Huang, Y., Liu, F., Zhao, Y., Cao, L., Wang, T., Sun, Q., Ming, Z., Zhang, L., Ge, J., Zheng, L., Zhang, Y., Wang, H., Zhu, Y., Zhu, C., Hu, T., Hua, T., Zhang, B., . . . Rao, Z. (2020). Structure of the RNA-dependent RNA polymerase from COVID-19 virus. *Science*, 368(6492), 779-782. <https://doi.org/10.1126/science.abb7498>
- GH, M., MB, T., JD, B., BA, R., M, F., D, P., L, T., GJ, K., Y, H., JT, C., & DJ, M. (2009). Identification and characterization of ambroxol as an enzyme enhancement agent for Gaucher disease. *The Journal of biological chemistry*, 284(35). <https://doi.org/10.1074/jbc.M109.012393>
- Gil, C., Ginex, T., Maestro, I., Nozal, V., Barrado-Gil, L., Cuesta-Geijo, M. A., Urquiza, J., Ramirez, D., Alonso, C., Campillo, N. E., & Martinez, A. (2020). COVID-19: Drug Targets and Potential Treatments. *J Med Chem*, 63(21), 12359-12386. <https://doi.org/10.1021/acs.jmedchem.0c00606>
- GonnetPedro. (2007). P-SHAKE [article]. <https://doi.org/10.1016/j.jcp.2006.05.032>
- Gordon, C. J., Tchesnokov, E. P., Feng, J. Y., Porter, D. P., & Gotte, M. (2020). The antiviral compound remdesivir potently inhibits RNA-dependent RNA polymerase from Middle East respiratory syndrome coronavirus. *J Biol Chem*, 295(15), 4773-4779. <https://doi.org/10.1074/jbc.AC120.013056>
- Gordon, C. J., Tchesnokov, E. P., Woolner, E., Perry, J. K., Feng, J. Y., Porter, D. P., & Gotte, M. (2020). Remdesivir is a direct-acting antiviral that inhibits RNA-dependent RNA polymerase from severe acute respiratory syndrome coronavirus 2 with high potency. *J Biol Chem*, 295(20), 6785-6797. <https://doi.org/10.1074/jbc.RA120.013679>
- Grein, J., Ohmagari, N., Shin, D., Diaz, G., Asperges, E., Castagna, A., Feldt, T., Green, G., Green, M. L., Lescure, F. X., Nicastri, E., Oda, R., Yo, K., Quiros-Roldan, E., Studemeister, A., Redinski, J., Ahmed, S., Bennett, J., Chelliah, D., . . . Flanigan, T. (2020). Compassionate Use of Remdesivir for Patients with Severe Covid-19. *N Engl J Med*, 382(24), 2327-2336. <https://doi.org/10.1056/NEJMoa2007016>
- Gross, O., Moerer, O., Weber, M., Huber, T. B., & Scheithauer, S. (2020). COVID-19-associated nephritis: early warning for disease severity and complications? *Lancet*, 395(10236), e87-e88. [https://doi.org/10.1016/S0140-6736\(20\)31041-2](https://doi.org/10.1016/S0140-6736(20)31041-2)
- Group, A.-T. B. S., Lundgren, J. D., Grund, B., Barkauskas, C. E., Holland, T. L., Gottlieb, R. L., Sandkovsky, U., Brown, S. M., Knowlton, K. U., Self, W. H., Files, D. C., Jain, M.

- K., Benfield, T., Bowdish, M. E., Leshnowar, B. G., Baker, J. V., Jensen, J. U., Gardner, E. M., Ginde, A. A., . . . Neaton, J. D. (2022). Responses to a Neutralizing Monoclonal Antibody for Hospitalized Patients With COVID-19 According to Baseline Antibody and Antigen Levels : A Randomized Controlled Trial. *Ann Intern Med*, 175(2), 234-243. <https://doi.org/10.7326/M21-3507>
- Group, A.-T. L.-C. S., Lundgren, J. D., Grund, B., Barkauskas, C. E., Holland, T. L., Gottlieb, R. L., Sandkovsky, U., Brown, S. M., Knowlton, K. U., Self, W. H., Files, D. C., Jain, M. K., Benfield, T., Bowdish, M. E., Leshnowar, B. G., Baker, J. V., Jensen, J. U., Gardner, E. M., Ginde, A. A., . . . Neaton, J. D. (2021). A Neutralizing Monoclonal Antibody for Hospitalized Patients with Covid-19. *N Engl J Med*, 384(10), 905-914. <https://doi.org/10.1056/NEJMoa2033130>
- Group, A. C.-T. f. I. w. C.-S. (2021). Efficacy and safety of two neutralising monoclonal antibody therapies, sotrovimab and BR11-196 plus BR11-198, for adults hospitalised with COVID-19 (TICO): a randomised controlled trial. *Lancet Infect Dis*. [https://doi.org/10.1016/S1473-3099\(21\)00751-9](https://doi.org/10.1016/S1473-3099(21)00751-9)
- Group, R. C. (2022). Casirivimab and imdevimab in patients admitted to hospital with COVID-19 (RECOVERY): a randomised, controlled, open-label, platform trial. *Lancet*, 399(10325), 665-676. [https://doi.org/10.1016/S0140-6736\(22\)00163-5](https://doi.org/10.1016/S0140-6736(22)00163-5)
- Guan, W. J., Ni, Z. Y., Hu, Y., Liang, W. H., Ou, C. Q., He, J. X., Liu, L., Shan, H., Lei, C. L., Hui, D. S. C., Du, B., Li, L. J., Zeng, G., Yuen, K. Y., Chen, R. C., Tang, C. L., Wang, T., Chen, P. Y., Xiang, J., . . . China Medical Treatment Expert Group for, C. (2020). Clinical Characteristics of Coronavirus Disease 2019 in China. *N Engl J Med*, 382(18), 1708-1720. <https://doi.org/10.1056/NEJMoa2002032>
- Gupta, A., Gonzalez-Rojas, Y., Juarez, E., Crespo Casal, M., Moya, J., Falci, D. R., Sarkis, E., Solis, J., Zheng, H., Scott, N., Cathcart, A. L., Hebner, C. M., Sager, J., Mogalian, E., Tipple, C., Peppercorn, A., Alexander, E., Pang, P. S., Free, A., . . . Investigators, C.-I. (2021). Early Treatment for Covid-19 with SARS-CoV-2 Neutralizing Antibody Sotrovimab. *N Engl J Med*, 385(21), 1941-1950. <https://doi.org/10.1056/NEJMoa2107934>
- Gupta, A., Madhavan, M. V., Sehgal, K., Nair, N., Mahajan, S., Sehrawat, T. S., Bikdeli, B., Ahluwalia, N., Ausiello, J. C., Wan, E. Y., Freedberg, D. E., Kirtane, A. J., Parikh, S. A., Maurer, M. S., Nordvig, A. S., Accili, D., Bathon, J. M., Mohan, S., Bauer, K. A., . . . Landry, D. W. (2020). Extrapulmonary manifestations of COVID-19. *Nat Med*, 26(7), 1017-1032. <https://doi.org/10.1038/s41591-020-0968-3>
- H, D., F, H., S, G., & F, M. (1987). Mucociliary clearance in early simple chronic bronchitis. *European journal of respiratory diseases. Supplement*, 153. <https://www.ncbi.nlm.nih.gov/pubmed/3322859>
- H, I., A, K., & Y, T. (2022). Teratology studies with ambroxol (NA872) in rats and rabbits. *応用薬理*, 21(2), 271-279. https://jglobal.jst.go.jp/en/detail?JGLOBAL_ID=200902042198997737
- H, W., B, X., Y, Z., Y, D., R, G., H, H., X, L., & J, L. (2021). Efficacy and Safety of Traditional Chinese Medicine in Coronavirus Disease 2019 (COVID-19): A Systematic Review and Meta-Analysis. *Frontiers in pharmacology*, 12. <https://doi.org/10.3389/fphar.2021.609213>

- Hammond, J., Leister-Tebbe, H., Gardner, A., Abreu, P., Bao, W., Wisemandle, W., Baniecki, M., Hendrick, V. M., Damle, B., Simón-Campos, A., Pypstra, R., & Rusnak, J. M. (2022). Oral Nirmatrelvir for High-Risk, Nonhospitalized Adults with Covid-19 [research-article]. <https://doi.org/10.1056/NEJMoa2118542>.
<https://doi.org/NJ202202163861504>
- Hanwell, M. D., Curtis, D. E., Lonie, D. C., Vandermeersch, T., Zurek, E., & Hutchison, G. R. (2012). Avogadro: an advanced semantic chemical editor, visualization, and analysis platform [OriginalPaper]. *Journal of Cheminformatics*, 4(1), 1-17.
<https://doi.org/doi:10.1186/1758-2946-4-17>
- Harmer, D., Gilbert, M., Borman, R., & Clark, K. L. (2002). Quantitative mRNA expression profiling of ACE 2, a novel homologue of angiotensin converting enzyme. *FEBS Lett*, 532(1-2), 107-110. [https://doi.org/10.1016/s0014-5793\(02\)03640-2](https://doi.org/10.1016/s0014-5793(02)03640-2)
- Hilgenfeld, R. (2014). From SARS to MERS: crystallographic studies on coronaviral proteases enable antiviral drug design. *FEBS J*, 281(18), 4085-4096.
<https://doi.org/10.1111/febs.12936>
- Hoffmann, M., Kleine-Weber, H., Schroeder, S., Kruger, N., Herrler, T., Erichsen, S., Schiergens, T. S., Herrler, G., Wu, N. H., Nitsche, A., Muller, M. A., Drosten, C., & Pohlmann, S. (2020). SARS-CoV-2 Cell Entry Depends on ACE2 and TMPRSS2 and Is Blocked by a Clinically Proven Protease Inhibitor. *Cell*, 181(2), 271-280 e278.
<https://doi.org/10.1016/j.cell.2020.02.052>
- Huang, F., Guo, J., Zou, Z., Liu, J., Cao, B., Zhang, S., Li, H., Wang, W., Sheng, M., Liu, S., Pan, J., Bao, C., Zeng, M., Xiao, H., Qian, G., Hu, X., Chen, Y., Chen, Y., Zhao, Y., . . . Li, L. (2014). Angiotensin II plasma levels are linked to disease severity and predict fatal outcomes in H7N9-infected patients. *Nat Commun*, 5, 3595.
<https://doi.org/10.1038/ncomms4595>
- I, B.-B., G, M., M, F., & M, H. (2013). Ambroxol as a pharmacological chaperone for mutant glucocerebrosidase. *Blood cells, molecules & diseases*, 50(2).
<https://doi.org/10.1016/j.bcmd.2012.10.007>
- I, K., P, R., M, N., & M, G. (2019). The pharmacokinetic properties of HIV-1 protease inhibitors: A computational perspective on herbal phytochemicals. *Heliyon*, 5(10). <https://doi.org/10.1016/j.heliyon.2019.e02565>
- Imai, Y., Kuba, K., Rao, S., Huan, Y., Guo, F., Guan, B., Yang, P., Sarao, R., Wada, T., Leong-Poi, H., Crackower, M. A., Fukamizu, A., Hui, C. C., Hein, L., Uhlig, S., Slutsky, A. S., Jiang, C., & Penninger, J. M. (2005). Angiotensin-converting enzyme 2 protects from severe acute lung failure. *Nature*, 436(7047), 112-116.
<https://doi.org/10.1038/nature03712>
- J, Z., H, Z., & L, S. (2022). Therapeutic antibodies for COVID-19: is a new age of IgM, IgA and bispecific antibodies coming? *mAbs*, 14(1).
<https://doi.org/10.1080/19420862.2022.2031483>
- Jackson, C. B., Farzan, M., Chen, B., & Choe, H. (2022). Mechanisms of SARS-CoV-2 entry into cells. *Nat Rev Mol Cell Biol*, 23(1), 3-20. <https://doi.org/10.1038/s41580-021-00418-x>
- Jayk Bernal, A., Gomes da Silva, M. M., Musungaie, D. B., Kovalchuk, E., Gonzalez, A., Delos Reyes, V., Martin-Quiros, A., Caraco, Y., Williams-Diaz, A., Brown, M. L., Du,

- J., Pedley, A., Assaid, C., Strizki, J., Grobler, J. A., Shamsuddin, H. H., Tipping, R., Wan, H., Paschke, A., . . . Group, M. O.-O. S. (2022). Molnupiravir for Oral Treatment of Covid-19 in Nonhospitalized Patients. *N Engl J Med*, *386*(6), 509-520. <https://doi.org/10.1056/NEJMoa2116044>
- JM, L., C, H., T, K., SA, H., MS, M., LD, T., C, M., E, C., B, M., E, M., N, C., I, C., CM, B., EL, S., C, C., JA, S., A, B., & PS, N. (2014). The androgen-regulated protease TMPRSS2 activates a proteolytic cascade involving components of the tumor microenvironment and promotes prostate cancer metastasis. *Cancer discovery*, *4*(11). <https://doi.org/10.1158/2159-8290.CD-13-1010>
- Jordan, P. C., Stevens, S. K., & Deval, J. (2018). Nucleosides for the treatment of respiratory RNA virus infections. *Antivir Chem Chemother*, *26*, 2040206618764483. <https://doi.org/10.1177/2040206618764483>
- Jorgensen, W. L., Chandrasekhar, J., Madura, J. D., Impey, R. W., & Klein, M. L. (1998). Comparison of simple potential functions for simulating liquid water [research-article]. <https://doi.org/1.445869>
- K, N., M, F., Y, I., S, M., & S, N. (2006). Ambroxol for the prevention of acute upper respiratory disease. *Clinical and experimental medicine*, *6*(2). <https://doi.org/10.1007/s10238-006-0099-2>
- Kabinger, F., Stiller, C., Schmitzova, J., Dienemann, C., Kokic, G., Hillen, H. S., Hobartner, C., & Cramer, P. (2021). Mechanism of molnupiravir-induced SARS-CoV-2 mutagenesis. *Nat Struct Mol Biol*, *28*(9), 740-746. <https://doi.org/10.1038/s41594-021-00651-0>
- Khan, A., Benthin, C., Zeno, B., Albertson, T. E., Boyd, J., Christie, J. D., Hall, R., Poirier, G., Ronco, J. J., Tidswell, M., Harges, K., Powley, W. M., Wright, T. J., Siederer, S. K., Fairman, D. A., Lipson, D. A., Bayliffe, A. I., & Lazaar, A. L. (2017). A pilot clinical trial of recombinant human angiotensin-converting enzyme 2 in acute respiratory distress syndrome. *Crit Care*, *21*(1), 234. <https://doi.org/10.1186/s13054-017-1823-x>
- Kim, D., Kim, S., Park, J., Chang, H. R., Chang, J., Ahn, J., Park, H., Park, J., Son, N., Kang, G., Kim, J., Kim, K., Park, M. S., Kim, Y. K., & Baek, D. (2021). A high-resolution temporal atlas of the SARS-CoV-2 transcriptome and transcriptome. *Nat Commun*, *12*(1), 5120. <https://doi.org/10.1038/s41467-021-25361-5>
- Kim, D., Lee, J. Y., Yang, J. S., Kim, J. W., Kim, V. N., & Chang, H. (2020). The Architecture of SARS-CoV-2 Transcriptome. *Cell*, *181*(4), 914-921 e910. <https://doi.org/10.1016/j.cell.2020.04.011>
- KM, B., J, B., A, E., & LD, P. (2008). Antiinflammatory properties of ambroxol. *European journal of medical research*, *13*(12). <https://www.ncbi.nlm.nih.gov/pubmed/19073395>
- Kuba, K., Imai, Y., Rao, S., Gao, H., Guo, F., Guan, B., Huan, Y., Yang, P., Zhang, Y., Deng, W., Bao, L., Zhang, B., Liu, G., Wang, Z., Chappell, M., Liu, Y., Zheng, D., Leibbrandt, A., Wada, T., . . . Penninger, J. M. (2005). A crucial role of angiotensin converting enzyme 2 (ACE2) in SARS coronavirus-induced lung injury. *Nat Med*, *11*(8), 875-879. <https://doi.org/10.1038/nm1267>

- Lefkowitz, E. J., Dempsey, D. M., Hendrickson, R. C., Orton, R. J., Siddell, S. G., & Smith, D. B. (2018). Virus taxonomy: the database of the International Committee on Taxonomy of Viruses (ICTV). *Nucleic Acids Res*, *46*(D1), D708-D717. <https://doi.org/10.1093/nar/gkx932>
- Lei, C., Qian, K., Li, T., Zhang, S., Fu, W., Ding, M., & Hu, S. (2020). Neutralization of SARS-CoV-2 spike pseudotyped virus by recombinant ACE2-Ig. *Nat Commun*, *11*(1), 2070. <https://doi.org/10.1038/s41467-020-16048-4>
- Li, M., Wang, Jin. (2020). Prospect of ambroxol in the treatment of COVID-2019. <https://doi.org/ppcovidwho-4376>
- Liu, Y., Yang, Y., Zhang, C., Huang, F., Wang, F., Yuan, J., Wang, Z., Li, J., Li, J., Feng, C., Zhang, Z., Wang, L., Peng, L., Chen, L., Qin, Y., Zhao, D., Tan, S., Yin, L., Xu, J., . . . Liu, L. (2020). Clinical and biochemical indexes from 2019-nCoV infected patients linked to viral loads and lung injury. *Sci China Life Sci*, *63*(3), 364-374. <https://doi.org/10.1007/s11427-020-1643-8>
- Lu, R., Zhao, X., Li, J., Niu, P., Yang, B., Wu, H., Wang, W., Song, H., Huang, B., Zhu, N., Bi, Y., Ma, X., Zhan, F., Wang, L., Hu, T., Zhou, H., Hu, Z., Zhou, W., Zhao, L., . . . Tan, W. (2020). Genomic characterisation and epidemiology of 2019 novel coronavirus: implications for virus origins and receptor binding. *Lancet*, *395*(10224), 565-574. [https://doi.org/10.1016/S0140-6736\(20\)30251-8](https://doi.org/10.1016/S0140-6736(20)30251-8)
- M, L., A, L., E, C., & G, Z. (1987). An alternative to steroids for prevention of respiratory distress syndrome (RDS): multicenter controlled study to compare ambroxol and betamethasone. *Journal of perinatal medicine*, *15*(3). <https://doi.org/10.1515/jpme.1987.15.3.227>
- M, M., & B, R. (2008). Ambroxol in the 21st century: pharmacological and clinical update. *Expert opinion on drug metabolism & toxicology*, *4*(8). <https://doi.org/10.1517/17425255.4.8.1119>
- M, S., M, R., K, B., R, D., DK, M., & RM, C. (2021). Clinical Efficacy of Remdesivir and Favipiravir in the Treatment of Covid-19 Patients: Scenario So Far. *Current drug research reviews*. <https://doi.org/10.2174/2589977513666210806122901>
- M, Y., H, N., LK, N., C, O., H, K., & R, N. (2014). Ambroxol inhibits rhinovirus infection in primary cultures of human tracheal epithelial cells. *Archives of pharmacal research*, *37*(4). <https://doi.org/10.1007/s12272-013-0210-7>
- Magalhaes, J., Gegg, M. E., Migdalska-Richards, A., & Schapira, A. H. (2018). Effects of ambroxol on the autophagy-lysosome pathway and mitochondria in primary cortical neurons [OriginalPaper]. *Scientific reports*, *8*(1), 1-12. <https://doi.org/doi:10.1038/s41598-018-19479-8>
- Malone, B., Urakova, N., Snijder, E. J., & Campbell, E. A. (2022). Structures and functions of coronavirus replication-transcription complexes and their relevance for SARS-CoV-2 drug design. *Nat Rev Mol Cell Biol*, *23*(1), 21-39. <https://doi.org/10.1038/s41580-021-00432-z>
- Mariano, G., Farthing, R. J., Lale-Farjat, S. L. M., & Bergeron, J. R. C. (2020). Structural Characterization of SARS-CoV-2: Where We Are, and Where We Need to Be. *Front Mol Biosci*, *7*, 605236. <https://doi.org/10.3389/fmolb.2020.605236>

- Mason, R. J. (2020). Pathogenesis of COVID-19 from a cell biology perspective. *Eur Respir J*, 55(4). <https://doi.org/10.1183/13993003.00607-2020>
- McCreary, E. K., Division of Infectious Diseases, D. o. M., UPMC Health System and The University of Pittsburgh School of Medicine, Pittsburgh, Pennsylvania, Angus, D. C., Department of Critical Care Medicine, U. H. S. a. T. U. o. P. S. o. M., Pittsburgh, Pennsylvania, & Associate Editor, J. (2022). Efficacy of Remdesivir in COVID-19. *JAMA*, 324(11), 1041-1042. <https://doi.org/10.1001/jama.2020.16337>
- Meyer, B., Chiaravalli, J., Gellenoncourt, S., Brownridge, P., Bryne, D. P., Daly, L. A., Grauslys, A., Walter, M., Agou, F., Chakrabarti, L. A., Craik, C. S., Eysers, C. E., Eysers, P. A., Gambin, Y., Jones, A. R., Sierrecki, E., Verdin, E., Vignuzzi, M., & Emmott, E. (2021). Characterising proteolysis during SARS-CoV-2 infection identifies viral cleavage sites and cellular targets with therapeutic potential [OriginalPaper]. *Nature Communications*, 12(1), 1-16. <https://doi.org/doi:10.1038/s41467-021-25796-w>
- Michel, C. J., Mayer, C., Poch, O., & Thompson, J. D. (2020). Characterization of accessory genes in coronavirus genomes. *Virology*, 17(1), 131. <https://doi.org/10.1186/s12985-020-01402-1>
- Molnupiravir for treatment of COVID-19. (2022). *Med Lett Drugs Ther*, 64(1642), 10-11. <https://www.ncbi.nlm.nih.gov/pubmed/35134041>
- Monteil, V., Kwon, H., Prado, P., Hagelkruys, A., Wimmer, R. A., Stahl, M., Leopoldi, A., Garreta, E., Hurtado Del Pozo, C., Prosper, F., Romero, J. P., Wirnsberger, G., Zhang, H., Slutsky, A. S., Conder, R., Montserrat, N., Mirazimi, A., & Penninger, J. M. (2020). Inhibition of SARS-CoV-2 Infections in Engineered Human Tissues Using Clinical-Grade Soluble Human ACE2. *Cell*, 181(4), 905-913 e907. <https://doi.org/10.1016/j.cell.2020.04.004>
- Morales, A., Rello, S. R., Cristóbal, H., Fiz-López, A., Arribas, E., Marí, M., Tutusaus, A., Cal-Sabater, P. d. I., Nicolaes, G. A. F., Ortiz-Pérez, J. T., Bernardo, D., & Frutos, P. G. d. (2021). Growth Arrest-Specific Factor 6 (GAS6) Is Increased in COVID-19 Patients and Predicts Clinical Outcome [Communication]. *Biomedicines*, 9(4), 335. <https://doi.org/10.3390/biomedicines9040335>
- Morens, D. M., & Fauci, A. S. (2020). Emerging Pandemic Diseases: How We Got to COVID-19. *Cell*, 182(5), 1077-1092. <https://doi.org/10.1016/j.cell.2020.08.021>
- N, C., M, Z., X, D., J, Q., F, G., Y, H., Y, Q., J, W., Y, L., Y, W., J, X., T, Y., X, Z., & L, Z. (2020). Epidemiological and clinical characteristics of 99 cases of 2019 novel coronavirus pneumonia in Wuhan, China: a descriptive study. *Lancet (London, England)*, 395(10223). [https://doi.org/10.1016/S0140-6736\(20\)30211-7](https://doi.org/10.1016/S0140-6736(20)30211-7)
- N, Z., D, Z., W, W., X, L., B, Y., J, S., X, Z., B, H., W, S., R, L., P, N., F, Z., X, M., D, W., W, X., G, W., GF, G., & W, T. (2020). A Novel Coronavirus from Patients with Pneumonia in China, 2019. *The New England journal of medicine*, 382(8). <https://doi.org/10.1056/NEJMoa2001017>
- Ni, W., Yang, X., Yang, D., Bao, J., Li, R., Xiao, Y., Hou, C., Wang, H., Liu, J., Yang, D., Xu, Y., Cao, Z., & Gao, Z. (2020). Role of angiotensin-converting enzyme 2 (ACE2) in

- COVID-19 [ReviewPaper]. *Critical Care*, 24(1), 1-10.
<https://doi.org/doi:10.1186/s13054-020-03120-0>
- Nie, J., Li, Q., Wu, J., Zhao, C., Hao, H., Liu, H., Zhang, L., Nie, L., Qin, H., Wang, M., Lu, Q., Li, X., Sun, Q., Liu, J., Fan, C., Huang, W., Xu, M., & Wang, Y. (2020). Quantification of SARS-CoV-2 neutralizing antibody by a pseudotyped virus-based assay. *Nat Protoc*, 15(11), 3699-3715. <https://doi.org/10.1038/s41596-020-0394-5>
- Nobata, K., Fujimura, M., Ishiura, Y., Myou, S., & Nakao, S. (2006). Ambroxol for the prevention of acute upper respiratory disease. *Clin Exp Med*, 6(2), 79-83.
<https://doi.org/10.1007/s10238-006-0099-2>
- O, T., & AJ, O. (2010). AutoDock Vina: improving the speed and accuracy of docking with a new scoring function, efficient optimization, and multithreading. *Journal of computational chemistry*, 31(2). <https://doi.org/10.1002/jcc.21334>
- OA, O., M, K., C, O., & T, A. (2021). Discovery of Clioquinol and analogues as novel inhibitors of Severe Acute Respiratory Syndrome Coronavirus 2 infection, ACE2 and ACE2 - Spike protein interaction in vitro. *Heliyon*, 7(3).
<https://doi.org/10.1016/j.heliyon.2021.e06426>
- Olaleye, O. A., Kaur, M., & Onyenaka, C. C. (2020). Ambroxol Hydrochloride Inhibits the Interaction between Severe Acute Respiratory Syndrome Coronavirus 2 Spike Protein's Receptor Binding Domain and Recombinant Human ACE2. *bioRxiv*.
<https://doi.org/10.1101/2020.09.13.295691>
- Olivieri, D., Zavattini, G., Tomasini, G., Daniotti, S., Bonsignore, G., Ferrara, G., Carnimeo, N., Chianese, R., Catena, E., Marcatili, S., & et al. (1987). Ambroxol for the prevention of chronic bronchitis exacerbations: long-term multicenter trial. Protective effect of ambroxol against winter semester exacerbations: a double-blind study versus placebo. *Respiration*, 51 Suppl 1, 42-51.
<https://doi.org/10.1159/000195274>
- Ou, X., Liu, Y., Lei, X., Li, P., Mi, D., Ren, L., Guo, L., Guo, R., Chen, T., Hu, J., Xiang, Z., Mu, Z., Chen, X., Chen, J., Hu, K., Jin, Q., Wang, J., & Qian, Z. (2020). Characterization of spike glycoprotein of SARS-CoV-2 on virus entry and its immune cross-reactivity with SARS-CoV. *Nat Commun*, 11(1), 1620.
<https://doi.org/10.1038/s41467-020-15562-9>
- Owen, D. R., Allerton, C. M. N., Anderson, A. S., Aschenbrenner, L., Avery, M., Berritt, S., Boras, B., Cardin, R. D., Carlo, A., Coffman, K. J., Dantonio, A., Di, L., Eng, H., Ferre, R., Gajiwala, K. S., Gibson, S. A., Greasley, S. E., Hurst, B. L., Kadar, E. P., . . . Zhu, Y. (2021). An oral SARS-CoV-2 M(pro) inhibitor clinical candidate for the treatment of COVID-19. *Science*, 374(6575), 1586-1593.
<https://doi.org/10.1126/science.abl4784>
- P, B., & P, B. (1989). [Prophylaxis and treatment of bronchopulmonary complications with ambroxol administered by infusion in elderly patients undergoing surgery]. *Il Giornale di chirurgia*, 10(10). <https://www.ncbi.nlm.nih.gov/pubmed/2518303>
- P, D., I, M., V, P., H, C., J, C., & N, d. B. (2020). The four horsemen of a viral Apocalypse: The pathogenesis of SARS-CoV-2 infection (COVID-19). *EBioMedicine*, 58.
<https://doi.org/10.1016/j.ebiom.2020.102887>

- P, D., & M, F. (2021). Channels and Transporters of the Pulmonary Lamellar Body in Health and Disease. *Cells*, 11(1). <https://doi.org/10.3390/cells11010045>
- P, Z., XL, Y., XG, W., B, H., L, Z., W, Z., HR, S., Y, Z., B, L., CL, H., HD, C., J, C., Y, L., H, G., RD, J., MQ, L., Y, C., XR, S., X, W., . . . ZL, S. (2020). A pneumonia outbreak associated with a new coronavirus of probable bat origin. *Nature*, 579(7798). <https://doi.org/10.1038/s41586-020-2012-7>
- Paces, J., Strizova, Z., Smrz, D., & Cerny, J. (2020). COVID-19 and the immune system. *Physiol Res*, 69(3), 379-388. <https://doi.org/10.33549/physiolres.934492>
- Painter, G. R., Bowen, R. A., Bluemling, G. R., DeBergh, J., Edpuganti, V., Gruddanti, P. R., Guthrie, D. B., Hager, M., Kuiper, D. L., Lockwood, M. A., Mitchell, D. G., Natchus, M. G., Sticher, Z. M., & Kolykhalov, A. A. (2019). The prophylactic and therapeutic activity of a broadly active ribonucleoside analog in a murine model of intranasal venezuelan equine encephalitis virus infection. *Antiviral Res*, 171, 104597. <https://doi.org/10.1016/j.antiviral.2019.104597>
- Paladugu, S., & Donato, A. A. (2020). Remdesivir improved time to recovery in adults hospitalized with COVID-19 and lower respiratory tract involvement. *Ann Intern Med*, 173(2), JC4. <https://doi.org/10.7326/ACPJ202007210-005>
- Paleari, D., Rossi, G. A., Nicolini, G., & Olivieri, D. (2011). Ambroxol: a multifaceted molecule with additional therapeutic potentials in respiratory disorders of childhood [research-article]. <https://doi.org/10.1517/17460441.2011.629646>. <https://doi.org/10.1517/17460441.2011.629646>
- Paxlovid for treatment of COVID-19. (2022). *Med Lett Drugs Ther*, 64(1642), 9-10. <https://www.ncbi.nlm.nih.gov/pubmed/35134040>
- PC, N., & JO, M. (2014). Molecular dynamics simulations: from structure function relationships to drug discovery. *In silico pharmacology*, 2. <https://doi.org/10.1186/s40203-014-0004-8>
- Pillaiyar, T., Manickam, M., Namasivayam, V., Hayashi, Y., & Jung, S. H. (2016). An Overview of Severe Acute Respiratory Syndrome-Coronavirus (SARS-CoV) 3CL Protease Inhibitors: Peptidomimetics and Small Molecule Chemotherapy. *J Med Chem*, 59(14), 6595-6628. <https://doi.org/10.1021/acs.jmedchem.5b01461>
- Pirofski, L. A., & Casadevall, A. (2018). The Damage-Response Framework as a Tool for the Physician-Scientist to Understand the Pathogenesis of Infectious Diseases. *J Infect Dis*, 218(suppl_1), S7-S11. <https://doi.org/10.1093/infdis/jiy083>
- Polack, F. P., Thomas, S. J., Kitchin, N., Absalon, J., Gurtman, A., Lockhart, S., Perez, J. L., Perez Marc, G., Moreira, E. D., Zerbini, C., Bailey, R., Swanson, K. A., Roychoudhury, S., Koury, K., Li, P., Kalina, W. V., Cooper, D., Frenck, R. W., Jr., Hammitt, L. L., . . . Group, C. C. T. (2020). Safety and Efficacy of the BNT162b2 mRNA Covid-19 Vaccine. *N Engl J Med*, 383(27), 2603-2615. <https://doi.org/10.1056/NEJMoa2034577>
- PR, G. (2010). Ambroxol - Resurgence of an old molecule as an anti-inflammatory agent in chronic obstructive airway diseases. *Lung India : official organ of Indian Chest Society*, 27(2). <https://doi.org/10.4103/0970-2113.63603>
- Pushpakom, S., Iorio, F., Eyers, P. A., Escott, K. J., Hopper, S., Wells, A., Doig, A., Guilliams, T., Latimer, J., McNamee, C., Norris, A., Sanseau, P., Cavalla, D., &

- Pirmohamed, M. (2019). Drug repurposing: progress, challenges and recommendations. *Nat Rev Drug Discov*, 18(1), 41-58.
<https://doi.org/10.1038/nrd.2018.168>
- R, G., JJ, P., C, C., MB, L., JC, W., M, F., & RB, G. (1987). Influence of ambroxol on amoxicillin levels in bronchoalveolar lavage fluid. *Arzneimittel-Forschung*, 37(8).
<https://www.ncbi.nlm.nih.gov/pubmed/3675695>
- RayBiotech. (2022). COVID-19 Spike-ACE2 Binding Assay Kit.
<https://www.raybiotech.com/covid-19-spike-ace2-binding-assay-kit-en/>
- Reynard, O., Nguyen, X. N., Alazard-Dany, N., Barateau, V., Cimarelli, A., & Volchkov, V. E. (2015). Identification of a New Ribonucleoside Inhibitor of Ebola Virus Replication. *Viruses*, 7(12), 6233-6240. <https://doi.org/10.3390/v7122934>
- RR, W., G, S., B, B., J, A., & D, L. (1992). Randomized double blind trial of Ambroxol for the treatment of respiratory distress syndrome. *European journal of pediatrics*, 151(5). <https://doi.org/10.1007/BF02113258>
- Ryckaert, J.-P. (2022). (PDF) Numerical-Integration of Cartesian Equations of Motion of a System with Constraints – Molecular-Dynamics of N-Alkanes.
[https://doi.org/http://dx.doi.org/10.1016/0021-9991\(77\)90098-5](https://doi.org/http://dx.doi.org/10.1016/0021-9991(77)90098-5)
- Ryckaert, J.P., Ciccotti, G. and Berendsen, H.J. (1977) Numerical Integration of the Cartesian Equations of Motion of a System with Constraints Molecular Dynamics of n-Alkanes. *Journal of Computational Physics*, 23, 327-341. - References - Scientific Research Publishing. (2022).
[https://www.scirp.org/\(S\(lz5mqp453edsnp55rrgict55\)\)/reference/ReferencesPers.aspx?ReferenceID=1318824](https://www.scirp.org/(S(lz5mqp453edsnp55rrgict55))/reference/ReferencesPers.aspx?ReferenceID=1318824)
- S, K., PA, T., EE, B., J, C., G, F., A, G., L, H., J, H., S, H., BA, S., J, W., B, Y., J, Z., & SH, B. (2016). PubChem Substance and Compound databases. *Nucleic acids research*, 44(D1). <https://doi.org/10.1093/nar/gkv951>
- S, M., L, S., K, L., G, D. S., P, W., J, E., J, H., M, T., A, S., J, H., WE, H., R, K., P, C., J, H., S, C., K, M., H, Z., P, L., V, L., . . . AHV, S. (2020). Ambroxol for the Treatment of Patients With Parkinson Disease With and Without Glucocerebrosidase Gene Mutations: A Nonrandomized, Noncontrolled Trial. *JAMA neurology*, 77(4).
<https://doi.org/10.1001/jamaneurol.2019.4611>
- S, P., G, Z., K, K., & J, M.-Q. (1997). Reduction of cytokine release of blood and bronchoalveolar mononuclear cells by ambroxol. *European journal of medical research*, 2(3). <https://www.ncbi.nlm.nih.gov/pubmed/9113503>
- Sadoff, J., Gray, G., Vandebosch, A., Cardenas, V., Shukarev, G., Grinsztejn, B., Goepfert, P. A., Truyers, C., Fennema, H., Spiessens, B., Offergeld, K., Scheper, G., Taylor, K. L., Robb, M. L., Treanor, J., Barouch, D. H., Stoddard, J., Ryser, M. F., Marovich, M. A., . . . Group, E. S. (2021). Safety and Efficacy of Single-Dose Ad26.COV2.S Vaccine against Covid-19. *N Engl J Med*, 384(23), 2187-2201.
<https://doi.org/10.1056/NEJMoa2101544>

- Saul, S., & Einav, S. (2020). Old Drugs for a New Virus: Repurposed Approaches for Combating COVID-19. *ACS Infect Dis*, 6(9), 2304-2318. <https://doi.org/10.1021/acscinfecdis.0c00343>
- SB, B., C, Y., EC, C., S, K., GS, T., & V, D. (2020). Ambroxol and Ciprofloxacin Show Activity Against SARS-CoV2 in Vero E6 Cells at Clinically-Relevant Concentrations. *bioRxiv : the preprint server for biology*. <https://doi.org/10.1101/2020.08.11.245100>
- Shang, Y., Li, H., & Zhang, R. (2021). Effects of Pandemic Outbreak on Economies: Evidence From Business History Context. *Front Public Health*, 9, 632043. <https://doi.org/10.3389/fpubh.2021.632043>
- Sheahan, T. P., Sims, A. C., Zhou, S., Graham, R. L., Pruijssers, A. J., Agostini, M. L., Leist, S. R., Schafer, A., Dinnon, K. H., 3rd, Stevens, L. J., Chappell, J. D., Lu, X., Hughes, T. M., George, A. S., Hill, C. S., Montgomery, S. A., Brown, A. J., Bluemling, G. R., Natchus, M. G., . . . Baric, R. S. (2020). An orally bioavailable broad-spectrum antiviral inhibits SARS-CoV-2 in human airway epithelial cell cultures and multiple coronaviruses in mice. *Sci Transl Med*, 12(541). <https://doi.org/10.1126/scitranslmed.abb5883>
- Shrimp, J. H., Kales, S. C., Sanderson, P. E., Simeonov, A., Shen, M., & Hall, M. D. (2020). An Enzymatic TMPRSS2 Assay for Assessment of Clinical Candidates and Discovery of Inhibitors as Potential Treatment of COVID-19 [research-article]. <https://doi.org/10.1021/acscptsci.0c00106>
- Siegel, D., Hui, H. C., Doerffler, E., Clarke, M. O., Chun, K., Zhang, L., Neville, S., Carra, E., Lew, W., Ross, B., Wang, Q., Wolfe, L., Jordan, R., Soloveva, V., Knox, J., Perry, J., Perron, M., Stray, K. M., Barauskas, O., . . . Mackman, R. L. (2017). Discovery and Synthesis of a Phosphoramidate Prodrug of a Pyrrolo[2,1-f][triazin-4-amino] Adenine C-Nucleoside (GS-5734) for the Treatment of Ebola and Emerging Viruses. *J Med Chem*, 60(5), 1648-1661. <https://doi.org/10.1021/acs.jmedchem.6b01594>
- Skeggs, L. T., Dorer, F. E., Levine, M., Lentz, K. E., & Kahn, J. R. (1980). The biochemistry of the renin-angiotensin system. *Adv Exp Med Biol*, 130, 1-27. https://doi.org/10.1007/978-1-4615-9173-3_1
- SN, H., S, K., & Z, A. (2021). The Duplicitous Nature of ACE2 in COVID-19 Disease. *EBioMedicine*, 67. <https://doi.org/10.1016/j.ebiom.2021.103356>
- Sun, J., He, W. T., Wang, L., Lai, A., Ji, X., Zhai, X., Li, G., Suchard, M. A., Tian, J., Zhou, J., Veit, M., & Su, S. (2020). COVID-19: Epidemiology, Evolution, and Cross-Disciplinary Perspectives. *Trends Mol Med*, 26(5), 483-495. <https://doi.org/10.1016/j.molmed.2020.02.008>
- SW, C., Y, G., RS, P., P, S., JJ, E., GS, T., & V, D. (2018). Ambroxol Induces Autophagy and Potentiates Rifampin Antimycobacterial Activity. *Antimicrobial agents and chemotherapy*, 62(9). <https://doi.org/10.1128/AAC.01019-18>
- Tao, S., Zandi, K., Bassit, L., Ong, Y. T., Verma, K., Liu, P., Downs-Bowen, J. A., McBrayer, T., LeCher, J. C., Kohler, J. J., Tedbury, P. R., Kim, B., Amblard, F., Sarafianos, S. G., & Schinazi, R. F. (2021). Comparison of anti-SARS-CoV-2 activity and intracellular metabolism of remdesivir and its parent nucleoside. *Curr Res Pharmacol Drug Discov*, 2, 100045. <https://doi.org/10.1016/j.crphar.2021.100045>

- Teoh, S. L., Lim, Y. H., Lai, N. M., & Lee, S. W. H. (2020). Directly Acting Antivirals for COVID-19: Where Do We Stand? *Front Microbiol*, *11*, 1857. <https://doi.org/10.3389/fmicb.2020.01857>
- Tikellis, C., & Thomas, M. C. (2012). Angiotensin-Converting Enzyme 2 (ACE2) Is a Key Modulator of the Renin Angiotensin System in Health and Disease. *Int J Pept*, *2012*, 256294. <https://doi.org/10.1155/2012/256294>
- Tipnis, S. R., Hooper, N. M., Hyde, R., Karran, E., Christie, G., & Turner, A. J. (2000). A human homolog of angiotensin-converting enzyme. Cloning and functional expression as a captopril-insensitive carboxypeptidase. *J Biol Chem*, *275*(43), 33238-33243. <https://doi.org/10.1074/jbc.M002615200>
- Towler, P., Staker, B., Prasad, S. G., Menon, S., Tang, J., Parsons, T., Ryan, D., Fisher, M., Williams, D., Dales, N. A., Patane, M. A., & Pantoliano, M. W. (2004). ACE2 X-ray structures reveal a large hinge-bending motion important for inhibitor binding and catalysis. *J Biol Chem*, *279*(17), 17996-18007. <https://doi.org/10.1074/jbc.M311191200>
- V, D., & GS, T. (2019). Enhancement of lung levels of antibiotics by ambroxol and bromhexine. *Expert opinion on drug metabolism & toxicology*, *15*(3). <https://doi.org/10.1080/17425255.2019.1578748>
- VanBlargan, L., Errico, J., Halfmann, P., Zost, S., Crowe, J., Purcell, L., Kawaoka, Y., Corti, D., Fremont, D., & Diamond, M. (2021). An infectious SARS-CoV-2 B.1.1.529 Omicron virus escapes neutralization by therapeutic monoclonal antibodies. *Res Sq*. <https://doi.org/10.21203/rs.3.rs-1175516/v1>
- Vangeel, L., Chiu, W., De Jonghe, S., Maes, P., Slechten, B., Raymenants, J., Andre, E., Leysen, P., Neyts, J., & Jochmans, D. (2022). Remdesivir, Molnupiravir and Nirmatrelvir remain active against SARS-CoV-2 Omicron and other variants of concern. *Antiviral Res*, *198*, 105252. <https://doi.org/10.1016/j.antiviral.2022.105252>
- Vickers, C., Department of Metabolic Disease, M. P., Inc., Cambridge, Massachusetts 02139, Hales, P., Department of Lead Discovery, M. P., Inc., Cambridge, Massachusetts 02139, Kaushik, V., Department of Metabolic Disease, M. P., Inc., Cambridge, Massachusetts 02139, Dick, L., Department of Lead Discovery, M. P., Inc., Cambridge, Massachusetts 02139, Gavin, J., Department of Lead Discovery, M. P., Inc., Cambridge, Massachusetts 02139, Tang, J., Department of Protein Sciences, M. P., Inc., Cambridge, Massachusetts 02139, Godbout, K., Department of Technology Platform, M. P., Inc., Cambridge, Massachusetts 02139, Parsons, T., Department of Protein Sciences, M. P., Inc., Cambridge, Massachusetts 02139, Baronas, E., Department of Technology Platform, M. P., Inc., Cambridge, Massachusetts 02139, Hsieh, F., . . . Department of Metabolic Disease, M. P., Inc., Cambridge, Massachusetts 02139. (2002). Hydrolysis of Biological Peptides by Human Angiotensin-converting Enzyme-related Carboxypeptidase *. *Journal of Biological Chemistry*, *277*(17), 14838-14843. <https://doi.org/10.1074/jbc.M200581200>
- VP, C., AB, P., & DD, V. (2022). SARS-CoV-2 variants and vulnerability at the global level. *Journal of medical virology*. <https://doi.org/10.1002/jmv.27717>

- VP, C., C, K., S, S., R, P., SC, C., MM, Y., & V, A. (2022). A global picture: therapeutic perspectives for COVID-19. *Immunotherapy*, 14(5). <https://doi.org/10.2217/imt-2021-0168>
- W, L., MJ, M., N, V., J, S., SK, W., MA, B., M, S., JL, S., K, L., TC, G., H, C., & M, F. (2003). Angiotensin-converting enzyme 2 is a functional receptor for the SARS coronavirus. *Nature*, 426(6965). <https://doi.org/10.1038/nature02145>
- Walls, A. C., Park, Y. J., Tortorici, M. A., Wall, A., McGuire, A. T., & Velesler, D. (2020). Structure, Function, and Antigenicity of the SARS-CoV-2 Spike Glycoprotein. *Cell*, 181(2), 281-292 e286. <https://doi.org/10.1016/j.cell.2020.02.058>
- Walsh, E. E., Frencck, R. W., Jr., Falsey, A. R., Kitchin, N., Absalon, J., Gurtman, A., Lockhart, S., Neuzil, K., Mulligan, M. J., Bailey, R., Swanson, K. A., Li, P., Koury, K., Kalina, W., Cooper, D., Fontes-Garfias, C., Shi, P. Y., Tureci, O., Tompkins, K. R., . . . Gruber, W. C. (2020). Safety and Immunogenicity of Two RNA-Based Covid-19 Vaccine Candidates. *N Engl J Med*, 383(25), 2439-2450. <https://doi.org/10.1056/NEJMoa2027906>
- Wang, J., Reiss, K., Shi, Y., Lolis, E., Lisi, G. P., & Batista, V. S. (2021). Mechanism of Inhibition of the Reproduction of SARS-CoV-2 and Ebola Viruses by Remdesivir. *Biochemistry*, 60(24), 1869-1875. <https://doi.org/10.1021/acs.biochem.1c00292>
- Wang, M., Cao, R., Zhang, L., Yang, X., Liu, J., Xu, M., Shi, Z., Hu, Z., Zhong, W., & Xiao, G. (2020). Remdesivir and chloroquine effectively inhibit the recently emerged novel coronavirus (2019-nCoV) in vitro [Letter]. *Cell Research*, 30(3), 269-271. <https://doi.org/doi:10.1038/s41422-020-0282-0>
- Wang, P., Nair, M. S., Liu, L., Iketani, S., Luo, Y., Guo, Y., Wang, M., Yu, J., Zhang, B., Kwong, P. D., Graham, B. S., Mascola, J. R., Chang, J. Y., Yin, M. T., Sobieszczyk, M., Kyratsous, C. A., Shapiro, L., Sheng, Z., Huang, Y., & Ho, D. D. (2021). Antibody resistance of SARS-CoV-2 variants B.1.351 and B.1.1.7. *Nature*, 593(7857), 130-135. <https://doi.org/10.1038/s41586-021-03398-2>
- Wang, Q., Zhang, Y., Wu, L., Niu, S., Song, C., Zhang, Z., Lu, G., Qiao, C., Hu, Y., Yuen, K. Y., Wang, Q., Zhou, H., Yan, J., & Qi, J. (2020). Structural and Functional Basis of SARS-CoV-2 Entry by Using Human ACE2. *Cell*, 181(4), 894-904 e899. <https://doi.org/10.1016/j.cell.2020.03.045>
- Wang, S., Qiu, Z., Hou, Y., Deng, X., Xu, W., Zheng, T., Wu, P., Xie, S., Bian, W., Zhang, C., Sun, Z., Liu, K., Shan, C., Lin, A., Jiang, S., Xie, Y., Zhou, Q., Lu, L., Huang, J., & Li, X. (2021). AXL is a candidate receptor for SARS-CoV-2 that promotes infection of pulmonary and bronchial epithelial cells [OriginalPaper]. *Cell Research*, 31(2), 126-140. <https://doi.org/doi:10.1038/s41422-020-00460-y>
- WE, S., N, S., M, S., T, F., EL, W., S, A., & CB, J. (2007). Development and validation of a high-throughput screen for inhibitors of SARS CoV and its application in screening of a 100,000-compound library. *Journal of biomolecular screening*, 12(1). <https://doi.org/10.1177/1087057106296688>
- Wei, C., Wan, L., Yan, Q., Wang, X., Zhang, J., Yang, X., Zhang, Y., Fan, C., Li, D., Deng, Y., Sun, J., Gong, J., Yang, X., Wang, Y., Wang, X., Li, J., Yang, H., Li, H., Zhang, Z., . . . Zhong, H. (2020). HDL-scavenger receptor B type 1 facilitates SARS-CoV-2 entry

- [OriginalPaper]. *Nature Metabolism*, 2(12), 1391-1400.
<https://doi.org/doi:10.1038/s42255-020-00324-0>
- Weinreich, D. M., Sivapalasingam, S., Norton, T., Ali, S., Gao, H., Bhore, R., Xiao, J., Hooper, A. T., Hamilton, J. D., Musser, B. J., Rofail, D., Hussein, M., Im, J., Atmodjo, D. Y., Perry, C., Pan, C., Mahmood, A., Hosain, R., Davis, J. D., . . . Trial, I. (2021). REGEN-COV Antibody Combination and Outcomes in Outpatients with Covid-19. *N Engl J Med*, 385(23), e81. <https://doi.org/10.1056/NEJMoa2108163>
- Wettstein, L., Kirchoff, F., & Munch, J. (2022). The Transmembrane Protease TMPRSS2 as a Therapeutic Target for COVID-19 Treatment. *Int J Mol Sci*, 23(3).
<https://doi.org/10.3390/ijms23031351>
- Wouters, O. J., McKee, M., & Luyten, J. (2020). Estimated Research and Development Investment Needed to Bring a New Medicine to Market, 2009-2018. *JAMA*, 323(9), 844-853. <https://doi.org/10.1001/jama.2020.1166>
- Wrapp, D., Wang, N., Corbett, K. S., Goldsmith, J. A., Hsieh, C. L., Abiona, O., Graham, B. S., & McLellan, J. S. (2020). Cryo-EM structure of the 2019-nCoV spike in the prefusion conformation. *Science*, 367(6483), 1260-1263.
<https://doi.org/10.1126/science.abb2507>
- Wu, Z., & McGoogan, J. M. (2020). Characteristics of and Important Lessons From the Coronavirus Disease 2019 (COVID-19) Outbreak in China: Summary of a Report of 72314 Cases From the Chinese Center for Disease Control and Prevention. *JAMA*, 323(13), 1239-1242. <https://doi.org/10.1001/jama.2020.2648>
- X, S., L, W., Y, S., & C, B. (2004). Inhibition of inflammatory responses by ambroxol, a mucolytic agent, in a murine model of acute lung injury induced by lipopolysaccharide. *Intensive care medicine*, 30(1).
<https://doi.org/10.1007/s00134-003-2001-y>
- Xia, S., Lan, Q., Su, S., Wang, X., Xu, W., Liu, Z., Zhu, Y., Wang, Q., Lu, L., & Jiang, S. (2020). The role of furin cleavage site in SARS-CoV-2 spike protein-mediated membrane fusion in the presence or absence of trypsin [Letter]. *Signal Transduction and Targeted Therapy*, 5(1), 1-3.
<https://doi.org/doi:10.1038/s41392-020-0184-0>
- Y, I., K, K., S, R., Y, H., F, G., B, G., P, Y., R, S., T, W., H, L.-P., MA, C., A, F., CC, H., L, H., S, U., AS, S., C, J., & JM, P. (2005). Angiotensin-converting enzyme 2 protects from severe acute lung failure. *Nature*, 436(7047).
<https://doi.org/10.1038/nature03712>
- Y, K., S, K., H, O., & G, U. (1995). Antenatal ambroxol usage in the prevention of infant respiratory distress syndrome. Beneficial and adverse effects. *Clinical and experimental obstetrics & gynecology*, 22(3).
<https://www.ncbi.nlm.nih.gov/pubmed/7554258>
- Y, T., A, K., M, H., J, N., & T, S. (2022). Toxicity studies with ambroxol (NA872) in rats, mice and rabbits. *応用薬理*, 21(2), 281-311.
https://jglobal.jst.go.jp/en/detail?JGLOBAL_ID=200902061809579329
- Yan, R., Zhang, Y., Li, Y., Xia, L., Guo, Y., & Zhou, Q. (2020). Structural basis for the recognition of SARS-CoV-2 by full-length human ACE2. *Science*, 367(6485), 1444-1448. <https://doi.org/10.1126/science.abb2762>

- Yan, W., Zheng, Y., Zeng, X., He, B., & Cheng, W. (2022). Structural biology of SARS-CoV-2: open the door for novel therapies. *Signal Transduct Target Ther*, 7(1), 26. <https://doi.org/10.1038/s41392-022-00884-5>
- Yang, X., Yu, Y., Xu, J., Shu, H., Xia, J., Liu, H., Wu, Y., Zhang, L., Yu, Z., Fang, M., Yu, T., Wang, Y., Pan, S., Zou, X., Yuan, S., & Shang, Y. (2020). Clinical course and outcomes of critically ill patients with SARS-CoV-2 pneumonia in Wuhan, China: a single-centered, retrospective, observational study. *Lancet Respir Med*, 8(5), 475-481. [https://doi.org/10.1016/S2213-2600\(20\)30079-5](https://doi.org/10.1016/S2213-2600(20)30079-5)
- Ylilauri, M., & Pentikäinen, O. T. (2013). MMGBSA As a Tool To Understand the Binding Affinities of Filamin–Peptide Interactions [research-article]. <https://doi.org/10.1021/ci4002475>
- Yoon, J. J., Toots, M., Lee, S., Lee, M. E., Ludeke, B., Luczo, J. M., Ganti, K., Cox, R. M., Sticher, Z. M., Edpuganti, V., Mitchell, D. G., Lockwood, M. A., Kolykhalov, A. A., Greninger, A. L., Moore, M. L., Painter, G. R., Lowen, A. C., Tompkins, S. M., Fearn, R., . . . Plemper, R. K. (2018). Orally Efficacious Broad-Spectrum Ribonucleoside Analog Inhibitor of Influenza and Respiratory Syncytial Viruses. *Antimicrob Agents Chemother*, 62(8). <https://doi.org/10.1128/AAC.00766-18>
- Z, X., L, S., Y, W., J, Z., L, H., C, Z., S, L., P, Z., H, L., L, Z., Y, T., C, B., T, G., J, S., P, X., J, D., J, Z., & FS, W. (2020). Pathological findings of COVID-19 associated with acute respiratory distress syndrome. *The Lancet. Respiratory medicine*, 8(4). [https://doi.org/10.1016/S2213-2600\(20\)30076-X](https://doi.org/10.1016/S2213-2600(20)30076-X)
- Z, Y., K, L., D, S.-D., B, W., CC, H., EF, P., TD, G., EC, M., A, S., & TE, F. (2012). UCSF Chimera, MODELLER, and IMP: an integrated modeling system. *Journal of structural biology*, 179(3). <https://doi.org/10.1016/j.jsb.2011.09.006>
- Zhang, L., Lin, D., Sun, X., Curth, U., Drosten, C., Sauerhering, L., Becker, S., Rox, K., & Hilgenfeld, R. (2020). Crystal structure of SARS-CoV-2 main protease provides a basis for design of improved alpha-ketoamide inhibitors. *Science*, 368(6489), 409-412. <https://doi.org/10.1126/science.abb3405>
- Zhang, Q., Chen, C. Z., Swaroop, M., Xu, M., Wang, L., Lee, J., Wang, A. Q., Pradhan, M., Hagen, N., Chen, L., Shen, M., Luo, Z., Xu, X., Xu, Y., Huang, W., Zheng, W., & Ye, Y. (2020). Heparan sulfate assists SARS-CoV-2 in cell entry and can be targeted by approved drugs in vitro [OriginalPaper]. *Cell Discovery*, 6(1), 1-14. <https://doi.org/doi:10.1038/s41421-020-00222-5>
- Zhang, Y. Z., & Holmes, E. C. (2020). A Genomic Perspective on the Origin and Emergence of SARS-CoV-2. *Cell*, 181(2), 223-227. <https://doi.org/10.1016/j.cell.2020.03.035>
- Zhou, S., Hill, C. S., Sarkar, S., Tse, L. V., Woodburn, B. M. D., Schinazi, R. F., Sheahan, T. P., Baric, R. S., Heise, M. T., & Swanstrom, R. (2021). beta-d-N4-hydroxycytidine Inhibits SARS-CoV-2 Through Lethal Mutagenesis But Is Also Mutagenic To Mammalian Cells. *J Infect Dis*, 224(3), 415-419. <https://doi.org/10.1093/infdis/jiab247>